TOPICS IN BLACK-HOLE PHYSICS:

GEOMETRIC CONSTRAINTS ON NONCOLLAPSING, GRAVITATING SYSTEMS

and

TIDAL DISTORTIONS OF A SCHWARZSCHILD BLACK HOLE

Thesis by

Ian H. Redmount

In Partial Fulfillment of the Requirements

for the Degree of

Doctor of Philosophy

California Institute of Technology

Pasadena, California

1984

(Submitted September 23, 1983)

ACKNOWLEDGEMENTS

I wish to express my deepest gratitude to Kip S. Thorne: advisor, teacher, friend, and transmitter of that heritage of scholarship and learning of which the degree of Doctor of Philosophy is a symbol. I would also like to thank Richard H. Price, with whom I worked during the last year of my tenure at Caltech, to my great benefit, and Steven C. Frautschi, with whom I worked at various times and who was always willing to give me needed help and advice.

My thanks go also to my classmates and colleagues at Caltech, especially to my comrades in the Theoretical Astrophysics Group. I offer special thanks to my office-mates Yekta Gürsel and Douglas A. Macdonald. They taught me much and helped me unstintingly; their friendship is a cherished part of my life at Caltech.

I wish to acknowledge here my debt to my father, mother, sister, and brother. My family is a never-failing source of strength to me, and I have reached the milestone this work represents only by building upon the foundation they provide.

Those whose friendship has enriched me these past five years are too numerous to list, but I must recognize three very special people: Kim Aaron, Camille Kunze, and Marga Stya. They have helped to make my life rounded and whole; I offer them heartfelt thanks.

During my tenure as a graduate student at Caltech, I have been supported by a National Science Foundation Predoctoral Fellowship, a Robert Andrews Millikan Fellowship, a Caltech teaching assistantship, a J. S. Fluor Graduate Fellowship, and research assistantships provided by K. S. Thorne and S. C. Frautschi. I gratefully acknowledge all these sources of financial support.

ABSTRACT

This dissertation consists of two studies on the general-relativistic theory of black holes. The first work concerns the fundamental issue of black-hole formation: in it I seek geometric constraints on gravitating matter systems, in the special case of axial symmetry, which determine whether or not those systems undergo gravitational collapse to form black holes. The second project deals with mechanical behavior of a black hole: specifically, I study the tidal deformation of a static black hole by the gravitational fields of external bodies.

In the first paper I approach the problem of geometric constraints determining gravitational collapse or non-collapse through the initial-value formalism of general relativity. I construct initial-value data representing noncollapsing, nonsingular, axisymmetric matter systems and examine the constraints imposed on this construction by the initial-value equation derived from the Einstein field equations. The construction consists of a nonsingular, momentarily static interior geometry with nonnegative mass-energy density, matched smoothly to a static, vacuum exterior geometry (described by a Weyl solution of the Einstein field equations) at a boundary surface. The initial-value equation is found to impose restrictions on the choice of the boundary surface for such a system. Two such constraints are obtained here, appropriate to spherical and toroidal interior-region topologies. These constraints are studied by applying them to simple examples of Weyl exterior geometries. The "hoop conjecture" for the general geometric-constraints problem states that a system must collapse to a black hole unless its circumference in some direction exceeds a lower bound of the order of the system's mass. The examples examined here show, however, that the constraints derived in this study are not generally correlated with any simple measure of system size, and thus that they do not embody the hoop conjecture.

The second paper examines the tidal distortion of a Schwarzschild black hole by bodies ("moons") suspended above the horizon on "ropes." A solution of the Einstein field equations is constructed describing this configuration, using the Weyl formalism for axisymmetric, static, vacuum geometries. The intrinsic geometry of the tidally deformed black-hole horizon is obtained from this solution; I construct embedding diagrams to represent the shape of the horizon and the tidal bulges raised on it for both weak and strong perturbations. The relations among the masses of the hole and moons, the binding energy of the system, and the rope density and tension are calculated from the solution and shown to be mutually consistent. Also, the Riemann curvature tensor representing the tidal fields near the horizon is calculated. This solution is found to agree with a previous calculation by Hartle of black-hole tides, in the limit of perturbing moons far from the horizon. In the opposite case of moons very near the horizon, this solution approaches the static limit of the distorted horizon in Rindler space calculated by Suen and Price. The results of this study thus support the use of the Rindler approximation to Schwarzschild spacetime in calculating static black-hole tides, and its extension to dynamical situations.

TABLE OF CONTENTS

INTRODUCTION

Solutions of Einstein's General Theory of Relativity which can describe black holes were found within just a few years after the theory itself was first announced--the spherically symmetric, uncharged Schwarzschild solution in 1916 and the spherically symmetric, charged Reissner-Nordstrom solution in 1918. But for decades the idea of such "ultimately collapsed" objects was regarded as, at best, an unrealizable mathematical abstraction. Such thinking began to change in the early 1960's, when observations began to reveal unexpectedly violent phenomena in the universe, phenomena which might involve extremely strong gravitational fields. These discoveries sparked a renewal of interest in general relativity theory and in black holes in particular. In the succeeding two decades a great deal of research has been done on the fundamental theory of black holes. Questions on the formation and stability of black holes, on their local and global properties, on their classical and quantum dynamics, have been and are the subjects of extensive investigation. In recent years black holes have become part of the stock-in-trade of the astrophysicist as well as the relativist; attention is being focussed on the behavior of black holes as real physical objects in astrophysical situations.[1,2]

This dissertation consists of two studies in general relativity theory germane to black-hole physics: first, a search for geometric constraints on noncollapsing, gravitating systems; second, a description of a Schwarzschild black hole distorted by the tidal effects of fixed external masses. The first work deals with an issue of fundamental theory, seeking conditions on the geometry of matter systems which determine whether or not gravitational collapse to a black hole is inevitable. The second project concerns the mechanics of an interacting black hole, specifically, the gravitational deformations of a static black hole by external bodies. In both studies consideration is restricted to axially symmetric

systems, so that the powerful Weyl formalism[3,4] for static, axisymmetric geometries can be used to describe the gravitational fields.

Part One: Geometric Constraints on Nonsingular, Momentarily Static, Axisymmetric Systems in General Relativity

The only mechanism by which black holes can be formed, other than primordially, is gravitational collapse of matter systems. It is held that any sufficiently compact assemblage of matter and energy will collapse under its own gravity to form an event horizon and thus a black hole. The proper characterization of "sufficiently compact" is an unsolved problem. Indeed, the relationship between system size and black-hole formation might be considered the oldest problem in black-hole theory. In 1795 Laplace[5] calculated that the escape velocity from the surface of a spherical body of fixed density and sufficiently large radius would exceed the speed of light; such a body would render itself invisible by means of its own gravity. Laplace's result, expressed in terms of a relation between the mass of the body and its radius, coincides with that of the Schwarzschild radius for a spherical, uncharged black hole--despite the fact that Laplace's calculation used Newtonian gravity and Newton's corpuscular theory of light.

In this century the size-constraint problem has been solved only for the case of spherical symmetry. An uncharged, spherically symmetric body must lie outside its Schwarzschild radius, i.e., it must have circumference greater than $2\pi r_S$, where r_S is related to the mass M of the body by $r_S = 2M$ $(G=c=1)$, else it will be inside the horizon of a black hole and in a state of dynamical collapse. Studies of gravitational collapse in less symmetric situations have led to the formulation of the "hoop conjecture": for a body of mass M the formation of a horizon and a black hole is inevitable if and only if the body is compacted such

that its circumference in every direction is less than a bound of order $4\pi M$ (i.e., if and only if a hoop of this circumference can be passed around the body in every direction.)[1,2] The aim of the research presented in Part One is to gain insight into the hoop conjecture by considering the case of axial symmetry.

The size-constraint question lends itself to treatment as an initial-value problem. If a matter system is described on an initial-value hypersurface (i.e., at an initial "moment of time"), what constraints on the initial data ensure that collapse to a black hole is inevitable or can be avoided in the course of the subsequent evolution? The field equations of general relativity can be cast in the form of equations for such a Cauchy problem; in this formulation, six of the ten independent Einstein field equations describe the evolution of the system, and the remaining four are conditions governing the initial-value data.[6] The full dynamical problem is too intractable, even under the simplifying assumption of axial symmetry, to yield useful results on this question. So in Part One I consider a more manageable question: if I demand that the system be noncollapsing on the initial hypersurface (which guarantees that subsequent collapse can be avoided in principle), how is its geometry constrained by the field equations which govern the initial-value data? That is, what geometric conditions must the system satisfy in order to be even momentarily noncollapsing?

The hypothetical noncollapsing system is described by a three-dimensional initial-value hypersurface consisting of a bounded interior region occupied by matter and an asymptotically flat, vacuum exterior region. The interior is required to be axisymmetric and momentarily static, embodying non-collapse. It must also satisfy the physical requirements that the locally measured mass-energy density be nonnegative, and that no physical singularities be present. The exterior is required to be axisymmetric and to be a slice of a fully static region (i.e., the exterior region outside the light cones of the interior at its

moment of stasis is required to be static); the latter condition embodies the absence of gravitational waves. These conditions imply that the exterior can be described by a Weyl solution of the Einstein field equations.[3,4] Such solutions have singular, unphysical "sources"; in this construction a region of the solution containing the singular source is replaced by the nonsingular interior geometry described above. I seek geometric constraints related to the hoop conjecture from the limitations on this construction imposed by the initial-value field equations.

On a hypersurface of momentary stasis such as described above, the four initial-value field equations reduce to one, which equates the three-dimensional curvature scalar of the hypersurface to a multiple of the locally measured energy density.[6] This equation can be manipulated into a form which equates a total divergence with a quantity which is nonnegative by virtue of the nonnegativity of the energy density. Integrating this equation over the interior region gives an integral over the matter/vacuum boundary surface which consequently is required to be nonnegative. This requirement constitutes a geometric constraint on the system. By using different descriptions of the interior geometry, I obtain two such constraints, one applicable primarily to sources of spherical topology, the other applicable to sources with toroidal topology. (The technique of obtaining surface integrals constrained to be nonnegative from volume integrals of manifestly nonnegative integrands is one that has proven useful for other problems in gravitation theory as well. For example, recent work on the positivity of mass of isolated systems has utilized this method.[7])

The constraints thus obtained can, in appropriate circumstances, be expressed entirely in terms of quantities characterizing the exterior geometry. Their significance is that in any given exterior, surfaces for which a constraint inequality is violated are forbidden as matter/vacuum boundaries for a

momentarily static system as described here. In Part One I apply these constraints to simple cases of Weyl exterior geometries with both spherical and toroidal interior topologies. Applied to the Schwarzschild exterior, the spherical-topology constraint is in accord with the result given above: the source must extend outside its own Schwarzschild radius. In some more complicated examples the constraints forbid the matter boundary surface to be arbitrarily near the singular source of the full Weyl geometry, i.e., the constraints identify a forbidden region in these exterior geometries within which the matter boundary surface cannot lie.

The geometric constraints obtained in Part One do not, however, embody or support the hoop conjecture. The example calculations show that the constraints are not, in general, correlated with any simple measure of boundary-surface size. Furthermore, in some examples the constraints forbid as boundaries of momentarily static systems surfaces with arbitrarily large circumferences, in contrast to the hoop conjecture. But these results do not disprove the hoop conjecture either. The constraints of Part One and the hoop conjecture are logically distinct. The hoop conjecture, as formulated above, is a necessary and sufficient condition for the inevitability of collapse to a black hole: a system compacted as described in the conjecture must form a black hole, while a system not so compacted can avoid such a fate. The constraints obtained here are necessary but not sufficient conditions for the construction of a momentarily static system as described above: a surface in an exterior Weyl geometry for which either of these constraints is violated cannot be the boundary of a nonsingular, noncollapsing system with positive mass-energy density; a surface satisfying the constraints may or may not be suitable as the boundary of such a system. Additionally, the initial-value formalism used here does not establish the inevitable formation of a black hole from systems violating the constraints.

Thus the fact that the constraints forbid some surfaces with arbitrarily large circumferences does not contradict the hoop conjecture. And there is no example in these results of a momentarily static system with circumference in every direction much less than its mass. In fact the Weyl geometries studied here provide no possibility for such a counterexample: all the source-surrounding surfaces examined in them have largest circumferences larger than a bound of order $4\pi M$.

The hoop conjecture and the size-constraint problem remain subjects of active study. For example, Schoen and Yau[8] in recent work motivated by Part One of this thesis, prove a size constraint reminiscent of the original Laplace[5] result. They show that a bounded system, in which the proper or comoving density of mass-energy is bounded below by a positive constant Λ, possesses an apparent horizon (and eventually forms a black hole) if its "radius," suitably defined, exceeds a certain limit of order $\Lambda^{-1/2}$. (The quantity they define as the measure of radius is essentially the largest minor radius of any torus that can be enclosed in the matter region.) Thus Schoen and Yau do obtain a size constraint for noncollapsing systems, though it differs considerably from the hoop conjecture. Notably, the constraint is given in terms of the local mass-energy density rather than the total mass measured remotely; also, the size measure used depends on the detailed nature of the interior geometry.

In their proof Schoen and Yau use techniques of functional analysis far removed from the methods I employ in Part One, but in both works the problem of conditions ensuring collapse or non-collapse is treated as an initial-value problem; in both cases geometric constraints are derived on the initial-value data. Perhaps other applications of this approach might yield results more directly related to the hoop conjecture than those discussed above. The results of Part One also indicate another possible approach to the size constraint

question: geometric conditions bearing on the hoop conjecture may be derivable from the static, vacuum Einstein field equations themselves, at least in the axisymmetric case. The observation that all the source-surrounding surfaces in examples of Weyl geometries studied here have circumferences in some direction larger than a bound of the order of the system mass M suggests this possibility.

Part Two: Tidal Distortions of a Schwarzschild Black Hole

By the early 1970's the principal features of the fundamental theory of black holes were becoming well established, and interest turned to the problem of finding black holes in nature.[9] This stimulated research efforts on the roles black holes might play in various areas of astrophysics.[2] In addition, discoveries in the 1970's on the quantum mechanical and thermodynamic properties of holes suggested interesting consequences of black-hole physics for statistical mechanics, particle physics, and other fields.[10] Both of these lines of inquiry require further understanding of the interaction of black holes with other physical systems.

The research to be described in Part Two of this dissertation grew out of a program of studies in black-hole dynamics in which I participated in collaboration with K. S. Thorne, R. H. Price, R. J. Crowley, W. H. Zurek, D. A. Macdonald, W.-M. Suen, M. Mijic, L. S. Finn, and X.-H. Zhang. The aim of this program is to express and understand the laws of black-hole physics in a form which accords with an interpretation of the black-hole horizon as a time-evolving, two-dimensional membrane in three-dimensional space. Such a membrane is assigned physical properties, such as conductivity and viscosity, the values of which are consequences of these laws. This reformulation provides an intuitive conceptual framework for dealing with questions on the physical interactions of

black holes. It has been applied successfully to problems involving the electrodynamics of holes[11,12]; the study discussed in Part Two is part of an extension of this formalism to gravitational problems.

One important aspect of the gravitational interaction of black holes with other systems is tidal deformation of black holes by the gravitational fields of external bodies. Black-hole tides play an important role in the exchange of angular momentum between a rotating black hole and external matter[13,14,15,16]; they may also be important in processes invoked in speculations on the statistical mechanics of holes.[17] As part of the program of studies described above, Suen and Price[18] have calculated static and dynamical tidal effects on the horizon in the space seen by a uniformly accelerated observer (Rindler space). This horizon is planar; Rindler space is an approximation to Schwarzschild spacetime in a region very close to the horizon, so close that the horizon curvature (i.e., its spherical shape) is not evident. In Part Two I present a detailed examination of tidal distortion of an actual Schwarzschild black hole, in the static case. These calculations provide means to corroborate the results of Suen and Price and verify the validity of the deformed Rindler-space approximation to a real, deformed black hole. Further, they extend the Rindler-space results (for the static case) to a full, curved, Schwarzschild horizon and link those results with the findings of previous studies on black-hole tides.

The calculations in Part Two begin with the construction of an approximate (perturbative) solution of the Einstein field equations describing a Schwarzschild black hole tidally distorted by the gravitational fields of bodies fixed on the polar axis of the hole outside its horizon. As this configuration is static, axially symmetric, and vacuum outside of the hole and the perturbing bodies or "moons," the desired solution is obtained via the Weyl formalism applicable to just such geometries.[3,4] Because the solution must be static, the formalism implies the

presence of "ropes" from infinity supporting the moons and specifies their properties. Moreover, all the masses, binding energies, and rope tensions in the solution are found to obey completely consistent relations.

Various features of the static tidal deformation of a Schwarzschild black hole are extracted from this solution: The shape of the distorted horizon is obtained directly from the solution metric. "Embedding diagrams" (surfaces in Euclidean three-space having the same intrinsic geometry as the horizon) are calculated to represent the shape of the horizon and its tidal bulges, both for weak and for strong deformations. Also, the components of the Riemann curvature tensor measuring the tidal gravitational fields in the vicinity of the horizon are calculated from the metric of the solution.

The solution thus obtained for the static, tidally deformed Schwarzschild black hole provides the desired comparisons discussed above. In the limit in which the perturbing moons are far from the horizon in comparison to its size, the horizon geometry derived from this solution is in agreement with the results obtained by Hartle,[13,14] for the same physical situation, using different perturbation techniques. The opposite limit, in which the moons are very close to the horizon compared to its size, is the configuration describable by the Rindler approximation. The intrinsic horizon geometry and the Riemann curvature components calculated from this solution can be compared with the same quantities calculated by Suen and Price[18] for the distorted horizon in Rindler space. Complete agreement is found between the two sets of results, in the appropriate limit. Hence the calculations of Part Two confirm the validity of the Rindler approximation for calculating black-hole tidal effects in the (strongly perturbed) static case, and they therefore lend support to the results obtained using that approximation in dynamical calculations.

REFERENCES

[1]C. W. Misner, K. S. Thorne, and J. A. Wheeler, *Gravitation* (W. H. Freeman, San Francisco, 1973), pp. 817-940.

[2]R. D. Blandford and K. S. Thorne, in *General Relativity: An Einstein Centenary Survey*, edited by S. W. Hawking and W. Israel (Cambridge University Press, Cambridge, 1979), pp. 454-503.

[3]H. Weyl, Ann. Phys. (Leipzig) 54 , 117-145 (1918).

[4]J. L. Synge, *Relativity: The General Theory* (North Holland, Amsterdam, 1966), pp. 309-317.

[5]P. S. Laplace, *Le Systeme du monde*, vol. II, Paris, 1795. Published in English as *The System of the World*, W.Flint, London, 1809. Quoted in Reference 1, p. 872.

[6]C. W. Misner, K. S. Thorne, and J. A. Wheeler, *Gravitation* (W. H. Freeman, San Francisco, 1973), pp. 484-556.

[7]Martin Walker, *On the positivity of total gravitational energy at retarded times*, Lectures at the 1982 Les Houches summer school on gravitational radiation, May 1982.

[8]Richard Schoen and S. T. Yau, preprint, 1983.

[9]K. S. Thorne, Sci. Am. vol. 231, no. 6, pp. 32-43, (December 1974).

[10]Jacob D. Bekenstein, Gen. Relativ. Gravit. 14 , 355-359 (1982).

[11]Kip S. Thorne and Douglas Macdonald, Mon. Not. R. astr. Soc. 198 , 339-343 (1982).

[12]Douglas Macdonald and Kip S. Thorne, Mon. Not. R. astr. Soc. 198 , 345-382 (1982).

[13]James B. Hartle, Phys. Rev. D 8, 1010-1024 (1973).

[14]James B. Hartle, Phys. Rev. D 9, 2749-2759 (1974).

[15]S. W. Hawking and J. B. Hartle, Commun. math. Phys. 27, 283-290 (1972).

[16]Saul A. Teukolsky, Ph. D. thesis, California Institute of Technology, University Microfilms #74-14,289 (1974).

[17]William G. Unruh and Robert M. Wald, Phys. Rev. D. 25, 942-958 (1982).

[18]Wai-Mo Suen and Richard H. Price, unpublished.

PART ONE: GEOMETRIC CONSTRAINTS ON NONSINGULAR, MOMENTARILY STATIC, AXISYMMETRIC SYSTEMS IN GENERAL RELATIVITY

[Published in Physical Review D 27, 699-718 (15 February 1983).]

Geometric Constraints on Nonsingular, Momentarily Static, Axisymmetric Systems in General Relativity

Ian H. Redmount

Theoretical Astrophysics 130-33
California Institute of Technology
Pasadena, California 91125

ABSTRACT

This paper attempts to examine the relationship between system size and gravitational collapse for the case of axial symmetry. The approach here is to construct non-collapsing systems, with momentarily static matter interiors and static vacuum exteriors, and to find limitations on the validity of the construction. Specifically, the exteriors are static, axisymmetric, asymptotically flat, vacuum geometries, described by Weyl solutions of the Einstein field equations. These solutions have singular sources (naked singularities, except for the Schwarzschild solution); here, regions of the Weyl solutions containing the singularities are replaced by momentarily static material bodies. These are described by axisymmetric solutions of Brill's time-symmetric initial-value equation, with nonnegative energy density, joining smoothly to the Weyl geometries at the bodies' boundaries. The consistency requirements of such a construction limit the choice of surfaces in the exterior geometry suitable as matter/vacuum boundaries; general constraints on the boundary location and geometry are derived here. For the explicit examples of the Γ-metric and the Bach-Weyl ring metric as exteriors, these constraints forbid the boundary surface to be arbitrarily near the Weyl

singularity.

The "hoop conjecture" demands, roughly, that the largest circumference of the boundary surface of such a non-collapsing system always exceed a limit of the order of the system's mass. The specific examples studied here are all consistent with the hoop conjecture, but they show that the boundary constraints derived in this paper are not in general related to boundary-surface size and thus that these constraints do not embody the hoop conjecture.

I. INTRODUCTION

In astrophysical calculations and speculations about black holes one usually takes for granted several "articles of faith" that relativity theorists have not yet proved with any rigor.[1] These include the hypothesis of cosmic censorship, the rapid-loss-of-hair conjecture, and the hoop conjecture. Of these, the one for which we have the least concrete evidence is the hoop conjecture. This states that a black hole forms when and only when a mass M gets compacted into a region with circumference in any direction $C \leq 4\pi M$, so a hoop of that circumference can be slipped over the region and rotated through 360 degrees.[2,3] This statement of the conjecture is deliberately imprecise, but it indicates the form which a rigorous result linking system size and black hole formation is expected to take. The proof of such a result is also likely to require certain physical constraints such as a positive-energy-density condition. The motivation of this paper is to seek insight into this size-constraint problem by considering a special case.

More specifically, I restrict attention to axisymmetric systems and approach the problem not by examining black hole formation but the opposite--I ask what conditions must obtain for a material system to be non-collapsing. Specifically, I consider a bounded matter system (occupying the "interior" region I) which is axisymmetric and momentarily static; the latter embodies non-collapse and implies that the system can be described with Brill's time-symmetric initial-value formalism.[4] The exterior region E, i.e., the region outside the light cones of the interior at the moment of stasis, is required to be axisymmetric, fully (not just momentarily) static, asymptotically flat, and vacuum. These conditions embody the absence of gravitational waves and imply that the exterior is a slice of a Weyl solution of the vacuum Einstein equations.[5] This shows that the boundary surface of the matter interior lies outside the

absolute event horizon (if there is one), since the Weyl solutions are devoid of horizons except possibly at the edge of the Weyl coordinate patch.[6,7] I further impose the physical conditions that the local energy density be everywhere non-negative, and that no physical singularities occur. I then formulate the question thus: given a specific Weyl solution, and assuming a general interior geometry satisfying the above conditions and matched smoothly to the Weyl exterior, what constraints are imposed on the matter/vacuum boundary surface? Do these constraints have any bearing on the size of the boundary surface, which the hoop conjecture suggests should be "larger in all directions" than $\sim 4\pi M$?

I am aware of one previous calculation of this sort: a cursory study by Thorne[8] of constraints on interior solutions for the Weyl-type gravitational field of a thin-ring torus. Thorne's calculation showed that the location of the interior's surface in the Weyl exterior is bounded away from the immediate neighborhood of the Weyl toroidal singularity. However, this gave no substantial insight into the hoop conjecture.

My analysis of constraints on momentarily static, axisymmetric systems proceeds as follows: in Section II I introduce the time-symmetric initial- value formalism which forms the basis of my calculations, and I derive the junction conditions for matching interior and exterior geometries. In Section III I describe the exterior and interior geometries, and using the initial-value equation and the junction conditions I derive a constraint on the matter/vacuum boundary surface; in Section IV I utilize an alternative description of the interior to derive a second such boundary constraint, particularly suited to toroidal systems. In Section V and Section VI I apply the boundary constraints of Section III and Section IV, respectively, to simple examples of Weyl exterior geometries, and examine the implications of these constraints and their possible interpretations. In Section VII I discuss the possible extension of these results to exterior

geometries more general than the Weyl solutions.

The principal conclusions of this analysis are: there *do* exist constraints on the location of the matter/vacuum boundary in the Weyl exterior, for non-collapsing systems as described here. For systems with toroidal topology, equation (4.11) represents a rigorous constraint. For spherical-topology systems, constraints are given by equations (3.24), (3.30), and (3.43), although the derivation of the most generally applicable of these, equation (3.43), relies on an unproved assumption; see Appendix C. It may well be possible to close this gap in the derivation, though I have not been able to do so.

Applied to the spherical-topology Γ-metric (Section V) and to the toroidal Bach-Weyl ring metric (Section VI), my constraints imply the existence of a forbidden region near the Weyl singularity, within which the boundary of the matter system cannot lie. These examples further show that the constraints are not, in general, related in any obvious way to a minimum size for the matter system, and do not in any obvious sense embody the hoop conjecture. On the other hand, I have found no violation of the hoop conjecture in these examples; more precisely, the examples do not test my constraints against the hoop conjecture, because none of the candidate boundary surfaces in the Γ-metric or ring metric exteriors have arbitrarily small circumference in all directions.

Although I have not accomplished the original goal of this research--to prove a special case of the hoop conjecture or to find a counterexample to it--the formalism I have used and the results I have obtained here may prove useful in the hands of other researchers. Specifically, further manipulations of this formalism may yield additional boundary constraints for non-collapsing systems which are stronger than the ones I have derived, more generally applicable, or more amenable to interpretation as size constraints or manifestations of the hoop conjecture. It may also be possible to clarify the geometric meaning of the

constraints derived here, perhaps by applying them to additional explicit examples of Weyl geometries.

II. GOVERNING EQUATIONS AND JUNCTION CONDITIONS

A. Initial-Value Equations

The requirements of a momentarily static interior and a fully static exterior allow this problem to be treated using the time-symmetric initial-value formalism,[4] the hypersurface of constant time at the moment of interior stasis being time-symmetric. The three-dimensional geometry of the system on this hypersurface (hereafter denoted Σ) is governed by the single initial-value equation

$$^{(3)}R = 16\pi\varepsilon \tag{2.1}$$

where $^{(3)}R$ is the three-dimensional curvature scalar and ε is the locally measured energy density. I further assume the weak energy condition

$$\varepsilon \geq 0 \quad \text{throughout } \Sigma \tag{2.2}$$

and the absence of any physical singularity on Σ. The approach I take is to restrict all calculations to the hypersurface Σ and to study the two-dimensional boundary surface between its interior and exterior regions. The above relations and assumptions determine the matching conditions across and constraints upon that boundary.

B. Junction Conditions Across a 2-Surface

The derivation of junction conditions across a two-surface in Σ is similar to that of junction conditions across a three-dimensional hypersurface in spacetime.[9] Let $\mathscr{T}$ be a two-dimensional surface in Σ. The first step in this derivation

is to express the three-dimensional curvature scalar ${}^{(3)}R$ in the vicinity of $\mathscr{T}$ in terms of the intrinsic and extrinsic curvatures of $\mathscr{T}$. This may be done by contracting the Gauss-Codazzi equations written in Gaussian normal coordinates, in a manner analogous to that for the higher-dimensional calculation cited above. After some manipulation, one obtains

$$ {}^{(3)}R = {}^{(2)}R + 2\partial(\mathrm{Tr}\mathbf{S})/\partial n - (\mathrm{Tr}\mathbf{S})^2 - \mathrm{Tr}(\mathbf{S}^2) \tag{2.3} $$

where ${}^{(2)}R$ is the curvature scalar for the two-dimensional geometry of $\mathscr{T}$, $\mathrm{Tr}\mathbf{S} = S^{\alpha}{}_{\alpha}$ is the trace of the extrinsic curvature of $\mathscr{T}$, $\mathrm{Tr}(\mathbf{S}^2) = S^{\alpha}{}_{\beta} S^{\beta}{}_{\alpha}$ is the trace of its square (the sums over α and β extend over the two dimensions of $\mathscr{T}$), and $\partial/\partial n$ is the derivative with respect to proper distance normal to $\mathscr{T}$. The second step of the derivation is to integrate equation (2.1) over an infinitesimal interval of proper length across $\mathscr{T}$ in the normal direction, using the above result for ${}^{(3)}R$. That the intrinsic geometry of $\mathscr{T}$ be well defined requires that the metric restricted to $\mathscr{T}$ and the curvature scalar ${}^{(2)}R$ be continuous across $\mathscr{T}$, and consequently that $\mathrm{Tr}\mathbf{S}$ and $\mathrm{Tr}(\mathbf{S}^2)$ have no delta function discontinuities at $\mathscr{T}$. Given the assumption that the energy density ε contains no singular surface layer, this integration thus implies the junction condition

$$ \Delta(\mathrm{Tr}\mathbf{S}) \equiv \lim_{\delta \to 0} (\mathrm{Tr}\mathbf{S}) \Big|_{n=-\delta}^{+\delta} = 0 \tag{2.4} $$

where n is the proper distance normal to the surface $\mathscr{T}$.

In summary, the junction conditions across a two-surface $\mathscr{T}$ in the time-symmetric hypersurface Σ are: the intrinsic geometry of $\mathscr{T}$ must be continuous across the surface, and (in the absence of a singular surface layer) the trace of the extrinsic curvature of $\mathscr{T}$ must be likewise continuous.

III. DERIVATION OF A BOUNDARY CONSTRAINT

My approach to the derivation of constraints on the two-dimensional matter/vacuum boundary surface is to write the three-dimensional curvature scalar ${}^{(3)}R$ in the interior region of Σ as a total divergence plus a nonpositive quantity; equation (2.1) and the inequality (2.2) then imply that the divergence so obtained must be nonnegative. By integrating this divergence over the interior volume and invoking the assumption of nonsingularity to apply the divergence theorem, I obtain surface integrals over the boundary which are constrained to be nonnegative. Applying the above junction conditions to these integrals yields integrals, involving exterior quantities, which likewise are required to be nonnegative. To carry out this approach it is necessary to describe the interior and exterior geometries of Σ with appropriate coordinate systems.

A. Exterior Coordinate System, Metric, and Field Equations.

Since the exterior region is a slice of a static, axially symmetric, vacuum four-geometry, it can be described in complete generality by the Weyl formalism.[5] The four-metric of the exterior spacetime can be put in the form

$$ds_E^2=-\exp\{2\psi_E(\rho_E,z_E)\}dt^2+\exp\{2[\gamma_E(\rho_E,z_E)-\psi_E(\rho_E,z_E)]\}[d\rho_E^2+dz_E^2]$$

$$+\rho_E^2\exp\{-2\psi_E(\rho_E,z_E)\}d\varphi^2 \quad . \tag{3.1}$$

Restricted to Σ, this gives the three-metric

$$d\sigma_E^2=\exp\{2(\gamma_E-\psi_E)\}[d\rho_E^2+dz_E^2]+\rho_E^2\exp\{-2\psi_E\}d\varphi^2 \tag{3.2}$$

(the subscript E denotes "exterior"). For metric (3.1) in vacuum, the Einstein field equations reduce to

$$\partial^2\psi_E/\partial\rho_E^2+(1/\rho_E)\partial\psi_E/\partial\rho_E+\partial^2\psi_E/\partial z_E^2=0 \quad , \tag{3.3}$$

$$\partial\gamma_E/\partial\rho_E=\rho_E[(\partial\psi_E/\partial\rho_E)^2-(\partial\psi_E/\partial z_E)^2] \quad , \tag{3.4}$$

$$\partial\gamma_E/\partial z_E=2\rho_E(\partial\psi_E/\partial\rho_E)(\partial\psi_E/\partial z_E) \quad . \tag{3.5}$$

It is also required that $\gamma_E=0$ for $\rho_E=0$ to avoid a conical singularity on the z (symmetry) axis, and that far from a bounded source ψ_E approach the Newtonian potential:

$$\lim_{r\to\infty}\psi_E=-M/r+O(M^3/r^3) \tag{3.6}$$

where $r\equiv(\rho_E^2+z_E^2)^{1/2}$ and M is the total gravitational mass of the system as measured at infinity. Condition (3.6) ensures that the metric (3.1) has the appropriate asymptotic behavior at infinity.[10] Equation (3.3) means that ψ_E is a harmonic potential in a Euclidean "background space" with cylindrical coordinates (ρ_E,φ,z_E). Since γ_E can be determined from ψ_E by integrating equations (3.4) and (3.5), the entire exterior geometry is specified if ψ_E, or its fictitious "source" in the flat background space, is given.

The matter/vacuum boundary surface can be defined in terms of the exterior Weyl coordinates by specifying a meridian (φ=constant) curve for the surface. In general two cases of interest arise. In the "spherical topology" case, the interior region includes a segment of the symmetry axis. The boundary meridian in this case is an open curve with end points on the symmetry axis; I assume the curve intersects the axis orthogonally at its ends so that the boundary surface has no cusps. The other case is that of "toroidal topology"; here the symmetry axis lies wholly outside the matter (interior) region. In this case the boundary meridian is a closed curve, which I assume to be simple, i.e., non-self-intersecting. It is convenient to specify the meridian for either case parametrically, using proper length λ along the meridian as parameter and

defining the meridian with two functions $\rho_E = R(\lambda)$, $z_E = Z(\lambda)$; I take these to be twice differentiable. With λ and φ as coordinates on the boundary surface, the intrinsic geometry of the surface approached from the exterior is given by the two-metric

$$ds_2^2 = d\lambda^2 + R^2(\lambda)\exp\{-2\psi_E(R(\lambda), Z(\lambda))\}d\varphi^2 \quad . \tag{3.7}$$

The coordinate basis vectors tangent to the boundary are $\partial / \partial\varphi$ and

$$d / d\lambda = R'(\lambda)\partial / \partial\rho_E + Z'(\lambda)\partial / \partial z_E \tag{3.8}$$

where here and below primes denote derivatives with respect to λ. The normal to the surface is

$$d / dn = -Z'(\lambda)\partial / \partial\rho_E + R'(\lambda)\partial / \partial z_E \quad . \tag{3.9}$$

I choose the direction of increasing λ on the meridian so that (3.9) gives the outward-directed normal; this orientation of λ is analogous to the orientation of the coordinate θ in ordinary three-dimensional spherical coordinates. The metric (3.2), restricted to a boundary meridian, shows that both $d / d\lambda$ and d / dn are unit vectors. Figure 1 illustrates possible boundary geometries, coordinates, and associated vectors.

The trace of the boundary surface extrinsic curvature, for use in the junction conditions of Subsection II.B, can be calculated directly given the above boundary coordinates, vectors, and metric. I obtain

$$\mathrm{Tr}\mathbf{S}_E = \frac{R'Z'' - Z'R''}{R'^2 + Z'^2} + Z' / R + d(2\psi_E - \gamma_E) / dn$$

$$= -\alpha_E' + Z' / R + d(2\psi_E - \gamma_E) / dn \tag{3.10}$$

where

$$\alpha_E(\lambda)\equiv-\tan^{-1}(Z'/R') \tag{3.11}$$

is the angle between the vectors $\partial/\partial\rho_E$ and $d/d\lambda$, as indicated in Figure 1. (Since the metric (3.2), restricted to a φ=constant surface, is conformally flat, α_E is this angle as measured both in the physical space and in the background space). Here, as above, the subscript E denotes quantities calculated on the exterior side of the boundary.

B. Interior Coordinate System, Metric, and Field Equations

Because the interior geometry is only momentarily static, it is not constrained as strongly as is the exterior; it can be described in several ways. One simple description uses a three-metric similar to that of the vacuum Weyl metric:

$$d\sigma_I^2=\exp\{2[\gamma_I(\rho_I,z_I)-\psi_I(\rho_I,z_I)]\}[d\rho_I^2+dz_I^2]+\rho_I^2\exp\{-2\psi_I(\rho_I,z_I)\}d\varphi^2 \tag{3.12}$$

where here and below the subscript I denotes "interior." Since g_{00} is not specified, no generality is lost in this description.

Under the assumptions made here, it is always possible to cover the interior region with coordinates (ρ_I,φ,z_I) such that the metric takes the form (3.12). The φ coordinate derives from the axial symmetry. The existence of these interior coordinates hinges on the existence of coordinates (ρ_I,z_I) in which the metric has the above-indicated isothermal (conformally flat) form on a two-dimensional φ=constant slice of the interior. The uniformization theorem for Riemann surfaces (Appendix A) guarantees the existence of such an isothermal coordinate patch covering this slice, provided that the slice is simply connected. Since vacuum regions may be included as part of the interior if

necessary, the φ=constant slices of the interior can be assumed simply connected without loss of generality. The uniformization theorem further ensures that these coordinates (ρ_I, z_I) can be chosen so that their values fill any desired bounded, simply connected region in the plane $\mathbf{R}^2$. (Here this choice is limited by regularity requirements of the full three-dimensional interior coordinate system; in particular, $\rho_I=0$ on the symmetry axis is required, with $\rho_I>0$, say, off that axis, in order that γ_I and ψ_I be nonsingular). For example, for a toroidal-topology interior, the coordinates (ρ_I, z_I) might be chosen to fill a unit disk in the right half of the plane; for a spherical-topology interior, the right half of the unit disk centered on the origin is convenient. The latter choice makes the coordinates regular even at the "corners" of the interior slice, where the meridian meets the symmetry axis. (See Appendix A).

Since the metric (3.12) has the same form as (3.2), the description of the boundary surface from the interior is similar to that from the exterior. The boundary meridians are defined by two functions, $\rho_I=P(\lambda)$ and $z_I=\mathcal{Z}(\lambda)$. The intrinsic geometry of the boundary is given by the two-metric

$$ds_2^2=d\lambda^2+P^2(\lambda)\exp\{-2\psi_I(P(\lambda),\mathcal{Z}(\lambda))\}d\varphi^2 \quad . \tag{3.13}$$

The coordinate basis vectors tangent to the boundary are $\partial/\partial\varphi$ and

$$d/d\lambda=P'(\lambda)\partial/\partial\rho_I+\mathcal{Z}'(\lambda)\partial/\partial z_I \quad . \tag{3.14}$$

The normal vector is

$$d/dn=-\mathcal{Z}'(\lambda)\partial/\partial\rho_I+P'(\lambda)\partial/\partial z_I \quad . \tag{3.15}$$

With the orientation of λ already specified from the exterior, I make (3.15) the outward-directed normal by choosing the appropriate sign for the coordinate z_I. As above, both d/dn and $d/d\lambda$ are unit vectors. The configuration of interior

coordinates and vectors is as shown in Figure 1. The trace of the boundary extrinsic curvature is calculated as before, with the result

$$\mathrm{Tr}\mathbf{S}_I=\frac{P'\mathcal{Z}''-\mathcal{Z}'P''}{P'^2+\mathcal{Z}'^2}+\mathcal{Z}'/P+d(2\psi_I-\gamma_I)/dn$$

(3.16)

$$=-\alpha_I'+\mathcal{Z}'/P+d(2\psi_I-\gamma_I)/dn$$

with

$$\alpha_I(\lambda)\equiv-\tan^{-1}(\mathcal{Z}'/P') \quad . \tag{3.17}$$

The potentials $\gamma_I(\rho_I,z_I)$ and $\psi_I(\rho_I,z_I)$ in (3.12) need not satisfy equations like (3.3), (3.4) and (3.5), which are consequences of the vacuum Einstein field equations. The functions γ_I and ψ_I are constrained only by the initial-value equation (2.1). The calculation of the scalar curvature ${}^{(3)}R$ for the geometry described by the metric (3.12) is straightforward, and yields

$${}^{(3)}R_I=2\{2[\partial^2\psi_I/\partial\rho_I^2+(1/\rho_I)(\partial\psi_I/\partial\rho_I)+\partial^2\psi_I/\partial z_I^2]-[\partial^2\gamma_I/\partial\rho_I^2+\partial^2\gamma_I/\partial z_I^2]$$

$$-[(\partial\psi_I/\partial\rho_I)^2+(\partial\psi_I/\partial z_I)^2]\}\exp\{2(\psi_I-\gamma_I)\} \tag{3.18}$$

$$=16\pi\varepsilon\geq 0 \quad .$$

C. A Boundary Constraint Inequality

It is convenient to express (3.18) in terms of the covariant gradient ∇ for the three-metric (3.12). If this is done, a little rearrangement yields

$$\tfrac{1}{2}{}^{(3)}R_I+(\nabla\psi_I)^2=e^{-\psi_I}\nabla\cdot\{e^{\psi_I}[\nabla(2\psi_I-\gamma_I)+(\gamma_I/\rho_I)\nabla\rho_I]\} \tag{3.19}$$

where all the dot products in this equation are given by the metric (3.12). This form is suitable for deriving a boundary constraint via the approach outlined at the beginning of this section. Combined with (2.1) and (2.2), (3.19) implies

$$\nabla\cdot\{e^{\psi_I}[\nabla(2\psi_I-\gamma_I)+(\gamma_I/\rho_I)\nabla\rho_I]\}=e^{\psi_I}[8\pi\varepsilon+(\nabla\psi_I)^2]\geq 0 \ . \qquad (3.20)$$

I integrate this expression over the interior region I and apply the divergence theorem to the left-hand expression, obtaining a surface integral over the boundary ∂I:

$$\oint_{\partial I} d^2A\, e^{\psi_I}[d(2\psi_I-\gamma_I)/dn+(\gamma_I/\rho_I)d\rho_I/dn]=\int_I d^3V e^{\psi_I}[8\pi\varepsilon+(\nabla\psi_I)^2]\geq 0 \ . \qquad (3.21)$$

The metric (3.13) gives $d^2A=d\lambda P(\lambda)\exp\{-\psi_I(P(\lambda),\mathcal{Z}(\lambda))\}d\varphi$ and the operator (3.15) applied to ρ_I gives $d\rho_I/dn=-\mathcal{Z}'$. Dividing out the φ-integral, I obtain

$$\int_0^{\lambda_{max}} d\lambda[P(\lambda)d(2\psi_I-\gamma_I)/dn-\mathcal{Z}'(\lambda)\gamma_I]=[1/(2\pi)]\int_I d^3V e^{\psi_I}[8\pi\varepsilon+(\nabla\psi_I)^2]\geq 0 \qquad (3.22)$$

where the left-hand expression is a line integral taken over the boundary meridian, with all quantities evaluated at $\rho_I=P(\lambda)$, $z_I=\mathcal{Z}(\lambda)$.

The interior coordinates which give rise to the metric form (3.12) and thence to the inequality (3.22) are not unique, since the region of the plane filled by the coordinates (ρ_I,z_I) can be freely chosen (subject only to the requirement of simple connectivity, and the conditions $\rho_I=0$ on the symmetry axis, $\rho_I>0$ elsewhere). Any two such coordinate systems must be related by a conformal transformation on the coordinates (ρ_I,z_I), i.e., if (ρ_I,z_I) and $(\tilde{\rho}_I,\tilde{z}_I)$ are two sets of isothermal coordinates on a φ=constant slice of the interior, then $\tilde{\rho}_I\pm i\tilde{z}_I$ must be an injective analytic function of ρ_I+iz_I (allowing for a possible sign change for the z coordinate). Under these transformations, hereafter termed "gauge transformations," the potentials ψ_I and γ_I are not invariant; only the

combination $\rho_I e^{-\psi_I}=\|\partial/\partial\varphi\|$ and scalars constructible from the geometry (3.12) are. Thus the splitting off of the $(\nabla\psi_I)^2$ term in (3.19) and the weighting of the volume integrand in (3.21) by e^{ψ_I} are gauge-dependent, making the boundary constraint inequality (3.22) gauge- dependent.

To isolate this gauge dependence, and because exterior quantities are more completely and simply determined than interior ones, it is convenient to express (3.22) in terms of exterior quantities wherever possible. The junction conditions of Subsection II.B require that the two-metric (3.7) be continuous with (3.13), and that the extrinsic curvature trace (3.10) be continuous with (3.16). Solving the latter condition for $d(2\psi_I-\gamma_I)/dn$ and substituting the result into (3.22) gives

$$\int_0^{\lambda_{\max}} d\lambda\{P[d(2\psi_E-\gamma_E)/dn+Z'/R-\alpha_E'+\alpha_I']-\mathcal{F}'(1+\gamma_I)\}\geq 0 \quad . \qquad (3.23)$$

This constraint can be rendered a bit more tractable by specifying a choice of gauge. Let $\mathcal{M}$ be a φ=constant slice of the interior I; the boundary of $\mathcal{M}$, $\partial\mathcal{M}$, consists of a meridian for toroidal-topology interiors, a meridian plus a segment of the symmetry axis for the spherical-topology case. Let ${}^{(2)}\nabla$ denote the covariant derivative on $\mathcal{M}$ corresponding to the restriction of the metric (3.12) to $\mathcal{M}$. Let $\tilde{\rho}_I$ be the solution to the covariant Laplace equation ${}^{(2)}\nabla^2\tilde{\rho}_I=0$, where the Laplacian is also constructed from (3.12) restricted to $\mathcal{M}$, subject to the following boundary conditions: on the boundary meridian, $\tilde{\rho}_I=R(\lambda)$, as defined in Subsection III.A; if $\partial\mathcal{M}$ contains a segment of the symmetry axis, $\tilde{\rho}_I=0$ on that segment. Exactly one such $\tilde{\rho}_I$ always exists, since if $D\subset\mathbb{R}^2$ is the region of the plane filled by the interior coordinates (ρ_I,z_I), finding $\tilde{\rho}_I$ is equivalent to solving the Dirichlet problem on D with the corresponding boundary conditions on ∂D. Given $\tilde{\rho}_I$, the corresponding $\tilde{z}_I$ is determined by the Cauchy-Riemann equations, except for its overall sign and a possible overall translation. The sign

is fixed by the requirement that (3.15) represent the outward normal to ∂I; the translation is unimportant. Thus for any interior geometry considered here there exists a unique set of interior coordinates ("matched" coordinates) in which the metric has the form (3.12) and the radial coordinate $\tilde{\rho}_I$ matches the exterior radial coordinate ρ_E at the boundary, provided the map $(\tilde{\rho}_I,\tilde{z}_I):\mathcal{M}\to\mathbb{R}^2$ (or equivalently, $(\tilde{\rho}_I,\tilde{z}_I)$: $D\to\mathbb{R}^2$) is injective. A sufficient condition for this, relying only on exterior quantities, is that if the meridian exterior radial coordinate $R(\lambda)$ has only one local maximum, then injectivity of the matched coordinates is guaranteed for any interior geometry (see Appendix B). In matched interior coordinates, (3.23) takes the form

$$\int_0^{\lambda_{\max}} d\lambda\{R[d(2\psi_E-\gamma_E)/dn-\alpha_E'+\alpha_I']+Z'-\mathcal{F}'(1+\gamma_I)\}\geq 0 \quad . \tag{3.24}$$

Here α_I is given by (3.17), subject to the matching condition $P(\lambda)=R(\lambda)$; $\mathcal{F}(\lambda)$ and $\gamma_I(P(\lambda),\mathcal{F}(\lambda))$ are those appropriate to the matched interior coordinates $(\tilde{\rho}_I,\tilde{z}_I)$.

The inequality (3.24) may be further transformed by treating some of the terms as integrals in the Weyl "background" space, i.e., the exterior coordinate space with a flat Euclidean metric. Let dl be background-space length along the meridian, and ${}^{(B)}d/dn$ the unit outward normal derivative at the boundary surface in the background space. Since the metric (3.2), restricted to a φ=constant surface, is conformally flat, the scale factor between physical and background space meridian lengths is the same as that between physical and background space normal distances. Thus $d\lambda(d/dn)=dl({}^{(B)}d/dn)$. Consequently, I can write

$$\int_0^{\lambda_{\max}} d\lambda\, R(d\psi_E/dn)=[1/(2\pi)]\oint_{\partial I} d^2A_B\,{}^{(B)}d\psi_E/dn \quad , \tag{3.25}$$

where d^2A_B is the background space area measure. But the integral on the right side of (3.25) can be evaluated via Gauss's Law, i.e., by integrating (3.3) in the background space between ∂I and a coordinate sphere at infinity, applying the flat-space divergence theorem and utilizing (3.6). I obtain

$$\int_0^{\lambda_{max}} d\lambda R(d\psi_E/dn) = 2M \quad . \tag{3.26}$$

A similar transformation begins with

$$\int_0^{\lambda_{max}} d\lambda R(d\gamma_E/dn) = [1/(2\pi)] \oint_{\partial I} d^2A_B \, {}^{(B)}d\gamma_E/dn \quad . \tag{3.27}$$

The flat-space divergence theorem can be applied to the integral on the right side of this equation (equations (3.4), (3.5), and (3.6) imply that γ_E is of order $(M/r)^2$ as $r \to \infty$, so the integral over the sphere at infinity vanishes), with the result

$$\int_0^{\lambda_{max}} d\lambda R(d\gamma_E/dn) = -[1/(2\pi)] \int_E d^3V_B(\partial^2\gamma_E/\partial\rho_E^2 + \partial^2\gamma_E/\partial z_E^2)$$

$$-[1/(2\pi)] \int_E d^3V_B(1/\rho_E)(\partial\gamma_E/\partial\rho_E) \quad . \tag{3.28}$$

The integrals on the right are over the exterior volume E, with d^3V_B the coordinate-space volume measure. It follows from equations (3.4), (3.5), and (3.3) that the integrand of the first integral on the right equals the flat-space divergence of the vector field $-\psi_E {}^{(B)}\nabla\psi_E$, where ${}^{(B)}\nabla$ is the flat-space gradient. The integrand of the second integral is just the flat-space divergence of the vector field $(\gamma_E/\rho_E)(\partial/\partial\rho_E)$. Applying the divergence theorem to both integrals and converting the resulting surface integrals into line integrals in the physical space, I obtain

$$\int_0^{\lambda_{max}} d\lambda\, R(d\gamma_E/dn) = -\int_0^{\lambda_{max}} d\lambda[R\psi_E(d\psi_E/dn)+\gamma_E Z'] \quad . \qquad (3.29)$$

Using this and (3.26) in (3.24) gives

$$4M+\int_0^{\lambda_{max}} d\lambda\{R[\psi_E(d\psi_E/dn)-\alpha_E'+\alpha_I']+Z'(1+\gamma_E)-\mathcal{Z}'(1+\gamma_I)\} \geq 0 \quad . \qquad (3.30)$$

The boundary constraint (3.30) still depends on the interior geometry, but only through the coordinate derivative $\mathcal{Z}'$ and its derivative $\mathcal{Z}''$ along the meridian. These appear in α_I', as per (3.17), and in the last term of the integrand. The metric (3.12), specialized to a boundary meridian and in matched coordinates, yields the condition

$$1=\exp\{2[\gamma_I(R(\lambda),\mathcal{Z}(\lambda))-\psi_I(R(\lambda),\mathcal{Z}(\lambda))]\}[(R'(\lambda))^2+(\mathcal{Z}'(\lambda))^2] \quad . \qquad (3.31)$$

The junction conditions of Subsection II.B require that the boundary two-metrics (3.7) and (3.13) be continuous; coupled with the coordinate- matching condition $P(\lambda)=R(\lambda)$ this means ψ_I is continuous with ψ_E at the boundary. Thus γ_I at the boundary depends only on $\mathcal{Z}'$ and exterior quantities, i.e.,

$$\gamma_I(R(\lambda),\mathcal{Z}(\lambda))=\psi_E(R(\lambda),Z(\lambda))-\tfrac{1}{2}\log[(R'(\lambda))^2+(\mathcal{Z}'(\lambda))^2] \quad . \qquad (3.32)$$

This remaining dependence of (3.30) on interior quantities is dependence on the actual interior geometry rather than gauge dependence, since the choice of matched coordinates fixes the gauge. This may be seen by reexpressing (3.30) in terms of the matched interior coordinate ρ_I (dropping the tilde). This coordinate is uniquely and invariantly defined, as above, as the solution to ${}^{(2)}\nabla^2\rho_I=0$ on $\mathcal{M}$, with boundary conditions $\rho_I=R(\lambda)$ on the boundary meridian and $\rho_I=0$ on the symmetry axis if $\partial\mathcal{M}$ contains a segment thereof. Since $d\rho_I/dn=-\mathcal{Z}'$ on the meridian by (3.15), and similarly for $d\rho_E/dn$, inequality (3.30) may be written

$$4M+\int_0^{\lambda_{\max}} d\lambda\{R[\psi_E(d\psi_E/dn)+\alpha_I'-\alpha_E']$$

$$+(1+\gamma_I)(d\rho_I/dn)-(1+\gamma_E)(d\rho_E/dn)\}\geq 0 \quad . \tag{3.33}$$

Here α_I is defined as the angle from $\partial/\partial\rho_I$ to $d/d\lambda$, measured in accord with the orientation indicated in Figure 1; α_E is similarly defined. In terms of ρ_I and ρ_E, this means

$$\alpha_I=\tan^{-1}[(d\rho_I/dn)/(d\rho_I/d\lambda)] \;\; ; \;\; \alpha_E=\tan^{-1}[(d\rho_E/dn)/(d\rho_E/d\lambda)] \quad . \tag{3.34}$$

Also γ_I is given on the meridian by

$$\gamma_I=\psi_E-\tfrac{1}{2}\log[(d\rho_I/d\lambda)^2+(d\rho_I/dn)^2] \quad . \tag{3.35}$$

Hence the dependence of the boundary constraint (3.33) on interior quantities appears only through the function ρ_I. I have not been able to eliminate this dependence from this constraint in general.

The usefulness of the constraint (3.30) is in identifying surfaces in any given exterior geometry which are forbidden as boundaries of systems satisfying the $\varepsilon\geq 0$ and nonsingularity assumptions made here. The interior coordinates, specifically the coordinate derivative $\mathcal{Z}'$ for matched coordinates, must be specified in some way to evaluate the inequality (3.30); then, surfaces violating the inequality are forbidden. Surfaces satisfying the inequality may or may not be acceptable boundaries, since they may bound interiors satisfying (3.20) but violating the $\varepsilon\geq 0$ condition.

D. Double-Matched Coordinates

The boundary constraint (3.30) becomes very simple for cases in which the matched interior coordinates are also "double-matched," i.e., they satisfy

$\mathcal{Z}(\lambda)=Z(\lambda)$ as well as $P(\lambda)=R(\lambda)$. In such cases γ_I and γ_E are continuous at ∂I as well as ψ_I and ψ_E, and of course $\alpha_I'=\alpha_E'$. Inequality (3.30) reduces to

$$4M+\int_0^{\lambda_{max}} d\lambda\, R\psi_E(d\psi_E/dn)\geq 0 \quad . \tag{3.36}$$

If in addition the boundary surface is chosen to be an equipotential surface of ψ_E, then the integral can be evaluated via (3.26). The boundary constraint becomes

$$\psi_E|_{\partial I}\geq -2 \tag{3.37}$$

for a double-matched system with a ψ_E-equipotential boundary.

E. Maximization with respect to $\mathcal{Z}'$

It is also possible in certain cases to eliminate the interior coordinate dependence of (3.30) by maximizing the left side of the inequality with respect to the interior function $\mathcal{Z}'$. I denote the left side of (3.30) $\mathcal{I}_1[\mathcal{Z}']$, and regard it as a functional of $\mathcal{Z}'$; different functions $\mathcal{Z}'$ correspond to different interior geometries since matched interior coordinates are assumed in (3.30). If there exists a function $\mathcal{Z}_0'(\lambda)$ for which $\mathcal{I}_1$ is maximized, for a given exterior geometry and boundary surface, then the maximum value of $\mathcal{I}_1$ can serve to identify a forbidden surface. Specifically, a surface with $\mathcal{I}_1[\mathcal{Z}_0']<0$ is forbidden as a matter/vacuum boundary for any interior geometry under the assumptions made here.

It is a straightforward variational problem to extremize $\mathcal{I}_1$ with respect to $\mathcal{Z}'$. The first variation is

$$\delta\mathcal{I}_1=\int_0^{\lambda_{max}}[\tfrac{1}{2}\log(R'^2+\mathcal{Z}'^2)-\psi_E](\delta\mathcal{Z}')d\lambda=-\int_0^{\lambda_{max}}\gamma_I(\delta\mathcal{Z}')d\lambda \tag{3.38}$$

and the second variation is

$$\delta^2 \mathcal{I}_1 = \int_0^{\lambda_{max}} \frac{\mathcal{Z}'}{R'^2 + \mathcal{Z}'^2} (\delta \mathcal{Z}')^2 d\lambda \quad . \tag{3.39}$$

Thus the choice of $\mathcal{Z}'$ for which $\mathcal{I}_1$ is extremal is given by

$$\mathcal{Z}_0'(\lambda) = \pm \{ \exp[2\psi_E(R(\lambda), Z(\lambda))] - [R'(\lambda)]^2 \}^{1/2} \tag{3.40}$$

provided of course that

$$[R'(\lambda)]^2 \leq \exp[2\psi_E(R(\lambda), Z(\lambda))] \tag{3.41}$$

holds on the entire boundary meridian. This choice of $\mathcal{Z}_0'$ is equivalent to

$$\gamma_I(R(\lambda), \mathcal{Z}_0(\lambda)) = 0 \quad . \tag{3.42}$$

The choice of sign in (3.40) is fixed by the orientation of $d/d\lambda$ and d/dn on the boundary meridian. For those cases in which the negative square root applies along the entire meridian, (3.39) implies that $\mathcal{Z}_0'$ gives a maximum of $\mathcal{I}_1$. This is actually a local maximum in the space of functions $\mathcal{Z}'$; establishing it as a global maximum poses some difficulties (see Appendix C). In using this boundary constraint I assume the global maximality of $\mathcal{I}_1[\mathcal{Z}_0']$.

If condition (3.41) holds on the boundary meridian, and if the negative sign in (3.40) is admitted by the topology over the entire meridian, then the boundary constraint takes the form

$$\mathcal{I}_1[\mathcal{Z}_0'] = 4M + \int_0^{\lambda_{max}} d\lambda \{ R[\psi_E(d\psi_E/dn) - \alpha_E' + \alpha_J^{(0)'}] + Z'(1+\gamma_E) - \mathcal{Z}_0' \} \geq 0 \tag{3.43}$$

with $\mathcal{Z}_0'$ given by (3.40) and $\alpha_J^{(0)'}$ given by

$$\alpha_J^{(0)'} = -\frac{R'\mathcal{Z}_0'' - \mathcal{Z}_0' R''}{R'^2 + \mathcal{Z}_0'^2} = (d/d\lambda)[\tan^{-1}(-\mathcal{Z}_0'/R')] \quad . \tag{3.44}$$

Surfaces violating (3.43) are forbidden. Because of the aforementioned

conditions necessary to establish the existence and maximality of $\mathcal{F}_0'$, this form of the boundary constraint is most readily applied to systems of spherical topology, rather than toroidal systems with closed meridians.

IV. A SECOND BOUNDARY CONSTRAINT

A boundary constraint distinct from (3.30) or (3.43) can be derived via the same procedure as in Section III, starting from a slightly different interior description. I obtain the new boundary constraint by maintaining gauge invariance throughout the calculation.

A. Alternative Interior Description

The interior metric can be written

$$d\sigma_I^2 = \exp[2Q(\rho_I, z_I)]\,[d\rho_I^2 + dz_I^2] + \exp[2\beta(\rho_I, z_I)]\,d\varphi^2 \qquad (4.1)$$

The existence of coordinates in which the metric takes this form is guaranteed by the uniformization theorem, as in Subsection III.B. Since ρ_I does not appear as a factor in $g_{\varphi\varphi}$ here, the restrictions $\rho_I=0$ on the symmetry axis, $\rho_I>0$ elsewhere are not needed in this description. However, regularity of the geometry on the symmetry axis requires that the function β be singular there (i.e., that e^{β} vanish), if the axis passes within the interior region. The form of the metric (4.1) is preserved under gauge transformations of the type discussed in Subsection III.C; here the function β is gauge invariant, while Q is gauge-dependent.

The boundary surface is specified as before, by two functions $\rho_I = P(\lambda)$, $z_I = \mathcal{F}(\lambda)$; I make no assumption of matched coordinates here. The boundary's intrinsic geometry is given by the two-metric

$$ds_\Sigma^2 = d\lambda^2 + \exp[2\beta(P(\lambda), \mathcal{F}(\lambda))]\,d\varphi^2 \quad . \qquad (4.2)$$

The coordinate basis vectors on the boundary are $\partial/\partial\varphi$ and $d/d\lambda$ as given by (3.14); the normal vector d/dn is given by (3.15). The trace of the boundary extrinsic curvature is again calculated directly, with the result

$$\mathrm{Tr}\mathbf{S}_I=-[\alpha_I'+d(Q+\beta)/dn] \tag{4.3}$$

where α_I is as given by (3.17).

The scalar curvature ${}^{(3)}R$ for the geometry described by (4.1) is given by

$${}^{(3)}R_I=-2e^{-2Q}\{[(\partial/\partial\rho_I)^2+(\partial/\partial z_I)^2](Q+\beta)+(\partial\beta/\partial\rho_I)^2+(\partial\beta/\partial z_I)^2\} \ . \tag{4.4}$$

B. Derivation of the Alternate Boundary Constraint

In terms of the covariant derivative ∇ and covariant divergence corresponding to the metric (4.1), equation (4.4) takes the form

$${}^{(3)}R_I=-2[\nabla^2(Q+\beta)-\nabla Q\cdot\nabla\beta] \tag{4.5}$$

where the dot product in the last term is also that of (4.1). This expression for ${}^{(3)}R_I$ can be rearranged for integration over the interior volume in different ways; I maintain gauge invariance by rewriting it in the form

$$-[\tfrac{1}{2}{}^{(3)}R_I+(\nabla\beta)^2]=e^{\beta}\nabla\cdot[e^{-\beta}\nabla(Q+\beta)] \ . \tag{4.6}$$

Thus by the initial-value equation (2.1), I obtain

$$\nabla\cdot[e^{-\beta}\nabla(Q+\beta)]=-e^{-\beta}[8\pi\varepsilon+(\nabla\beta)^2]\leq 0 \ . \tag{4.7}$$

The divergence on the left is gauge invariant because the quantity on the right is.

I derive the desired boundary constraint by integrating (4.7) over the interior volume and applying the divergence theorem to obtain a surface integral.

Because of the singularity of β on the symmetry axis, that axis must be excluded from the integration volume if this is to be done. For spherical-topology systems, this means that the resulting surface integral consists of two terms, an integral over the boundary surface plus an integral over an infinitesimal "sheath" about the symmetry axis. But the integral over the sheath has the form

$$\int_{Sheath} d^2A[e^{-\beta}d(Q+\beta)/dn]=2\pi\int_{Sheath} d\lambda\, d(Q+\beta)/dn \quad . \tag{4.8}$$

In general dQ/dn will be finite at the symmetry axis. But $d\beta/dn=e^{-\beta}d(e^{\beta})/dn$ diverges to $-\infty$ there, since e^{β} vanishes while $d(e^{\beta})/dn$ approaches -1 by elementary flatness (the negative sign appears because the outward normal from the interior at the sheath points toward the symmetry axis). With the sheath term negative and infinite, the integral over the actual matter/vacuum boundary surface is not constrained at all by the inequality in (4.7). Thus the boundary constraint to be derived by integrating (4.7) is useful only for toroidal-topology systems, in which the interior region contains no segment of the symmetry axis.

For such toroidal systems, integrating (4.7) over the interior volume and using the divergence theorem yields

$$\int_0^{\lambda_{max}} d\lambda\, d(Q+\beta)/dn=-[1/(2\pi)]\int_I d^3V e^{-\beta}[8\pi\varepsilon+(\nabla\beta)^2]\leq 0 \quad . \tag{4.9}$$

By the junction condition (2.4), the trace (4.3) must be equal to (3.10). Solving this equality for $d(Q+\beta)/dn$ in (4.9) gives

$$\int_0^{\lambda_{max}} d\lambda [d(2\psi_E - \gamma_E)/dn + Z'/R - \alpha_E' + \alpha_I'] = [1/(2\pi)] \int_I d^3V e^{-\beta} [8\pi\varepsilon + (\nabla\beta)^2] \tag{4.10}$$

$$\geq 0 \quad .$$

The integral of α_I' around the boundary meridian gives 2π for an arbitrary regular interior; the integral of α_E' cannot be so given for all cases but can be evaluated in any given case (see Appendix D). Thus the boundary constraint has the form

$$\int_0^{\lambda_{max}} d\lambda [d(2\psi_E - \gamma_E)/dn + Z'/R - \alpha_E'] \geq -2\pi \quad . \tag{4.11}$$

This has the same significance as the constraint (3.24) or (3.30); it identifies surfaces in a given exterior geometry which are forbidden as matter/vacuum boundaries under the $\varepsilon \geq 0$ and nonsingularity assumptions. Surfaces for which (4.11) is violated are forbidden; the suitability of surfaces for which it is obeyed is undetermined. Although this condition, in contrast to that of Section III, has the disadvantage that it can only be applied to toroidal systems, it has the desirable feature that it can be evaluated using only exterior quantities, without further assumptions.

V. APPLICATION OF THE BOUNDARY CONSTRAINTS: A SPHERICAL-TOPOLOGY EXAMPLE

The boundary constraint derived in Section III can be examined by applying it to simple examples of Weyl exterior geometries. The simplest of these, in terms of the Weyl formalism, is the Curzon metric, for which the background-space source is a point monopole.[11] (This geometry is quite distinct from the Schwarzschild solution for a point monopole in the *physical* space; the Curzon geometry is not spherically symmetric.) Condition (3.43) may be applied to this geometry, but no particularly interesting results are obtained. A slightly more complicated set of Weyl geometries, those with a line source in the background

space, does reveal some important features of the constraint.

A. The Γ-Metrics

Specifically, the background source for these geometries is a line monopole, of linear density $\Gamma/2$, extending from $z_E=-a$ to $z_E=+a$ on the symmetry axis in the background space. This source is fictional; its linear density is the physical mass M of the system, measured at infinity, divided by its coordinate length, so that $\Gamma a=M$. Equation (3.3), the Laplace equation for ψ_E, is easily solved for such a source in prolate spheroidal coordinates (u,v,φ), related to the Weyl coordinates (ρ_E,z_E,φ) by $\rho_E=a\sinh u\sin v$, $z_E=a\cosh u\cos v$, with $u\in[0,+\infty)$, $v\in[0,\pi]$. In these coordinates the Weyl equations (3.3), (3.4), and (3.5) have the solution

$$\psi_E=\Gamma\log[\tanh(u/2)] \tag{5.1}$$

$$\gamma_E=-(\Gamma^2/2)\log\left[1+\frac{\sin^2 v}{\sinh^2 u}\right] \tag{5.2}$$

The resulting spacetime metric is[12]

$$\begin{aligned} ds_E^2=&-\tanh^{2\Gamma}(u/2)\,dt^2+\tanh^{-2\Gamma}(u/2)\left[1+\frac{\sin^2 v}{\sinh^2 u}\right]^{-\Gamma^2}[d\rho_E^2+dz_E^2] \\ &+\rho_E^2\tanh^{-2\Gamma}(u/2)\,d\varphi^2 \end{aligned} \tag{5.3}$$

$$\begin{aligned} =&-\tanh^{2\Gamma}(u/2)\,dt^2+(M/\Gamma)^2\sinh^2 u\tanh^{-2\Gamma}(u/2)\left[1+\frac{\sin^2 v}{\sinh^2 u}\right]^{1-\Gamma^2}[du^2+dv^2] \\ &+(M/\Gamma)^2\sinh^2 u\tanh^{-2\Gamma}(u/2)\sin^2 v\,d\varphi^2 \end{aligned}$$

The time-symmetric hypersurface Σ of concern here is given by any constant-t

hypersurface in this geometry.

The metric (5.3) describes a family of geometries parametrized by Γ. If $\Gamma=1$, so $a=M$, the geometry is just the Schwarzschild geometry[13]; the usual Schwarzschild coordinates (t,r,θ,φ) are related to the above (t,u,v,φ) coordinates by $r=2M\cosh^2(u/2)$, $\theta=v$. If $\Gamma\in(0,1)$, so $a>M$, the source is more elongated in the z-direction than in the spherical case; I term such geometries "prolate." Similarly, if $\Gamma\in(1,+\infty)$, $a<M$, the source is more compressed in the z-direction than in the spherical case; these geometries I label "oblate." In the limit $\Gamma\to+\infty$, $a\to0$, the Γ-metric becomes the Curzon metric.[13]

B. The Spherical-Topology Boundary Constraint

The surfaces of constant u in the Γ-metrics, equipotentials of ψ_E, provide a convenient one-parameter family of surfaces to which to apply the criterion (3.43). All the necessary quantities can be calculated from the metric (5.3) and the relations between (ρ_E,z_E) and (u,v). The $\mathcal{I}_1$-maximizing interior coordinate derivative $\mathcal{Z}_0'$, as per (3.40), is given by

$$\mathcal{Z}_0'=-\tanh^{\Gamma}(u/2)\left[1-\left(1+\frac{\sin^2 v}{\sinh^2 u}\right)^{\Gamma^2-1}\cos^2 v\right]^{1/2} . \tag{5.4}$$

This exists for all u if $\Gamma\le1$; if $\Gamma>1$, for small u the argument of the square root will be negative for v near 0 and π. I therefore apply criterion (3.43) only to the spherical (Schwarzschild) and prolate Γ-metrics. The functional $\mathcal{I}_1[\mathcal{Z}_0']$ of (3.43) takes the form

$$\mathcal{I}_1[\mathcal{Z}_0';u]=2M\{2-(\Gamma+1/\Gamma)\cosh u-(1/\Gamma-\Gamma)\sinh^2 u\log[\coth(u/2)]\}$$

$$+(M/\Gamma)\sinh u\int_0^{\pi}dv\left\{\sin^2 v\left[1+\frac{\sin^2 v}{\sinh^2 u}\right]^{\frac{\Gamma^2-3}{2}}\left[1+\frac{1-\Gamma^2\cos^2 v}{\sinh^2 u}\right]\left[1-\left[1+\frac{\sin^2 v}{\sinh^2 u}\right]^{\Gamma^2-1}\cos^2 v\right]^{-\frac{1}{2}}\right.$$

$$\left.+\left[1+\frac{\sin^2 v}{\sinh^2 u}\right]^{\frac{1-\Gamma^2}{2}}\left[1-\left[1+\frac{\sin^2 v}{\sinh^2 u}\right]^{\Gamma^2-1}\cos^2 v\right]^{+\frac{1}{2}}\right\}. \qquad (5.5)$$

The notation $\mathcal{I}_1[\mathcal{Z}_0';u]$ indicates that the functional $\mathcal{I}_1[\mathcal{Z}']$, evaluated at $\mathcal{Z}'=\mathcal{Z}_0'$, is a function of the u-value on the surface to be evaluated. Forbidden surfaces are those with $\mathcal{I}_1[\mathcal{Z}_0';u]<0$.

If $\Gamma=1$, the integral in (5.5) reduces to an elementary form; the resulting expression for $\mathcal{I}_1$ is

$$\mathcal{I}_1^{(S)}[\mathcal{Z}_0';u]=4M(1+\sinh u-\cosh u)=4M(1-e^{-u}) \qquad (5.6)$$

where the superscript (S) denotes the Schwarzschild case. This result means that for the Schwarzschild exterior geometry, none of the u=constant surfaces, with $u\geq 0$, are forbidden. That is, none of the surfaces of constant Schwarzschild radial coordinate r, with $r\geq 2M$, are forbidden. This is in accord with the existence of an exact interior solution which can be matched to the Schwarzschild exterior at any sphere of Schwarzschild radius $r\geq 2M$. Specifically, the Schwarzschild exterior four-geometry can be matched to a closed Friedmann interior geometry to describe an expanding or collapsing sphere of matter with uniform density and zero pressure.[14] At the moment of maximum expansion of the Friedmann interior, the geometry is momentarily static and time-symmetric; all of the hypotheses underlying the boundary constraint derivation apply here. The Schwarzschild coordinate radius of the matter/vacuum boundary at the moment of stasis can be freely chosen to be

any value $r \geq 2M$. The interior Friedmann metric on the hypersurface of time symmetry can be cast in the form (3.12), and the coordinates (ρ_I, z_I) can be chosen so that at the boundary surface ρ_I coincides with ρ_E of the Weyl coordinates for the Schwarzschild exterior. In that case one finds that $\gamma_I = 0$ holds throughout the interior, which means, as in Subsection III.E, that the interior coordinate derivative on the boundary, $\mathcal{Z}'$, coincides with the $\mathcal{I}_1$-maximizing function $\mathcal{Z}_0'$. That is, the $\mathcal{I}_1$-maximizing interior coordinate used to derive (5.6) actually occurs in the Friedmann/Schwarzschild system.

For prolate Γ-metrics, with $\Gamma < 1$, an analytic evaluation of the integral in (5.5) is not possible. It can, however, be studied with approximate and numerical calculations. I find that $\mathcal{I}_1$ has the limiting behavior

$$\lim_{u \to 0} \mathcal{I}_1[\mathcal{Z}_0'; u] = (2M/\Gamma)[-(1-\Gamma)^2 + B(1-\Gamma^2/2, 1-\Gamma^2/2)(u/2)^{\Gamma^2} + O(u^{2-\Gamma^2})] \qquad (5.7)$$

where B is the beta function. Thus at $u = 0$, $\mathcal{I}_1[\mathcal{Z}_0'; u]$ takes the value $-(2M/\Gamma)(1-\Gamma)^2$, which negative for all $\Gamma \in (0,1)$. The function $\mathcal{I}_1[\mathcal{Z}_0'; u]$ increases monotonically with u, approaching the limit $4M$ as $u \to +\infty$. Consequently in every prolate Γ-geometry there is a value u_0 such that $\mathcal{I}_1[\mathcal{Z}_0'; u_0]$ is zero, and $\mathcal{I}_1[\mathcal{Z}_0'; u]$ is negative for $u < u_0$, positive for $u > u_0$. If the higher order terms in u are neglected, equation (5.7) implies that the zero-crossing value u_0 is given by

$$u_0 = 2[(1-\Gamma)^2 / B(1-\Gamma^2/2, 1-\Gamma^2/2)]^{1/\Gamma^2} \quad . \qquad (5.8)$$

The neglect of the higher order terms is valid only if u is small and $2(1-\Gamma^2)$ is large; numerical calculations indicate that the fractional error in the value of u_0 given by (5.8) approaches 20% for Γ values near 1, is less than 1% for $\Gamma < 0.7$, and vanishes as $\Gamma \to 0$. By the boundary constraint (3.43), surfaces with $u < u_0$ are forbidden as boundary surfaces.

The constraint imposed by the condition $\mathscr{I}_1[\mathscr{Z}_0';u]\geq 0$ on u=constant boundary surfaces in the prolate Γ-metrics takes a simple form in the limit in which the background-space source is very large, i.e., the limit $a\to\infty$ or $\Gamma\to 0$. Equations (5.1) and (5.8) imply, in this limit,

$$\lim_{\Gamma\to 0}\psi_E(u_0)=-2+O(\Gamma) \quad . \tag{5.9}$$

Since ψ_E is a monotone increasing function of u, the boundary constraint $\mathscr{I}_1[\mathscr{Z}_0';u]\geq 0$, i.e., $u\geq u_0$, becomes equivalent to (3.37). This occurs because in the limit $\Gamma\to 0$, the "double match" of coordinates discussed in Subsection III.D is achieved; by equation (5.2), $\gamma_E\to 0$ as $\Gamma\to 0$, which means $\mathscr{Z}_0'\to Z'$ in that limit, as may also be seen directly.

C. Interpretation of the Boundary Constraint: Sizes and the Hoop Conjecture

The results of this example calculation indicate that the boundary constraints of Section III do not admit of interpretation as simple size constraints. The three simplest measures of the size of the u=constant surfaces in the Γ-geometries, consistent with axial symmetry, are the polar circumference $C_P=2\lambda_{\max}$, the equatorial circumference C_E, and the proper area A. These are given by

$$C_P(u)=(2M/\Gamma)\sinh^{\Gamma^2}u\tanh^{-\Gamma}(u/2)\int_0^{\pi}(\sinh^2u+\sin^2v)^{\frac{1-\Gamma^2}{2}}dv \quad , \tag{5.10}$$

$$C_E(u)=(2\pi M/\Gamma)\sinh u\tanh^{-\Gamma}(u/2) \quad , \tag{5.11}$$

$$A(u)=(2\pi M^2/\Gamma^2)\sinh^{1+\Gamma^2}u\tanh^{-2\Gamma}(u/2)\int_0^{\pi}(\sinh^2u+\sin^2v)^{\frac{1-\Gamma^2}{2}}\sin v\,dv \quad . \tag{5.12}$$

These equations show that in any prolate Γ-metric, for $u\ll 1$, C_P behaves as

$u^{\Gamma^2-\Gamma}$, C_E as $u^{1-\Gamma}$, and A as $u^{(1-\Gamma)^2}$. Thus as $u\to 0$, $C_P\to\infty$ while $C_E\to 0$ and $A\to 0$ in these prolate geometries.

The form of the boundary constraints of Section III suggests that these constraints might constitute lower bounds on C_P, i.e., that surfaces with C_P values less than some minimum might be forbidden. But among u=constant surfaces in a prolate Γ-metric, the forbidden surfaces are those with $0\le u<u_0$. Since $C_P\to\infty$ as $u\to 0$, the set of forbidden surfaces contains members with C_P values larger than any specified bound, larger than the C_P value of any given non-forbidden surface. Further, since $C_P\to\infty$ as $u\to 0$ and as $u\to\infty$, there exists a positive value of u, for $\Gamma<1$, at which $C_P(u)$ is a minimum. This is a property of the Γ-metric, without any reference to the boundary constraint. Numerical calculation reveals that u_0 is small compared to unity (e.g., $u_0<0.01$) for any value of Γ less than 1. Thus at u_0, C_P behaves as $u^{\Gamma^2-\Gamma}$; in particular, C_P is decreasing with increasing u. Therefore the minimum value of C_P must occur at a u-value greater than u_0, i.e., on a non-forbidden surface. The C_P values of the forbidden u=constant surfaces are bounded *below* by $C_P(u_0)$, given approximately by equations (5.8) and (5.10); neglecting higher order terms, I obtain

$$C_P(u_0)=(4M/\Gamma)[B(1-\Gamma^2/2,1-\Gamma^2/2)]^{1/\Gamma}(1-\Gamma)^{2-2/\Gamma} \quad . \tag{5.13}$$

There exists one forbidden and one non-forbidden u=constant surface having C_P equal to any given value greater than $C_P(u_0)$. These results appear to rule out any interpretation of the constraint (3.43) as a lower bound on C_P for acceptable boundary surfaces.

The other simple size measures for the u=constant surfaces, C_E and A, vanish at $u=0$ for $\Gamma<1$ and are monotone increasing with u. The condition $u\ge u_0$ for non-forbidden surfaces does put lower bounds on C_E and A for such surfaces, namely $C_E(u_0)$ and $A(u_0)$ respectively. Equations (5.8), (5.11), and (5.12), with

higher order terms neglected, give

$$C_E(u_0)=(4\pi M/\Gamma)[(1-\Gamma)^2/B(1-\Gamma^2/2,1-\Gamma^2/2)]^{\frac{1-\Gamma}{\Gamma^2}}\ , \tag{5.14}$$

$$A(u_0)=(16\pi M^2/\Gamma^2)B\left(\frac{3-\Gamma^2}{2},\frac{3-\Gamma^2}{2}\right)[(1-\Gamma)^2/B(1-\Gamma^2/2,1-\Gamma^2/2)]^{\frac{(1-\Gamma)^2}{\Gamma^2}}\ . \tag{5.15}$$

However these equations imply that both $C_E(u_0)\to 0$ and $A(u_0)\to 0$ as $\Gamma\to 0$. Thus given any positive lower bounds on C_E and A, there exists a prolate Γ-geometry with non-forbidden surfaces, according to (3.43), having C_E and A values smaller than those bounds. This indicates that condition (3.43) cannot be interpreted in general as a lower bound on C_E or A for acceptable boundary surfaces either.

Condition (3.43), as illustrated in this example, also does not appear to bear upon the hoop conjecture. The conjecture would place a lower bound on the largest circumference of allowed boundary surfaces, but the constraints of Section III serve to identify forbidden rather than allowed surfaces. If the Section III constraints placed an upper bound on the largest circumference of forbidden boundary surfaces, the result would support, though not prove, the conjecture. But as shown above, forbidden u=constant surfaces in prolate Γ-metrics can have arbitrarily large polar circumferences. In fact the example of u=constant surfaces in Γ-metrics does not even test the boundary constraints obtained here against the hoop conjecture; none has arbitrarily small circumference in every direction. Since the integral in (5.10) exceeds $\pi\sinh^{1-\Gamma^2}u$ for all $\Gamma<1$, C_P exceeds C_E for all u=constant surfaces in a prolate Γ-metric. Numerical calculations show that the minimum value of $C_P(u)$ decreases monotonically with increasing Γ, and therefore $C_P(u)$ for any prolate Γ-metric is bounded below by the Schwarzschild minimum $4\pi M$ (a similar result holds for the oblate, $\Gamma>1$, geometries, with the roles of C_P and C_E reversed). Consequently I have not been able to relate the $\mathscr{I}_1\geq 0$ boundary constraint to the hoop conjecture.

VI. AN EXAMPLE OF THE TOROIDAL-TOPOLOGY BOUNDARY CONSTRAINT

The toroidal boundary constraint (4.11) can also be examined by means of a simple example. One tractable toroidal exterior geometry has a ring source in the background space, given by $\rho_E=b$, $z_E=0$ in terms of the Weyl coordinates.[15] I shall call this exterior solution the "ring metric."

A. The Ring Metric

This geometry is most easily described using polar coordinates $(\tilde{r},\theta)$ centered on the ring, related to the Weyl cylindrical coordinates by $\rho_E=b+\tilde{r}\cos\theta$, $z_E=\tilde{r}\sin\theta$. The range of $\tilde{r}$ is from 0 to ∞; θ ranges from 0 to 2π if $\tilde{r}\leq b$. The coordinate φ is common to both systems. The solution to (3.3) and (3.6) for this system is

$$\psi_E=-(M/\pi)[m/(\rho_E b)]^{1/2}K(m) \tag{6.1}$$

where

$$m\equiv 4\rho_E b/[(\rho_E+b)^2+z_E^2]=4b(\tilde{r}\cos\theta+b)/[\tilde{r}^2+4b(\tilde{r}\cos\theta+b)] \tag{6.2}$$

and

$$K(m)=\int_0^{\pi/2}(1-m\sin^2\alpha)^{-1/2}d\alpha \tag{6.3}$$

is the complete elliptic integral of the first kind with parameter m. The solution to equations (3.4) and (3.5) for this function ψ_E is given by

$$\gamma_E=-[M^2m^2/(4\pi^2\rho_E b)][K^2(m)-4(1-m)K(m)\dot{K}(m)-4m(1-m)\dot{K}^2(m)]$$

$$-[M^2m^2/(4\pi^2b^2)][K^2(m)-4(1-m)K(m)\dot{K}(m)+4(1-m)(2-m)\dot{K}^2(m)] \tag{6.4}$$

where

$$\dot{K}(m)\equiv dK(m)/\,dm=\tfrac{1}{2}\int_0^{\pi/2}(1-m\sin^2\alpha)^{-3/2}\sin^2\alpha\,d\alpha\quad . \tag{6.5}$$

As before, M is the total mass of the system measured gravitationally at infinity.

The asymptotic forms of ψ_E and γ_E near the ring source ($\tilde{r}\to 0$) are useful for analyzing surfaces with condition (4.11). These forms are

$$\psi_E=-[M/(\pi b)]\{\log(8b/\tilde{r})-[\tilde{r}\cos\tilde{\theta}/(2b)]\log(8b/\tilde{r})+\tilde{r}\cos\tilde{\theta}/(2b)$$

$$+O[(\tilde{r}^2/b^2)\log(b/\tilde{r})]\} \tag{6.6}$$

$$\gamma_E=-[M^2/(4\pi^2b^2)]\{\cos\tilde{\theta}[4b/\tilde{r}-(\tilde{r}/b)\log^2(8b/\tilde{r})+(3\tilde{r}/b)\log(8b/\tilde{r})$$

$$-5\tilde{r}/(2b)]+2[\log^2(8b/\tilde{r})-2\log(8b/\tilde{r})+1]+O[(\tilde{r}^2/b^2)\log^2(b/\tilde{r})]\} \tag{6.7}$$

and are valid for $\tilde{r}\ll b$.

The three-metric of the Weyl exterior geometry for this solution is given by (3.2). In terms of the coordinates $(\tilde{r},\tilde{\theta},\varphi)$, this metric has the form

$$d\sigma_E^2=\exp\{2(\gamma_E-\psi_E)\}[d\tilde{r}^2+\tilde{r}^2d\tilde{\theta}^2]+\exp\{-2\psi_E\}(b+\tilde{r}\cos\tilde{\theta})^2\,d\varphi^2 \tag{6.8}$$

with ψ_E and γ_E as given above.

B. Application of the Boundary Constraint

The surfaces of constant $\tilde{r}$, $\tilde{r}\in(0,b)$, are a convenient family of surfaces to test as possible boundaries; equation (6.6) shows that these surfaces approach equipotentials of ψ_E as $\tilde{r}/b\to 0$, although they are not such in general. These surfaces cannot be tested by constraint (3.43); the necessary condition (3.41) for the existence of the $\mathscr{I}_1$-maximizing coordinate derivative $\mathscr{Z}_0'$ translates in this example into

$$\sin^2\tilde{\theta}\le\exp[2\gamma_E(\tilde{r},\tilde{\theta})]\qquad\forall\tilde{\theta}\in[0,2\pi] \tag{6.9}$$

Numerical calculations show this to be violated for every case I have examined. However these surfaces are ideal for testing with the constraint (4.11). All the necessary quantities can be calculated from the equations of Subsection VI.A. I label the left-hand side of (4.11) $\mathcal{I}_2$; it is given here by

$$\mathcal{I}_2(\tilde{r})=\int_0^{2\pi}\tilde{r}\,\partial(2\psi_E-\gamma_E)/\partial\tilde{r}\,d\tilde{\theta}+2\pi[(1-\tilde{r}^2/b^2)^{-1/2}-2] \tag{6.10}$$

where

$$\partial\psi_E/\partial\tilde{r}=[M/(2\pi)](m\rho_E b)^{-1/2}\{[(8\tilde{r}\rho_E b-4b\tilde{r}^2\cos\tilde{\theta})/(4\rho_E b+\tilde{r}^2)^2$$

$$+m\cos\tilde{\theta}/\rho_E]K(m)+2m\dot{K}(m)(8\tilde{r}\rho_E b-4b\tilde{r}^2\cos\tilde{\theta})/(4\rho_E b+\tilde{r}^2)^2\} \tag{6.11}$$

and

$$\partial\gamma_E/\partial\tilde{r}=[M^2/(4\pi^2 b)]\{(m\cos\tilde{\theta}/\rho_E^2)[K^2(m)-(1-m)L^2(m)]$$

$$+([2K(m)L(m)-(2-m)L^2(m)]/\rho_E+mL^2(m)/b)(8\tilde{r}\rho_E b-4b\tilde{r}^2\cos\tilde{\theta})/(4\rho_E b+\tilde{r}^2)^2\} \tag{6.12}$$

with

$$L(m)\equiv K(m)+2m\dot{K}(m) \tag{6.13}$$

and m as given by (6.2). Possible $\tilde{r}$=constant boundary surfaces must have $\mathcal{I}_2(\tilde{r})\geq-2\pi$; surfaces with $\mathcal{I}_2(\tilde{r})<-2\pi$ are forbidden.

Numerical calculations show that $\mathcal{I}_2(\tilde{r})$ increases monotonically with increasing $\tilde{r}/b$, with b fixed. A careful evaluation of equations (6.11) and (6.12) at $\tilde{r}=b$ shows that both $\partial\psi_E/\partial\tilde{r}$ and $\partial\gamma_E/\partial\tilde{r}$ are bounded at that limit; consequently the integral in (6.10) remains finite as $\tilde{r}\to b$. The second term diverges; thus

$$\lim_{\tilde{r}\to b} \mathcal{I}_2(\tilde{r}) = +\infty \quad . \tag{6.14}$$

The behavior of $\mathcal{I}_2$ in the limit $\tilde{r}\to 0$ can be determined using the asymptotic forms of ψ_E and γ_E, equations (6.6) and (6.7), or by expanding (6.11) and (6.12) in that limit. The resulting integral can be evaluated explicitly, with the result

$$\mathcal{I}_2(\tilde{r}) = 2\pi\{2M/(\pi b) - [M^2/(\pi^2 b^2)][\log(8b/\tilde{r}) - 1] - 1 + O(\tilde{r}^2/b^2)$$

$$+ O[(M/b)(\tilde{r}^2/b^2)\log(b/\tilde{r})] + O[(M^2/b^2)(\tilde{r}^2/b^2)\log^2(b/\tilde{r})]\} \tag{6.15}$$

for $\tilde{r} \ll b$. The three separate error terms are given because different error contributions dominate in different ranges of b/M values. This result implies

$$\lim_{\tilde{r}\to 0} \mathcal{I}_2(\tilde{r}) = -\infty \quad , \tag{6.16}$$

the limit taken at fixed b. Limits (6.14) and (6.16), plus the monotonicity of $\mathcal{I}_2(\tilde{r})$, show that for every ring geometry (every value of b), there exists a value $\tilde{r}_0 \in (0,b)$ at which $\mathcal{I}_2(\tilde{r}) = -2\pi$, with $\mathcal{I}_2 < -2\pi$ for $\tilde{r} < \tilde{r}_0$ and $\mathcal{I}_2 > -2\pi$ for $\tilde{r}$ between $\tilde{r}_0$ and b. Hence every ring geometry has a range of $\tilde{r}$=constant surfaces, viz., those with $\tilde{r} \in (0,\tilde{r}_0)$, which are forbidden as matter/vacuum boundaries by (4.11), and a range of such surfaces, with $\tilde{r} \in [\tilde{r}_0, b)$, not so forbidden. The value of $\tilde{r}_0$ can be obtained in the appropriate limit from equation (6.15); neglecting the error terms, I find

$$\tilde{r}_0 = 8b/\exp(1 + 2\pi b/M) \quad . \tag{6.17}$$

The approximation involved here is accurate for $\tilde{r}_0 \ll b, M$; because of the exponential in the denominator, this approximation is very good for $b \geq M$ and becomes arbitrarily accurate as b/M increases.

As in the example of Section V, the boundary constraint obtained in this calculation assumes a simple form in the limit of a large background-space source, which here means $b/M \to \infty$ (and there meant $\Gamma^{-1}=a/M \to \infty$). In this limit $\tilde{r}_0/b$ becomes very small so the surface $\tilde{r}=\tilde{r}_0$ becomes an equipotential of ψ_E. Then equations (6.6) and (6.17) imply

$$\lim_{b/M\to\infty} \psi_E|_{\tilde{r}=\tilde{r}_0} = -2 + O(M/b) \quad . \tag{6.18}$$

The function ψ_E increases outward from the ring "source," so in this limit the constraint $\tilde{r} \geq \tilde{r}_0$ on possible boundary surfaces becomes equivalent to (3.37). This is a somewhat serendipitous result, since (3.37) follows from the spherical-topology boundary constraint under the assumption that the interior coordinates are double-matched. The toroidal-topology constraint, however, does not specify or restrict the interior coordinates at all.

C. Interpretation of the Toroidal Constraint: Sizes and the Hoop Conjecture

Like the results of Section V, this toroidal example indicates that the boundary constraint (4.11) cannot be simply interpreted as a bound on surface size. The $\tilde{r}$=constant surfaces in the ring metrics have three simple size measures of interest, the meridian circumference λ_{max}, the outer equatorial circumference C_E^+ (defined as the circumference at θ=0), and the area A. These are given by

$$\lambda_{max}(\tilde{r}) = \int_0^{2\pi} \exp\{\gamma_E(\tilde{r},\theta) - \psi_E(\tilde{r},\theta)\}\tilde{r}\, d\theta \quad , \tag{6.19}$$

$$C_E^+(\tilde{r}) = 2\pi(b+\tilde{r})\exp\{-\psi_E(\tilde{r},\theta=0)\} \quad , \tag{6.20}$$

$$A(\tilde{r}) = 2\pi\int_0^{2\pi} \exp\{\gamma_E(\tilde{r},\theta) - 2\psi_E(\tilde{r},\theta)\}(b+\tilde{r}\cos\theta)\tilde{r}\, d\theta \quad , \tag{6.21}$$

where ψ_E and γ_E are given by (6.1) and (6.4), or (6.6) and (6.7) in the

appropriate limit. (The inner equatorial circumference C_E^-, that is, the equatorial circumference calculated at $\vartheta=\pi$, can also be obtained easily in a form like (6.20), but aside from the curious result that for certain values of b and $\tilde{r}$, $C_E^->C_E^+$, it provides little additional information). In the limit $\tilde{r}\ll b$, in which (6.6) and (6.7) are valid, the integrals in the above equations can be performed, giving

$$\lambda_{max}(\tilde{r})=2\pi\tilde{r}\exp\{[M/(\pi b)]\log(8b/\tilde{r})-[M^2/(2\pi^2b^2)][\log(8b/\tilde{r})-1]^2\}$$
$$\times I_0\{[M^2/(4\pi^2b^2)][4b/\tilde{r}-(\tilde{r}/b)\log^2(8b/\tilde{r})+(3\tilde{r}/b)\log(8b/\tilde{r})$$
$$-5\tilde{r}/(2b)]+[M/(\pi b)][\tilde{r}/(2b)][\log(8b/\tilde{r})-1]\}$$
$$\times\{1+O[(\tilde{r}^2/b^2)\log^2(b/\tilde{r})]\} \qquad (6.22)$$

$$C_E^+(\tilde{r})=2\pi(b+\tilde{r})\exp\{[M/(\pi b)][\log(8b/\tilde{r})-\tilde{r}/(2b)\log(8b/\tilde{r})+\tilde{r}/(2b)]\}$$
$$\times\{1+O[(\tilde{r}^2/b^2)\log(b/\tilde{r})]\} \qquad (6.23)$$

$$A(\tilde{r})=4\pi^2\tilde{r}\exp\{[2M/(\pi b)]\log(8b/\tilde{r})-[M^2/(2\pi^2b^2)][\log(8b/\tilde{r})-1]^2\}$$
$$\times(bI_0\{[M^2/(4\pi^2b^2)][4b/\tilde{r}-(\tilde{r}/b)\log^2(8b/\tilde{r})+(3\tilde{r}/b)\log(8b/\tilde{r})$$
$$-5\tilde{r}/(2b)]+[M/(\pi b)](\tilde{r}/b)[\log(8b/\tilde{r})-1]\}$$
$$-\tilde{r}I_1\{[M^2/(4\pi^2b^2)][4b/\tilde{r}-(\tilde{r}/b)\log^2(8b/\tilde{r})+(3\tilde{r}/b)\log(8b/\tilde{r})$$
$$-5\tilde{r}/(2b)]+[M/(\pi b)](\tilde{r}/b)[\log(8b/\tilde{r})-1]\})$$
$$\times\{1+O[(\tilde{r}^2/b^2)\log^2(b/\tilde{r})]\} \qquad (6.24)$$

where I_0 and I_1 are hyperbolic Bessel functions. As $\tilde{r}\to 0$ (with b fixed), equations (6.22) and (6.24) are dominated by the exponential behavior of I_0, while (6.23) is dominated by $\exp\{[M/(\pi b)]\log(8b/\tilde{r})\}$, so in this limit λ_{max}, C_E^+, and A

all diverge to $+\infty$.

This asymptotic behavior shows that the boundary constraint $\mathcal{I}_2 \geq -2\pi$, which in this example takes the form $\tilde{r} \geq \tilde{r}_0$, cannot be interpreted in general as identifying as forbidden surfaces with λ_{max}, C_E^+, or A values smaller than some lower bound. Every ring geometry contains forbidden $\tilde{r}$=constant surfaces with λ_{max}, C_E^+, and A values greater than any given bounds, greater than those values for any given non-forbidden surface. Thus for a boundary surface to have a size--as measured by λ_{max}, C_E^+, or A-- greater than some fixed bound is not equivalent to satisfying the constraint (4.11). In fact, numerical calculations show that in a wide range of ring geometries, the $\tilde{r}$=constant surfaces with the smallest values of λ_{max}, C_E^+, and A satisfy (4.11).

As $b/M \to \infty$, with $\tilde{r}/M$ fixed, $\lambda_{max}(\tilde{r})$ approaches the limit $2\pi\tilde{r}$. Thus $\tilde{r}$=constant surfaces exist in ring geometries with arbitrarily small values of λ_{max}, and since $\tilde{r}_0/M$ is dominated by the exponentially decreasing denominator of (6.17) in the $b/M \to \infty$ limit, ring geometries exist in which surfaces with arbitrarily small λ_{max} values are not forbidden by the toroidal boundary constraint.The constraint, therefore, does not imply a lower bound on λ_{max} for acceptable boundary surfaces. I cannot prove a similar result for the size measures C_E^+ and A using the ring geometries, however, because $\tilde{r}$=constant surfaces with arbitrarily small C_E^+ and A values do not exist in those geometries. Approximate and numerical calculations indicate that the A values for $\tilde{r}$=constant surfaces, for any b/M values, are bounded below by a value slightly in excess of $4M^2$. Similarly, C_E^+ values for these surfaces have a lower bound slightly greater than $18M$.

The above results indicate that the toroidal boundary constraint (4.11) is not directly connected with the hoop conjecture. Like the spherical-topology constraint, the inequality (4.11) serves to identify forbidden boundary surfaces

rather than to specify allowed ones; the hoop conjecture characterizes allowed surfaces. Also, the ring metric example shows that surfaces forbidden by (4.11) can have arbitrarily large circumferences, a result which, while not disproving the hoop conjecture, does not support it. Of course, like the Γ-metric calculation of Section V, the ring metric example does not actually test the hoop conjecture, since the $\tilde{r}$=constant surfaces examined all have circumferences (C_E^+) greater than a fixed bound of order M.

VII. EXTENSION OF THESE RESULTS

Some of the results of Sections III and IV can be applied to surfaces in a wider class of exterior geometries than the Weyl metrics. Specifically, the assumption of vacuum in the exterior can be relaxed. The spatial metric form (3.2) can be obtained in any axisymmetric, static exterior; the corresponding four-metric takes the form (3.1) only in special cases of this, including vacuum,[16] while the Weyl equations (3.3), (3.4), and (3.5) occur only for the vacuum case. The derivation of the spherical-topology boundary constraint, up to the inequality (3.24), depends only on the three-metric form (3.2); the Weyl vacuum field equations are used only in obtaining (3.30) from (3.24). Thus the spherical-topology constraint $\mathscr{I}_1[\mathscr{Z}']\geq 0$ can be applied to surfaces in any axisymmetric, static exterior geometry, provided $\mathscr{I}_1[\mathscr{Z}']$ is given by

$$\mathscr{I}_1[\mathscr{Z}']=\int_0^{\lambda_{\max}} d\lambda\{R[d(2\psi_E-\gamma_E)/d\eta-\alpha_E'+\alpha_I']+Z'-\mathscr{Z}'(1+\gamma_I)\} \qquad (7.1)$$

with all quantities defined as before, rather than by (3.30). The results (3.36) and (3.37) for the case of double-matched coordinates do not apply for non-vacuum exteriors, since these are derived from (3.30). The maximization of $\mathscr{I}_1$ with respect to $\mathscr{Z}'$ carried out in Subsection III.E can be performed in non-vacuum cases, however, since (3.24) has the same $\mathscr{Z}'$-dependence as (3.30). The

derivation of the toroidal-topology boundary constraint in Section IV never utilizes the Weyl field equations, so the constraint (4.11) can be applied in non-vacuum exteriors with no change.

It is thus possible to identify surfaces in arbitrary axisymmetric, static exterior geometries which are forbidden as boundaries of momentarily static, nonsingular matter systems by means of the inequalities (3.24) or (4.11), for either spherical or toroidal topology respectively. The usefulness of this generalization to non-vacuum exteriors is limited, however, by the fact that the exterior geometry, specifically the exterior coordinates and the potentials ψ_E and γ_E, must be known explicitly in order to evaluate the constraint inequalities. Consequently these constraints are likely to prove most useful for special exteriors, such as the Weyl vacuum geometries or electrovacuum generalizations thereof.

VIII. SUMMARY

Approaching the problem of boundary constraints for non-collapsing axisymmetric systems via the time-symmetric initial-value formalism, I have here obtained the two geometric conditions $\mathscr{I}_1 \geq 0$ and $\mathscr{I}_2 \geq -2\pi$ for spherical and toroidal topologies respectively, where $\mathscr{I}_1$ is given by the left side of (3.24) or (3.30), and $\mathscr{I}_2$ is given by the left side of (4.11). Both of these constraints identify surfaces in given exterior geometries which are forbidden as boundaries of momentarily static, nonsingular matter systems, i.e., surfaces for which the derived inequalities are violated are so forbidden. Applied to specific examples using as exterior geometries the prolate Γ-metrics and the toroidal ring metrics, these constraints define neighborhoods of the Weyl singularities within which the surfaces examined are forbidden; i.e., the constraints require that the surfaces of momentarily static material bodies giving rise to these exterior geometries

lie outside the delineated neighborhoods.

I have not been able to cast these boundary constraints in any form suggestive of bounds on surface size. Further, the results of the example calculations of Sections V and VI are not in accord with any interpretation of the constraints as limits on boundary circumference or area. Consequently these constraints do not in any obvious way embody or support the hoop conjecture. Neither do my results disprove the conjecture: since none of the source-surrounding surfaces in the geometries I have examined have circumferences much smaller than $4\pi M$ in all directions, no counterexample to the hoop conjecture could be found. Apparently the quantities $\mathscr{I}_1$ and $\mathscr{I}_2$ appearing in the constraint inequalities describe geometric properties of momentarily static axisymmetric systems, as constructed here, distinct from boundary size; my results show that these properties do impose limits on the construction of such systems. I have not succeeded in formulating an intuitive interpretation of these properties; perhaps their meaning can be clarified by further researches and by studying the application of these constraints to more examples of Weyl exterior geometries.

The initial-value formalism used here might prove useful in other investigations of size constraints and the hoop conjecture. Manipulations of the initial-value equation and junction conditions different from those I employed in Sections III and IV might yield different results and constraints, perhaps ones readily related to system size and to the hoop conjecture. It is also possible that results germane to the hoop conjecture might be obtained directly from the vacuum, static Einstein field equations, or from the Weyl form of those equations given in Subsection III.A. The fact that all source-surrounding surfaces in the Weyl geometries I have studied here have largest circumferences exceeding a limit of order M lends support to this possibility.

ACKNOWLEDGEMENTS

I wish to thank Professor Kip S. Thorne, who introduced me to this problem and provided many valuable ideas and suggestions.

This work was supported in part by the National Science Foundation via Grant AST79-22012. The author received support from a National Science Foundation Predoctoral Fellowship during part of the period in which this research was conducted, and from a J. S. Fluor Graduate Fellowship during another part.

APPENDIX A: EXISTENCE OF ISOTHERMAL INTERIOR COORDINATES

The uniformization theorem for simply connected Riemann surfaces states that a simply connected Riemann surface is conformally equivalent to (i.e., there exists a bijective function, analytic in the local complex coordinates on the Riemann surface, from that surface onto) exactly one of the following: the extended complex plane $\mathbf{C}\cup\{\infty\}$, the complex plane $\mathbf{C}$, or the unit disk $\Delta=\{z\in\mathbf{C}: |z|<1\}$, according as the surface is elliptic, parabolic, or hyperbolic respectively.[17] A Riemann surface is elliptic if it is compact (closed), hyperbolic if it is noncompact and carries a negative nonconstant subharmonic function, and parabolic if it is noncompact but carries no such function. Further, any simply connected domain in the extended complex plane which omits two or more points of $\mathbf{C}\cup\{\infty\}$ is hyperbolic.[18] Of interest here is the application of the uniformization theorem to the two-surface $\mathcal{M}=I|_{\varphi=\varphi_0}$, a φ=constant slice of the interior, to establish the existence of a single patch of isothermal coordinates covering all of $\mathcal{M}$, and thus a single patch of coordinates for I in which the metric has the form (3.12) or (4.1).

The nonsingularity assumption made here implies the existence of a C^1 two-metric[19] on $\mathcal{M}$. This, in turn, implies the existence of local C^1 isothermal

coordinates[20] in neighborhoods of all points of $\mathcal{M}$. Where two such coordinate patches, say (x,y) and (u,v), overlap, they must be related by the Cauchy-Riemann equations, hence $u \pm iv$ must be an analytic function of $x+iy$; that is, the local isothermal coordinates impart a Riemann-surface structure to $\mathcal{M}$. Let $\mathcal{N}=\Sigma|_{\varphi=\varphi_0}$ be a constant-φ slice of the entire hypersurface of time symmetry (interior I and exterior E). By the above arguments, $\mathcal{N}$ is also a Riemann surface. I assume that $\mathcal{N}$, like $\mathcal{M}$, is simply connected; the uniformization theorem then guarantees that $\mathcal{N}$ is conformally equivalent to some domain in $\mathbf{C}\cup\{\infty\}$. The function establishing this conformal equivalence maps $\mathcal{M}\subset\mathcal{N}$ into some subdomain of this; since $\mathcal{M}$ omits more than two points of $\mathcal{N}$ and the function is bijective, the image of $\mathcal{M}$ omits more than two points of $\mathbf{C}\cup\{\infty\}$ and is therefore hyperbolic. Consequently $\mathcal{M}$ is hyperbolic and conformally equivalent to the unit disk Δ and to any hyperbolic domain of $\mathbf{C}\cup\{\infty\}$. The functions on $\mathcal{M}$ establishing these equivalences are analytic in $x+iy$ for all local isothermal coordinates (x,y), so they preserve the isothermal form of the metric and provide the desired global isothermal coordinate patches on $\mathcal{M}$.

The interior coordinates (ρ_I,z_I) can be taken to fill any hyperbolic domain in the extended complex plane. For example, for a toroidal interior a unit disk translated into the right half plane, i.e., $\{z\in\mathbf{C}: z=a+re^{i\theta}, a>1, 0\le r<1, 0\le\theta\le 2\pi\}$, or simply the unit disk Δ (if the metric form (4.1) is used so that the restriction $\rho_I>0$ is not required), might be a convenient choice. Let $f:\mathcal{M}\to\Delta$ be the conformal map establishing these interior coordinates, neglecting the translation by a. Then f maps the boundary meridian $\partial\mathcal{M}$ onto the unit circle. Results from the mathematical theory of conformal representation serve to establish the regularity of this coordinate map at the boundary. Specifically, if $R\subset\mathbf{C}$ is a simply connected domain and $P\in\partial R$ a frontier point of R such that it is possible to construct two circles through P, one entirely inside R and one entirely outside, and

if $g: R \to \Delta$ is a conformal map of R into the unit disk, then as z approaches P in R, the derivative $g'(z)$ tends to a unique, finite, nonzero limit.[21] Here P is a boundary meridian point; let $N(P)$ be a local (isothermal) coordinate neighborhood of P on the φ=constant surface $\mathcal{N}$. I take R to be (the local-coordinate image of) $N(P) \cap \mathcal{M}$ and g to be the global coordinate map f composed with the local coordinate map on $N(P)$. The quoted theorem implies that the derivative of f is nonvanishing--the interior coordinates are regular--at any meridian point P at which the tangent vector $d/d\lambda$ is continuous. Most importantly, this means that $d\theta/d\lambda$, the derivative of coordinate polar angle with respect to meridian proper length, does not vanish anywhere on a C^1 or smoother meridian; the length λ and coordinate angle θ are monotonic functions of each other.

Similar conclusions obtain for spherical-topology interiors, except that for this case $\partial\mathcal{M}$ has "corners" where the meridian meets the symmetry axis. If a unit disk is chosen as the range of the interior coordinates, the coordinate map f must behave as $(z-z_0)^2$, in terms of a local complex coordinate z, in the vicinity of such a corner (at z_0), in order to convert the right angle of the corner into a straight angle on the unit circle. It is convenient to compose such a coordinate function with a function such as

$$\zeta(w) = -i\frac{[-i(w+1)/(w-1)]^{1/2}-1}{[-i(w+1)/(w-1)]^{1/2}+1} \quad , \; w \in \Delta \tag{A1}$$

which, using the principal branch of the square root, maps the unit disk bijectively onto the right half of the unit disk. The points $w=\pm 1$ are mapped to the corners $\zeta=\mp i$, the square root behavior of $\zeta(w)$ there converting straight angles to right angles. The composition of f as above, a Möbius transformation on the unit disk if needed to position the corner points, and the function ζ gives a conformal map of $\mathcal{M}$ onto the right half of the unit disk, providing isothermal interior coordinates appropriate to the spherical-topology case. These coordinates

are regular at all boundary points, the square root behavior of ζ at the corner points cancelling the square behavior of f there.

APPENDIX B: INJECTIVITY OF MATCHED INTERIOR COORDINATES

The existence of isothermal interior coordinates, the first of which matches the corresponding exterior Weyl coordinate (ρ_E) at the boundary, hinges on the injectivity of the analytic function $\tilde{\rho}_I+i\tilde{z}_I:\mathcal{M}\to\mathbf{C}$ defined by the stipulation that the real part $\tilde{\rho}_I$ is a harmonic function on $\mathcal{M}$ with boundary values $\tilde{\rho}_I=\rho_E$ on the boundary meridian and, in the spherical-topology case, $\tilde{\rho}_I=0$ on the symmetry axis. Alternatively, the function $\tilde{\rho}_I+i\tilde{z}_I$ can be regarded as an analytic function on the domain $D\subset\mathbf{C}$ occupied by some global isothermal interior coordinates (ρ_I,z_I), with the boundary values for $\tilde{\rho}_I$ appropriately mapped from $\partial\mathcal{M}$ to ∂D. By the results of Appendix A, D may without loss of generality be taken to be the unit disk Δ for the toroidal-topology case, or the right half thereof, $\Delta_+\equiv\{z\in\Delta:\ \mathrm{Re}z>0\}$, for the spherical-topology case.

The number of times an analytic function takes on a given value in its range can be counted by examining its behavior on the boundary of its domain. Let $\mathcal{D}\subset\mathbf{C}$ be a domain bounded by a simple closed curve $\mathcal{C}$, and let $w=f(z)$ be an analytic function regular in $\mathcal{D}$ and on $\mathcal{C}$; further let $\mathcal{C}'$ be the image of $\mathcal{C}$ under f, and suppose z_0 is a point in $\mathcal{D}$ with $f(z_0)$ not on $\mathcal{C}'$. Then the quantity

$$[1/(2\pi)]\Delta_{\mathcal{C}}\arg\{f(z)-f(z_0)\}=[1/(2\pi i)]\oint_{\mathcal{C}} d\log\{f(z)-f(z_0)\}\quad , \tag{B1}$$

where $\Delta_{\mathcal{C}}$ denotes variation around $\mathcal{C}$, equals the number of zeroes of $f(z)-f(z_0)$ in $\mathcal{D}$, a positive integer since z_0 is in $\mathcal{D}$. But this integral is equal to

$$[1/(2\pi i)]\oint_{\mathcal{C}'}[1/(w-w_0)]\,dw=[1/(2\pi)]\Delta_{\mathcal{C}'}\arg(w-w_0)\quad , \tag{B2}$$

which is just the number of times the curve $\mathcal{C}'$ encircles the point $w_0=f(z_0)$,

i.e., the number of times the point $f(z)$ circles w_0 as z is moved once around the curve $\mathscr{C}$. In particular, f is injective in $\mathscr{D}$ if $\mathscr{C}'$ is simple, i.e., unless the curve $\mathscr{C}'$ is traced multiple times by $f(z)$ as z circles $\mathscr{C}$ once or $\mathscr{C}'$ loops inside itself.[22]

Thus the image of ∂D under the map $\tilde{\rho}_I+i\tilde{z}_I$ reveals whether the matched interior coordinate function is injective. The complete image depends on the interior geometry, but the first coordinates of the image points are given by the boundary conditions on $\tilde{\rho}_I$. If the exterior radial coordinate on the meridian, $R(\lambda)$, has a single local maximum, then the image curve under the matched-coordinate map cannot be traced multiple times, nor can it loop inside itself. Consequently for $R(\lambda)$ to have a single local maximum is a sufficient condition for the injectivity of the matched-coordinate map $\tilde{\rho}_I+i\tilde{z}_I$, and thus for the existence of the matched coordinates described in Subsection III.C. It may be noted that this condition obtains in the examples discussed in Section V, where matched interior coordinates are assumed.

APPENDIX C: GLOBAL MAXIMALITY OF $\mathscr{I}_1[\mathscr{F}_0']$

In cases where the conditions for the existence and maximality of the $\mathscr{I}_1$-maximizing interior coordinate derivative $\mathscr{F}_0'$, described in Subsection III.E, are satisfied, the question whether $\mathscr{F}_0'$ gives a global (in the space of functions $\mathscr{F}'$) or just a local maximum of $\mathscr{I}_1$ can be examined by reducing the variational problem to a collection of maximization problems in one real variable. Let $\eta(\lambda)$ be a C^1 function on $[0,\lambda_{max}]$ with appropriate end-point values. If I take $\mathscr{F}'=\mathscr{F}_0'+q\eta$ then the functional $\mathscr{I}_1[\mathscr{F}']$ becomes a function of the variable q, a different function for each η, which I denote $\mathscr{I}_1(q;\eta)$. The variational problem with respect to $\mathscr{F}'$ is equivalent to the one-variable maximization problem with respect to q, considered for all possible functions η. In particular, $\mathscr{F}_0'$ gives a

global maximum of $\mathscr{I}_1[\mathscr{Z}']$ if and only if $q=0$ gives a global (over the domain of q) maximum of $\mathscr{I}_1(q;\eta)$ for every possible η.

The derivatives of $\mathscr{I}_1(q;\eta)$ are given by expressions similar to (3.38) and (3.39):

$$d\mathscr{I}_1(q;\eta)/dq=\int_0^{\lambda_{max}}\{\tfrac{1}{2}\log[R'^2+(\mathscr{Z}_0'+q\eta)^2]-\psi_E\}\eta\,d\lambda \tag{C1}$$

$$d^2\mathscr{I}_1(q;\eta)/dq^2=\int_0^{\lambda_{max}}\{(\mathscr{Z}_0'+q\eta)/[R'^2+(\mathscr{Z}_0'+q\eta)^2]\}\eta^2\,d\lambda \tag{C2}$$

The choice of $\mathscr{Z}_0'$, equation (3.40), ensures $d\mathscr{I}_1/dq=0$ at $q=0$ for every η, and if the topology of the system imposes $\mathscr{Z}_0'\le 0$ on the entire meridian, then $d^2\mathscr{I}_1/dq^2<0$ holds at $q=0$ for every η, so $\mathscr{Z}'=\mathscr{Z}_0'$ or $q=0$ is a local maximum of $\mathscr{I}_1$. It remains to be shown whether, for any particular η, there exist any other local (in q) maxima with larger values of $\mathscr{I}_1$ than $\mathscr{I}_1(0;\eta)$ or $\mathscr{I}_1$ takes on values larger than $\mathscr{I}_1(0;\eta)$ at the boundaries of the domain of q.

I have not been able to resolve these questions. A principal difficulty is delineating the domain of q, given η, i.e., characterizing the set of functions $\mathscr{Z}'$ which are possible second-coordinate derivatives for some interior geometry. If, for example, $\mathscr{Z}'\le 0$ on the entire meridian (by (3.15), this is equivalent to $d\rho_I/dn\ge 0$ on the entire meridian) holds for any admissible interior second coordinate, with matched first coordinate, then $d^2\mathscr{I}_1/dq^2<0$ holds on the entire domain of q for any η. If the domain of q is connected, this implies that $q=0$ is a global maximum for any η, hence that $\mathscr{Z}'=\mathscr{Z}_0'$ is a global maximum. The sufficient condition $\mathscr{Z}'\le 0$ is guaranteed if α_I', defined by (3.17), is required to be nonnegative, provided $R'>0, \mathscr{Z}'=0$ at $\lambda=0$, $R'<0, \mathscr{Z}'=0$ at $\lambda=\lambda_{max}$, and the matched interior coordinates are injective, so the interior coordinate image of the meridian does not "loop," as discussed in Appendix B. For these conditions imply $\tan^{-1}(\mathscr{Z}'/R')\in[-\pi,0]$, which precludes $\mathscr{Z}'>0$. I have not succeeded,

however, in establishing these or any other sufficient conditions for the global maximality of $\mathcal{F}_0'$ in general, nor in finding any constraints on exterior quantities under which such conditions obtain. The question of global maximality remains open; I assume it in applying the results of Subsection III.E.

APPENDIX D: THE INTEGRAL OF α_I' FOR TOROIDAL GEOMETRIES

It is easily shown that

$$\int_0^{\lambda_{max}} \alpha_I' d\lambda \equiv -\int_0^{\lambda_{max}} \frac{P'\mathcal{F}''-\mathcal{F}'P''}{P'^2+\mathcal{F}'^2} d\lambda = 2\pi \tag{D1}$$

holds for any toroidal geometry, with arbitrary nonsingular interior and with $P(\lambda)$and$\mathcal{F}(\lambda)$ the meridian values of any choice of isothermal interior coordinates. First, rearranging equation (4.10) gives

$$\int_0^{\lambda_{max}} \alpha_I' d\lambda = [1/(2\pi)] \int_I d^3V e^{-\beta}[8\pi\varepsilon+(\nabla\beta)^2] - \int_0^{\lambda max} d\lambda \, \mathrm{Tr}\mathbf{S}_E \tag{D2}$$

Everything on the right side of this equation is gauge invariant, i.e., invariant under conformal transformations of the interior coordinates, so the integral of α_I' over the meridian is likewise invariant. It can therefore be evaluated directly by making a convenient choice of interior coordinates. By the results described in Appendix A, the interior coordinates may be chosen to fill the unit disk, so that $P(\lambda)=\cos[\theta(\lambda)]$, $\mathcal{F}(\lambda)=\sin[\theta(\lambda)]$, with the polar angle θ a monotonic function of λ. Substituting these into the definition of α_I', I obtain

$$\int_0^{\lambda_{max}} \alpha_I' d\lambda = -\int_{2\pi}^{0} d\theta = +2\pi \tag{D3}$$

which is the desired result. The orientation of the end point values of $\theta(\lambda)$ is determined by the stipulation that (3.15) give the outward-directed normal

vector, which requires $d\theta/d\lambda<0$.

A similar result does not obtain for the integral of α_E'. In the ring-metric example of Section VI, the integral of α_E' over the meridian does equal 2π. In Thorne's[8] toroidal exterior solution, however, there are closed curves, candidates for boundary meridians, which are curves of constant ρ_E; the integral of α_E' over such curves is zero. Thus it is necessary to evaluate the integral of α_E' explicitly in each individual case.

REFERENCES

[1]R. D. Blandford and K. S. Thorne, in *General Relativity: An Einstein Centenary Survey*, edited by S. W. Hawking and W. Israel (Cambridge University Press, Cambridge, 1979), pp. 456-457.

[2]K. S. Thorne, in *Magic Without Magic: John Archibald Wheeler*, edited by J. R. Klauder (W. H. Freeman, San Francisco, 1972), pp. 231-258.

[3]C. W. Misner, K. S. Thorne, and J. A. Wheeler, *Gravitation* (W. H. Freeman, San Francisco, 1973), pp.867-868.

[4]D. R. Brill, Ann. Phys. (NY) 7 , 466-483 (1959).

[5]H. Weyl, Ann. Phys. (Leipzig) 54 , 117-145 (1918).

[6]W. Israel, Phys. Rev. 164 , 1776-1779 (1967).

[7]R. Geroch and J. B. Hartle, J. Math. Phys. (NY) 23 , 680-693 (1982).

[8]K. S. Thorne, J. Math. Phys. (NY) 16 , 1860-1865 (1975).

[9]C. W. Misner, K. S. Thorne, and J. A. Wheeler, *Gravitation* (W. H. Freeman, San Francisco, 1973), pp. 551-554.

[10]C. W. Misner, K. S. Thorne, and J. A. Wheeler, *Gravitation* (W. H. Freeman, San Francisco, 1973), p. 452.

[11]H. E. J. Curzon, Proc. London Math. Soc. 23 , 477-480 (1924).

[12]D. Papadopoulos, B. Stewart, and L. Witten, Phys. Rev. D 24 , 320-326 (1981).

[13]B. H. Voorhees, in *Methods of Local and Global Differential Geometry in General Relativity*, edited by D. Farnsworth, J. Fink, J. Porter, and A. Thompson (Springer Verlag, New York, 1970), pp. 138, 140.

[14]C. W. Misner, K. S. Thorne, and J. A. Wheeler, *Gravitation* (W. H. Freeman, San Francisco, 1973), pp. 851-856.

[15]R. Bach and H. Weyl, Math. Z. 13 , 134-145 (1922).

[16]J. L. Synge, *Relativity: The General Theory* (North Holland, Amsterdam, 1966), pp. 309-317.

[17]H. M. Farkas and I. Kra, *Riemann Surfaces* (Springer Verlag, New York, 1980), p. 180.

[18]H. M. Farkas and I. Kra, *Riemann Surfaces* (Springer Verlag, New York, 1980), p. 181.

[19]J. L. Synge, *Relativity: The General Theory* (North Holland, Amsterdam, 1966), pp. 1-2.

[20]M. Spivak, *A Comprehensive Introduction to Differential Geometry, Volume IV* (Publish or Perish, Inc., Berkeley, 1979), pp. 455-500.

[21]C. Caratheodory, *Conformal Representation* (Cambridge University Press, Cambridge, 1952), pp. 96-97.

[22]E. C. Titchmarsh, *The Theory of Functions*, 2nd ed. (Oxford University Press, London, 1939), p. 201.

Figure Caption

FIG. 1. Possible boundary and interior geometries, illustrated in exterior (Weyl) coordinate space. The configuration of the vectors $d/d\lambda$, d/dn, and the angle $\alpha(\lambda)$ appears the same whether these quantities are defined from the interior (I) or the exterior (E).

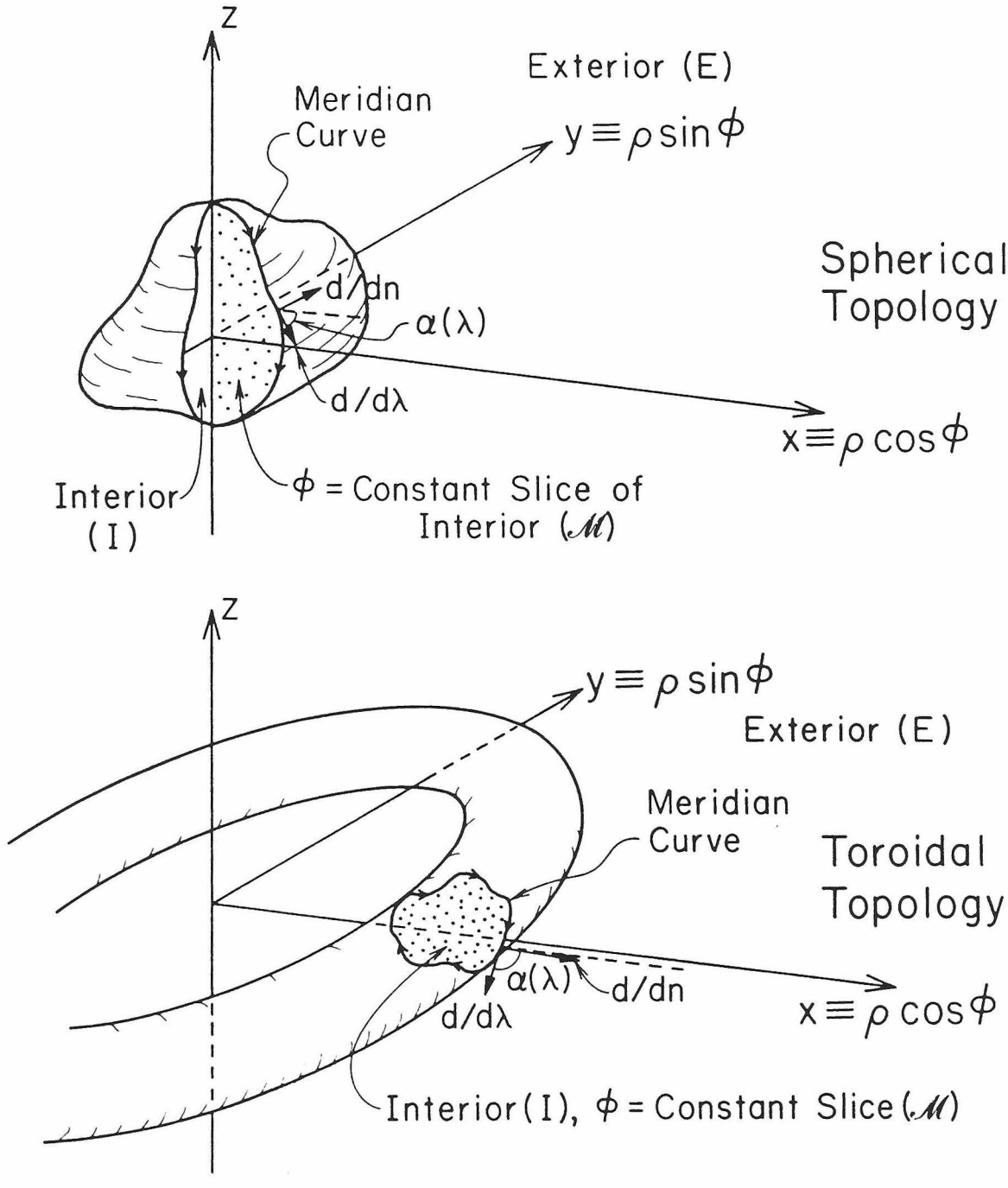
z
Exterior (E)
Meridian
Curve
$y \equiv \rho \sin\phi$
Spherical
Topology
d/dn
$\alpha(\lambda)$
d/dλ
$x \equiv \rho \cos\phi$
Interior
(I)
ϕ = Constant Slice of
Interior ($\mathcal{M}$)
z
$y \equiv \rho \sin\phi$
Exterior (E)
Meridian
Curve
Toroidal
Topology
$\alpha(\lambda)$
d/dn
d/dλ
$x \equiv \rho \cos\phi$
Interior(I), ϕ = Constant Slice ($\mathcal{M}$)

FIG. 1

PART TWO: TIDAL DISTORTIONS OF A SCHWARZSCHILD BLACK HOLE

Tidal Distortions of a Schwarzschild Black Hole

Ian H. Redmount

Theoretical Astrophysics 130-33
California Institute of Technology
Pasadena, California 91125

ABSTRACT

This paper examines the tidal distortions of a Schwarzschild black hole by static point masses ("moons") suspended on ropes above the horizon. A solution of the Einstein field equations for the hole plus moons is constructed, using the Weyl formalism for static, axisymmetric, vacuum geometries. This solution accounts for the masses of the moons and hole, the binding energy of the system, and the mass density and tension in the suspending "ropes" in a mutually consistent manner.

Various features of the tidal deformation of the hole are extracted from the solution: The intrinsic geometry of the distorted horizon is obtained; embedding diagrams representing the shape of the horizon and of the tidal bulges raised on it are calculated for both weak and strong perturbations; and the components of the Riemann curvature tensor measured in the orthonormal frame of a static observer near the horizon are also calculated.

These results corroborate the findings of other calculations of static black-hole tides: The horizon intrinsic geometry obtained here agrees with the results of a previous calculation by Hartle in the limit of moons far from the horizon. In the opposite limit of moons very close to the horizon, this solution approaches that of a

calculation by Price and Suen in which the Schwarzschild horizon is approximated by the flat horizon of Rindler space. Thus this calculation confirms the validity of the Rindler approximation to the Schwarzschild geometry for calculating the tidal effects of strong static perturbations, and provides support for the extension of that approximation to dynamical black-hole tides.

I. INTRODUCTION

In recent years much interest has centered on the study of black holes as real physical objects, and on the mechanics of their interactions with other physical systems. Tidal effects on black holes, a manifestation of the gravitational interaction between black holes and external bodies, are of particular interest. Such effects are expected to play a major role in the behavior of black holes in astrophysical contexts. The exchange of angular momentum between a rotating black hole and surrounding matter is affected by the behavior of black hole tides.[1,2,3,4] Tidal distortion should also contribute to the properties of black holes as sources of gravitational radiation. And tidal effects are potentially important (though thus far ignored) in *gedanken* experiments used to elucidate the quantum statistical mechanics of black holes and of the thermal (Hawking) radiation they emit. (Recent work by Unruh and Wald[5] and Bekenstein[6] on this subject involves hypothetical interactions between a black hole and "machines" lowered to and raised up from the vicinity of the hole's horizon. Such machines would produce tides on the horizon, which would alter these interactions in ways yet to be determined.)

The aim of this paper is to develop insight into the phenomenon of tidal distortion of a black hole by examining in great detail a simple case, and thus to provide a basis for future, more complex calculations. Several researchers have previously studied tidal distortion of black holes in a variety of contexts and with various methods. Hartle[1,2] and Hartle and Hawking[3] have calculated the effects of tidal perturbations on slowly rotating black holes and obtained results describing the shapes of tidal distortions produced and the rate of change of the black hole's angular momentum due to tidal friction. Teukolsky[4] has extended these tidal-friction results to rapidly rotating holes. Geroch and Hartle[7] have constructed the complete class of static, axisymmetric, distorted black hole

solutions, and examined some of the mathematical and physical properties of these solutions. The model solution for a tidally distorted black hole studied in this paper is a special case of the Geroch-Hartle solutions.

The study described in this paper was undertaken as part of a program of research into black-hole physics in collaboration with K. S. Thorne, R. H. Price, R. J. Crowley, W. H. Zurek, D. A. Macdonald, W.-M. Suen, M. Mijic, L. S. Finn, and X.-H. Zhang. This program aims to develop a general formalism for analyzing black-hole dynamics, which entails regarding the horizon as a time-evolving surface or membrane in three-space endowed with physical properties, e.g., electrical conductivity and shear viscosity. This membrane formalism has proved especially useful for treating electrodynamic processes involving black holes,[8,9] and the present paper is part of an effort to extend the formalism to gravitational processes. Suen and Price[10] have studied examples of static and dynamical tidal distortions of a horizon "viewed up close," using the planar horizon in Rindler space as an approximation to the curved horizon of a Schwarzschild hole. The reliability of their results, however, hinges on the initially untested validity of that Rindler approximation. The calculations of this paper generalize the work of Suen and Price, in the static case, to a complete, curved, Schwarzschild horizon--and lend support to their conclusions by substantiating the Rindler approximation.

The procedure used here is to model a simple physical situation featuring tidal distortion of a black hole: that of a Schwarzschild black hole perturbed by bodies fixed on the polar axis of the hole outside the horizon. This situation is static, axisymmetric, and vacuum except for the hole and the perturbing masses, making it possible to describe the spacetime geometry corresponding to this configuration by means of the Weyl formalism of general relativity.[11] The effects of black-hole tidal distortion are explored by examining the Weyl solution

obtained, and the results are compared to those of a variety of other calculations on black-hole tides. The general Weyl formalism and the solution obtained from it for the perturbed black hole are presented in Section II below. The intrinsic geometry of the distorted horizon is explored in Section III; Section IV contains a discussion of the various definitions of the masses of the hole and perturbing bodies and a discussion of the role of binding energy in the solution. In Section V the Riemann curvature tensor for the spacetime geometry in the vicinity of the distorted horizon is calculated, for purposes of comparison with other tidal-curvature calculations.

The solution obtained here succeeds in illustrating a number of aspects of the effects of tidal perturbations on a black hole, in the static limit. It yields expressions for the shape of the horizon with tides both for weak perturbations [equations (3.8), (3.14), and (3.33)] and for strong ones [equation (3.31)]. These agree with the results of other calculations in special limits: that of Hartle[1] for distant perturbing bodies and that of Suen and Price[10] in Rindler space, for bodies near the horizon. This solution provides a consistent account of the masses involved in the configuration, and of the relations among the masses measured locally, the masses measured at infinity, and the gravitational binding energy of the system. Finally, the solution gives values for the tidal Riemann-curvature components of the geometry near the horizon, which can also be compared with the results of the equivalent calculation in Rindler space; again, complete agreement is obtained.

II. GEOMETRY OF A SCHWARZSCHILD BLACK HOLE WITH TIDAL DISTORTIONS

A. General Formalism

Axisymmetric, static, vacuum solutions of the Einstein field equations can be described by the Weyl formalism.[11] This formalism uses coordinates (t,ρ,z,φ) in which the metric takes the form

$$ds^2 = -e^{2\psi(\rho,z)}dt^2 + e^{2[\gamma(\rho,z)-\psi(\rho,z)]}(d\rho^2+dz^2) + \rho^2 e^{2\psi(\rho,z)}d\varphi^2 \quad . \tag{2.1}$$

The vacuum Einstein equations in these coordinates reduce to

$$\partial^2\psi/\partial\rho^2 + (1/\rho)\partial\psi/\partial\rho + \partial^2\psi/\partial z^2 = 0 \quad , \tag{2.2}$$

$$\partial\gamma/\partial\rho = \rho[(\partial\psi/\partial\rho)^2-(\partial\psi/\partial z)^2] \quad , \tag{2.3}$$

$$\partial\gamma/\partial z = 2\rho(\partial\psi/\partial\rho)(\partial\psi/\partial z) \quad . \tag{2.4}$$

Equation (2.2) implies that ψ is a harmonic function in a fictitious Euclidean "background" space with cylindrical coordinates (ρ,z,φ). For asymptotically flat solutions with bounded sources, ψ approaches the Newtonian gravitational potential at spatial infinity:

$$\lim_{R\to\infty}\psi = -m/R + O(m^3/R^3) \quad , \tag{2.5}$$

where $R\equiv(\rho^2+z^2)^{1/2}$ and m is the total active gravitational mass of the system, as measured at infinity. The function ψ is determined by specifying a (usually singular) source for it in the background space. This source is artificial; its form is not closely connected with that of the physical object which generates the gravitational field.

Once ψ is known, the function γ is calculated by integrating equations (2.3) and (2.4), with the boundary condition that $\gamma=0$ on the symmetry axis in the absence of a conical singularity there. Thus the solution is completely characterized by the function ψ or its background-space source.

B. Description of a Schwarzschild Black Hole in the Weyl Formalism

The Schwarzschild solution, being static, axisymmetric, and vacuum, can be described with the Weyl formalism.[12] The background-space source for ψ in this description is not a point, and not spherically symmetric; this is a manifestation of the distortion inherent in the Weyl coordinates. The correct source is a line singularity of "linear density" $1/2$ and coordinate length $2M$, where M is the physical black-hole mass. The source occupies the segment $-M\leq z\leq M$, $\rho=0$ on the symmetry axis in the background space (see Figure 1). The "linear density" of the source is just the physical mass of the hole divided by the coordinate length of the source, and is unrelated to any physical density.

Equation (2.2) for ψ is most readily solved in the presence of such a source by transforming to prolate spheroidal coordinates (u,v), related to the cylindrical Weyl coordinates by

$$\rho = M\sinh u \sin v \quad , \tag{2.6}$$

$$z = M\cosh u \cos v \quad , \tag{2.7}$$

where $u\in[0,+\infty)$ and $v\in[0,\pi]$. The coordinates t and φ are of course unaltered. In these new coordinates, equations (2.2), (2.3), and (2.4) have the solution

$$\psi = \log[\tanh(u/2)] \quad , \tag{2.8}$$

$$\gamma = -\frac{1}{2}\log\left[1+\frac{\sin^2 v}{\sinh^2 u}\right] \quad . \tag{2.9}$$

In the (t,u,v,φ) coordinates, the metric (2.1) becomes

$$ds^2 = -\tanh^2(u/2)dt^2 + 4M^2\cosh^4(u/2)(du^2+dv^2)$$

$$+ 4M^2\cosh^4(u/2)\sin^2 v\, d\varphi^2 \quad . \tag{2.10}$$

Under the coordinate transformation

$$r = 2M\cosh^2(u/2) \quad , \tag{2.11}$$

$$\theta = v \quad , \tag{2.12}$$

with t and φ unchanged, the metric (2.10) becomes

$$ds^2 = -(1-2M/r)dt^2 + (1-2M/r)^{-1}dr^2 + r^2 d\theta^2 + r^2\sin^2\theta\, d\varphi^2 \quad . \tag{2.13}$$

This is the Schwarzschild metric in the usual Schwarzschild coordinates, which shows that (2.10) is indeed the desired solution. It describes a black hole of mass M, with the event horizon at the location $u=0$ of the "line-mass source." The cylindrical Weyl coordinates, and the prolate spheroidal coordinates, cover only that part of spacetime which lies outside the horizon.

C. A Schwarzschild Black Hole with Suspended "Moons"

An approximate solution for a black hole tidally distorted by the gravitational influence of nearby bodies can be constructed with the formalism of the preceding section. Beginning with the Schwarzschild solution described above, additional sources, representing the perturbing masses, are added to the Weyl background space. The function ψ for the new solution is obtained exactly by superposition. Equations (2.3) and (2.4) for γ are integrated approximately, for appropriate source configurations, by linearizing in the perturbing contribution to ψ.

The simplest perturbed configuration is that of a single "moon" fixed on the symmetry axis outside the black hole. This positioning preserves the stasis and axisymmetry required in the Weyl formalism, though it is only an approximation to a more realistic physical situation, such as a slowly orbiting moon. In the present calculation the moon is represented by a point monopole of "mass" μ at the point $\rho=0$, $z=b$ (with $b>M$) in the Weyl background space, as indicated in Figure 1. This choice simplifies the mathematics, but it introduces two subtleties into the problem. First, such a source in the background space corresponds to a Curzon singularity in the physical space.[13] The distinctive and bizarre gravitational features of the Curzon geometry manifest themselves in the strong-field region, i.e., near the singularity, where the contribution to ψ from the moon is at least of order unity. As these features probably do not correspond to the gravitational field near any real physical gravitating body, this solution is useful only in the moon's weak-field region, where the Curzon gravitational field closely resembles that of the Schwarzschild geometry. Second, the "mass" μ of the moon is related to the various dynamically defined masses of the configuration in somewhat complicated ways which emerge from the solution itself. These relationships are treated in detail in Section IV below; in the construction of the solution here it is simplest to regard μ as just a parameter characterizing the moon.

The "potential" ψ for the perturbed configuration is just the sum of the Schwarzschild potential (subscript 0) and that from the source representing the moon (subscript 1):

$$\begin{aligned}\psi &= \psi_0 + \psi_1^{(+)} \\ &= \log[\tanh(u/2)] - \mu[\rho^2+(z-b)^2]^{-1/2} \qquad (2.14) \\ &= \log[\tanh(u/2)] - \mu[M^2\sinh^2u\sin^2v+(b-M\cosh u\cos v)^2]^{-1/2} \quad .\end{aligned}$$

Here the superscript (+) refers to the configuration with a single moon above the hole. The coordinates (ρ,z) and (u,v) are as described above. The expression for $\psi_1^{(+)}$ is just the background-space harmonic potential for a "point" source at the designated location.

Since this is a static solution of the Einstein equations, the event horizon of the perturbed black hole can be identified as the surface on which the metric coefficient g_{tt} is zero.[14] By equation (2.1), this is the same as the surface on which ψ diverges to $-\infty$. As equation (2.14) shows, this is the surface $u=0$, since ψ_0 diverges to $-\infty$ there while $\psi_1^{(+)}$ remains finite. Thus for this particular coordinate representation of the geometry, the coordinate position of the black hole's horizon remains unchanged by the perturbation.

The primary aim of this calculation is to study the geometry of a gravitationally perturbed black hole and the tidal gravitational fields near the horizon. Since the source configuration used here is a physically reasonable model only for calculations restricted to the moon's weak-field region, this solution is of use only if the horizon lies in that region. Thus the model parameters μ, b, and M must be constrained so that the condition $|\psi_1^{(+)}| \ll 1$ holds for u near zero. With $\psi_1^{(+)}$ as given in (2.14), this is equivalent to the restriction $\mu \ll b - M$ on the model parameters.

The function γ is calculated by integrating $\partial\gamma/\partial v$ along a curve of constant u from the symmetry axis. Equations (2.3) and (2.4) imply the desired derivative of γ:

$$\partial\gamma/\partial v = \rho[(\partial\psi/\partial\rho)^2-(\partial\psi/\partial z)^2]\partial\rho/\partial v + 2\rho(\partial\psi/\partial\rho)(\partial\psi/\partial z)\partial z/\partial v$$

$$= \rho^2\cot v\,[(\partial\psi_0/\partial\rho)^2-(\partial\psi_0/\partial z)^2+2(\partial\psi_0/\partial\rho)(\partial\psi_1^{(+)}/\partial\rho)$$

$$-2(\partial\psi_0/\partial z)(\partial\psi_1^{(+)}/\partial z)] - 2\rho z\tan v\,[(\partial\psi_0/\partial\rho)(\partial\psi_0/\partial z) \qquad (2.15)$$

$$+(\partial\psi_0/\partial z)(\partial\psi_1^{(+)}/\partial\rho)+(\partial\psi_0/\partial\rho)(\partial\psi_1^{(+)}/\partial z)] + O[(\psi_1^{(+)})^2] \quad .$$

In (2.15) the terms of $\partial\gamma/\partial v$ are expanded in powers of the derivatives of $\psi_1^{(+)}$, and the terms of second order in $\psi_1^{(+)}$ are discarded, in accord with the perturbative scheme discussed above. The zeroth-order terms just give the derivative of the unperturbed Schwarzschild γ_0; the first-order terms give the desired perturbation term $\gamma_1^{(+)}$. That is,

$$\gamma = \gamma_0 + \gamma_1^{(+)} + O[(\psi_1^{(+)})^2] \quad , \qquad (2.16)$$

where

$$\gamma_0 = -\frac{1}{2}\log\left[1+\frac{\sin^2 v}{\sinh^2 u}\right] \qquad (2.17)$$

and

$$\partial\gamma_1^{(+)}/\partial v = 2\rho^2\cot v\,[(\partial\psi_0/\partial\rho)(\partial\psi_1^{(+)}/\partial\rho)-(\partial\psi_0/\partial z)(\partial\psi_1^{(+)}/\partial z)]$$

$$-2\rho z\tan v\,[(\partial\psi_0/\partial z)(\partial\psi_1^{(+)}/\partial\rho)+(\partial\psi_0/\partial\rho)(\partial\psi_1^{(+)}/\partial z)] \quad . \qquad (2.18)$$

(Actually in this case, with a single perturbing moon, the second-order terms in $\partial\gamma/\partial v$ could be integrated. They would give the γ function appropriate to the moon source by itself. But in this calculation such higher-order terms are not necessary, and in configurations involving more than one moon they could not be handled so easily, so here they are disregarded throughout.) The derivatives needed to evaluate $\partial\gamma_1^{(+)}/\partial v$ are obtained from equations (2.6), (2.7), and (2.14);

the result, after a bit of manipulation, is

$$\frac{\partial\gamma_1^{(+)}}{\partial v} = \frac{2\mu M}{[M^2\sinh^2 u\sin^2 v + (b - M\cosh u\cos v)^2]^{3/2}}(b - M\cosh u\cos v)\sin v \quad . \qquad (2.19)$$

This equation might be integrated exactly, but it is convenient at this point to restrict attention to the neighborhood of the horizon, and perform an approximate integration of (2.19) for u near zero. This specialization is done because the vicinity of the horizon is the region of interest in this calculation, and because the perturbation expansion in equation (2.15), which underlies (2.19), is valid only if the neglected $O[(\psi_1^{(+)})^2]$ terms are much smaller than the zeroth- and first-order terms. This is true near the horizon but not near the Curzon singularity. In the limit $u \to 0$, equation (2.19) becomes

$$\partial\gamma_1^{(+)}/\partial v = 2\mu M\sin v\,(b - M\cos v)^{-2}[1 + O(u^2)] \quad , \quad \text{for } u \ll 1 \, . \qquad (2.20)$$

This is easily integrated, with the result

$$\gamma_1^{(+)} = 2\mu[1/(b - M) - 1/(b - M\cos v)][1 + 0(u^2)] + C^{(+)} \quad , \quad \text{for } u \ll 1 \, , \qquad (2.21)$$

where $C^{(+)}$ is an integration constant.

Equations (2.14), (2.16), (2.17), and (2.21), put into the Weyl metric (2.1), constitute the solution for the geometry, near the horizon, of a Schwarzschild black hole perturbed by a single moon. A peculiar feature of this solution presents itself. It is not possible to choose the integration constant $C^{(+)}$ in (2.21) so that $\gamma_1^{(+)}$, and consequently γ, vanishes on the symmetry axis both above ($v = 0$) and below ($v = \pi$) the black hole. The form of the Weyl metric (2.1) implies that a nonvanishing γ on the symmetry axis corresponds to a conical singularity there. Such a singularity, in turn, corresponds to a singular distribution of stress-energy on the axis, which may be interpreted as that of a "rope" or "strut" supporting the gravitating masses.[15] This structure is inevitable in any

Weyl solution involving more than one separate (positive) mass; without it, the configuration could not be static. Dynamical information about the mass configuration can be extracted from quantitative studies of this "rope" or "strut" structure; see Section IV.

In the black-hole-plus-one-moon solution described above, different rope/strut structures are possible, depending on the choice of the integration constant $C^{(+)}$. If $C^{(+)}=0$, then $\gamma=0$ at $v=0$, i.e., on the segment of the symmetry axis between the "north pole" of the black hole and the moon (equation (2.4) implies that γ is constant along any segment of the symmetry axis not containing a singularity of ψ). But then $\gamma\neq 0$ at $v=\pi$, i.e., below the black hole, and it can also be shown that $\gamma\neq 0$ above the moon. (This is done by integrating $(\partial\gamma/\partial\rho)d\rho+(\partial\gamma/\partial z)dz$ along a small semicircle in the background space from just below the moon source to just above it.) In this case the black hole and moon may be described as suspended on, or held apart by, "ropes from infinity." Alternatively, if $C^{(+)}=-4\mu M/(b^2-M^2)$, then $\gamma=0$ at $v=\pi$, and also above the moon, but not at $v=0$, between the moon and the hole. This configuration corresponds to a black hole and moon held apart by a "strut" between them. Any other choice of $C^{(+)}$ entails a combination of rope and strut structures. As this solution is expected to reveal features of the black-hole geometry on the horizon directly under the moon, the version with $C^{(+)}=0$, with the black hole and moon suspended on ropes and no strut between them, is the most useful.

Of course a black hole cannot be suspended from a rope, even in principle: attaching the rope to the hole presents insurmountable problems. These difficulties can be avoided by adding a second moon, identical to the first, at the background-space position $\rho=0$, $z=-b$ (see Figure 1). Between symmetrically placed moons, the black hole requires no support; for a proper choice of integration constant, the moons are suspended by ropes from infinity and the

hole is unencumbered. The contributions of the lower moon to the Weyl potentials ψ and γ are exactly analogous to those of the upper moon:

$$\psi_1^{(-)} = -\mu[M^2\sinh^2 u \sin^2 v + (b + M\cosh u \cos v)^2]^{-1/2} \quad , \tag{2.22}$$

$$\frac{\partial \gamma_1^{(-)}}{\partial v} = \frac{-2\mu M}{[M^2\sinh^2\sin^2 v + (b + M\cosh u \cos v)^2]^{3/2}}(b + M\cosh u \cos v)\sin v$$

$$= -2\mu M \sin v\,(b + M\cos v)^{-2}[1 + O(u^2)] \qquad \text{for } u \ll 1, \tag{2.23}$$

and hence

$$\gamma_1^{(-)} = -2\mu[1/(b + M\cos v) - 1/(b + M)][1 + O(u^2)] + C^{(-)} \quad \text{for } u \ll 1\ , \tag{2.24}$$

where the superscript $(-)$ refers to the lower moon. The desired two-moon solution is obtained by adding the contributions of the upper and lower moons (since the equation for γ_1 is linearized in ψ_1), with integration constants $C^{(+)}=C^{(-)}=0$. The resulting total Weyl potentials are

$$\psi = \log[\tanh(u/2)] - \mu[M^2\sinh^2 u \sin^2 v + (b - M\cosh u \cos v)^2]^{-1/2}$$

$$-\mu[M^2\sinh^2 u \sin^2 v + (b + M\cosh u \cos v)^2]^{-1/2} \tag{2.25}$$

$$= \log[\tanh(u/2)] - 2\mu b/(b^2 - M^2\cos^2 v)[1 + O(u^2)] \quad \text{for } u \ll 1\ ,$$

$$\gamma = -\frac{1}{2}\log\left[1 + \frac{\sin^2 v}{\sinh^2 u}\right] + 4\mu b\,[1/(b^2 - M^2)$$

$$- 1/(b^2 - M^2\cos^2 v)][1 + O(u^2)] + O(\psi_1^2) \quad \text{for } u \ll 1\ , \tag{2.26}$$

where the last line of equation (2.25) and equation (2.26) are limits near the horizon. As desired, $\gamma=0$ at $v=0$ and at $v=\pi$, i.e., between the black hole and both moons.

III. INTRINSIC GEOMETRY OF THE DISTORTED HORIZON

One of the first questions which arises concerning the black hole perturbed by suspended moons, as described by the Weyl solution of the preceding section, is: What is the shape of the perturbed black-hole horizon? This can be answered by examining the intrinsic geometry of the horizon, as described by the metric given by (2.1), (2.25), and (2.26). Specializing this metric to a horizon section (t =constant, u =0) gives the horizon-section metric:

$$ds_H^2 = 4M^2 e^{-2\psi_1}(e^{2\gamma_1} dv^2 + \sin^2 v \, d\varphi^2) \quad , \tag{3.1}$$

where ψ_1 and γ_1 are the perturbation terms in the Weyl potentials of the solution. One way to elucidate the nature of this intrinsic geometry is by constructing embedding diagrams, two-dimensional surfaces in Euclidean three-space with the same surface metric.

Two regimes are of interest in this problem: the weak-perturbation regime, in which the change in the shape of the horizon from its unperturbed sphericity is small, and the strong-perturbation regime, in which the moons are close to the horizon and the change in horizon shape, at least in the immediate vicinity of the moons, is pronounced. In both regimes the magnitude of the perturbing potential ψ_1 is much less than unity near the horizon, since the solutions of Subsection II.C are derived under that assumption. Quantitative criteria distinguishing the two regimes are a bit more subtle; they emerge in the course of the embedding diagram calculations.

A. The Weak-Perturbation Regime

In the weak-perturbation regime it should be possible to represent the horizon geometry by a two-surface in Euclidean three-space defined by the

spherical coordinate equation $\tilde{r}=\mathcal{R}(\theta)$. (Here $\tilde{r}$ and θ are the usual spherical-polar radial and meridional coordinates, respectively. The tildes distinguish them from Schwarzschild coordinates.) The weakness of the perturbation should imply the condition $(d\mathcal{R}/d\theta)^2 \ll \mathcal{R}^2$. If this condition obtains, then the metric of the two-surface, denoted ds_2^2, is given by

$$ds_2^2 = \mathcal{R}^2 d\theta^2 + \mathcal{R}^2 \sin^2\theta \, d\tilde{\varphi}^2 \quad , \tag{3.2}$$

where the term $d\tilde{r}^2=(d\mathcal{R}/d\theta)^2 d\theta^2$ has been dropped. The equality of this metric and the horizon metric (3.1) is equivalent to the equations

$$\mathcal{R}\sin\theta = 2M e^{-\psi_1}\sin\upsilon \tag{3.3}$$

$$\mathcal{R}\, d\theta = 2M e^{\gamma_1-\psi_1} d\upsilon \quad . \tag{3.4}$$

Expanding the exponentials in these equations in powers of ψ_1 and γ_1 (retaining only the zeroth- and first-order terms), substituting the appropriate expressions for ψ_1 and γ_1 from equations (2.25) and (2.26) (evaluated at the horizon), and finally, dividing (3.4) by (3.3), gives the following differential equation for θ as a function of v:

$$d\theta/\sin\theta = [1+4\mu b/(b^2-M^2)](d\upsilon/\sin\upsilon) - [4\mu b/(b^2-M^2\cos^2\upsilon)](d\upsilon/\sin\upsilon) \tag{3.5}$$

Both sides of (3.5) are exact differentials; the equation has the solution

$$\tan(\theta/2) = \tan(\upsilon/2)\left[\frac{b+M\cos\upsilon}{b-M\cos\upsilon}\right]^{-2\mu M/(b^2-M^2)} \quad , \tag{3.6}$$

where the integration constant has been chosen to preserve symmetry about the black-hole equator: $\theta(\pi-\upsilon)=\pi-\theta(\upsilon)$. To use (3.6) to obtain $\mathcal{R}(\theta)$, I employ the identity

$$\left[\frac{b+M\cos\upsilon}{b-M\cos\upsilon}\right]^{-2\mu M/(b^2-M^2)} = \exp\left[-\frac{2\mu M}{b^2-M^2}\log\left[\frac{b+M\cos\upsilon}{b-M\cos\upsilon}\right]\right] \quad . \tag{3.7}$$

I assume, anticipating a result below, that the criterion defining the weak-perturbation regime ensures that the argument of the exponential in (3.7) is small, so that terms of second order and higher in the expansion of the exponential are negligible. (The factor $2\mu M/(b^2-M^2)$ is of order ψ_1; if the moon is not allowed to be arbitrarily near the horizon, so that $b-M$ is bounded below appropriately, the logarithm will not alter substantially the magnitude of the exponential argument.) I make such an expansion and apply the result to equation (3.3); the resulting solution for $\mathcal{R}$ is

$$\mathcal{R}(\theta) = 2M\left[1 + \frac{2\mu M\cos v}{b^2-M^2}\log\left(\frac{b+M\cos v}{b-M\cos v}\right) + \frac{2\mu b}{b^2-M^2\cos^2 v}\right]$$

$$= 2M\left[1 + \frac{2\mu M\cos\theta}{b^2-M^2}\log\left(\frac{b+M\cos\theta}{b-M\cos\theta}\right) + \frac{2\mu b}{b^2-M^2\cos^2\theta}\right] \quad , \tag{3.8}$$

where the higher-order terms have been dropped.

Equation (3.8) gives the desired embedding surface for the horizon-section shape, but its validity is restricted by the condition $(d\mathcal{R}/d\theta)^2 \ll \mathcal{R}^2$ employed in its derivation, and by the stronger condition that the discarded term $(d\mathcal{R}/d\theta)^2 d\theta^2$ must be negligible compared to the *perturbation terms* retained in $\mathcal{R}^2 d\theta^2$. The latter condition determines the range of model parameters for which the geometry of the perturbed horizon is faithfully represented by the embedding surface defined by $\tilde{r}=\mathcal{R}(\theta)$, with $\mathcal{R}(\theta)$ given by (3.8); it can be taken to be the quantitative criterion for the weak-perturbation regime. This condition is easily evaluated: Equation (3.8) implies

$$d\mathcal{R}/d\theta = -2M\left[\frac{2\mu M\sin v}{b^2-M^2}\log\left(\frac{b+M\cos v}{b-M\cos v}\right)\right.$$

$$\left. + \frac{4\mu M^2 b\cos v\sin v}{b^2-M^2\cos^2 v}\left[\frac{1}{b^2-M^2} + \frac{1}{b^2-M^2\cos^2 v}\right]\right] \tag{3.9}$$

(where again the higher order terms are dropped), which in turn implies

$$d\mathcal{R}/d\theta = 2M \times O\{\psi_1[M/(b-M)]^{1/2}\} \quad ; \tag{3.10}$$

i.e., the right hand side of (3.9) is of no larger order than this for any choice of model parameters. Thus the condition that $(d\mathcal{R}/d\theta)^2$ be negligible in comparison to the perturbation terms retained in $\mathcal{R}^2$ is equivalent to the parameter constraint

$$\psi_1^2 M/(b-M) \ll |\psi_1| \quad , \tag{3.11}$$

i.e.,

$$|\psi_1| M/(b-M) \ll 1 \quad , \tag{3.12}$$

plus the $|\psi_1| \ll 1$, i.e., $\mu \ll b-M$, constraint already imposed. As mentioned above, this is sufficient to ensure that the argument of the exponential in (3.7) is small (in this case, smaller than order $\psi_1 \log|\psi_1|$). It also means that the higher-order terms ignored in (3.8) and (3.9) are smaller than order $(\psi_1 \log|\psi_1|)^2$ and are thus safely negligible. Hence the weak-perturbation approximation is self-consistent. Criterion (3.12) for this regime can be expressed in the convenient form

$$b-M \gg (\mu M)^{1/2} \tag{3.13}$$

in terms of the model parameters.

For configurations satisfying (3.13) then, the embedding surface defined by (3.8) represents the intrinsic geometry of the horizon section. Both perturbation terms in $\mathcal{R}(\theta)$ are nonnegative and both assume their maximum values at the poles of the black hole, $\theta = v = 0$ and $\theta = v = \pi$, and their minimum values at the equator, $\theta = v = \pi/2$. Thus the perturbed horizon is prolate, elongated in the

direction of the moons; the polar circumference of the hole is greater than its equatorial circumference. In this sense the moons "raise a tide" on the black hole. Figure 2 illustrates the shape of the embedding surface.

Configurations with the moons very far from the hole, i.e., with $b \gg \max\{M, \mu\}$, are special cases of the weak-perturbation regime. In this case, which I term the "distant weak-perturbation limit," the embedding surface profile (3.8) assumes a simple form. Expanded in powers of μ/b and M/b, $\mathscr{R}(\theta)$ can be expressed in the form

$$\mathscr{R}(\theta) = 2M\exp[(2\mu/b)(1+M^2/b^2)][1+(4\mu M^2/b^3)P_2(\cos\theta)][1+O(\tilde{m}^4/b^4)] , \quad (3.14)$$

where $\tilde{m} \equiv \max\{\mu, M\}$ and $P_2(\cos\theta)$ is the Legendre polynomial of degree 2. This is the form of a prolate spheroid with small eccentricity; the distant moons produce a simple quadrupole tidal deformation of the horizon (see Figure 2). Hartle[1] obtains a similar result by different methods, as a consequence of a perturbative calculation of tidal effects on slowly rotating black holes. Hartle obtains, for the horizon of a Schwarzschild hole perturbed by a distant static moon, the embedding diagram

$$\tilde{r} = 2M\,[1 + 2\mu(M^2/R^3)P_2(\cos\theta)] \quad (3.15)$$

to leading order in the perturbation. The notation is as above, with R the Schwarzschild radial coordinate at the location of the moon. (This is related to the Weyl coordinate b used above by $b = R - M$. Since in this result $R \gg M$, b and R are interchangeable in (3.15).) The exponential factor in (3.14) absent in Hartle's result indicates that the mass parameter M must be interpreted differently in the two formalisms; this is discussed in Section IV. The factors containing the angular dependence, i.e., the shape of the surface, are the same in the two results, except for a factor of two in the perturbation term which

occurs because Hartle's configuration has one moon instead of the two used above. (The mass alteration implied in the exponential factor in (3.14) would contribute to the angular term in higher order in the perturbation, so it does not alter this agreement). Thus in the distant weak-perturbation limit, the tidally deformed black-hole geometry obtained from the Weyl solution of Subsection II.C is in accord with Hartle's calculation. It may be noted that the moon in Hartle's calculation is supported by tangential stresses in a spherical shell about the black hole, rather than by ropes from infinity as used here; in the distant weak-perturbation limit this difference does not alter the tides produced.

B. The Strong-Perturbation Regime

In the strong-perturbation regime, the horizon shape departs substantially from that of a sphere. In this case an embedding diagram of the type used in the preceding section, the construction of which relies on the smallness of the departure from sphericity, would not be suitable. Another type of embedding surface can be constructed, however, without assuming near-sphericity, by using cylindrical coordinates $(\tilde{\rho}, \tilde{z}, \tilde{\varphi})$ in the Euclidean three-space instead of the spherical polar coordinates used before. (The tildes serve to distinguish these coordinates from the Weyl coordinates.) The embedding surface is defined by the equation $\tilde{z} = Z(\tilde{\rho})$. Strictly, a single-valued function Z only defines an embedding surface from one pole to the equator, but the horizon is symmetric about its equator. The corresponding surface metric is

$$ds_2^2 = [1+(dZ/d\tilde{\rho})^2]d\tilde{\rho}^2 + \tilde{\rho}^2 d\tilde{\varphi}^2 \quad . \tag{3.16}$$

This is matched to the horizon-section metric (3.1) as the surface metric in the preceding section was. The azimuthal terms determine $\tilde{\rho}$; with that result the remaining terms yield $dZ/d\tilde{\rho}$. The results are:

$$\tilde{\rho} = 2M \sin v e^{-\psi_1} \tag{3.17}$$

$$(dZ/d\tilde{\rho})^2 = -1 + e^{2\gamma_1}(\cos v - \sin v\, \partial\psi_1/\partial v)^{-2} \quad . \tag{3.18}$$

Equation (3.18) has an inconvenient form; a change of variable gives a more manageable equation. Let ϖ be proper length in the meridional direction on the horizon section, measured from the "north pole," i.e., $v=0$. The metric (3.16) implies

$$d\tilde{\rho}/d\varpi = [1+(dZ/d\tilde{\rho})^2]^{-1/2} = e^{-\gamma_1}(\cos v - \sin v\, \partial\psi_1/\partial v) \tag{3.19}$$

and therefore

$$(dZ/d\varpi)^2 = 1 - e^{-2\gamma_1}(\cos v - \sin v\, \partial\psi_1/\partial v)^2 \quad . \tag{3.20}$$

Expanding this to linear order in ψ_1 and γ_1 and substituting their values from (2.25) and (2.26) yields

$$(dZ/d\varpi)^2 = \sin^2 v \left\{1 + \frac{8\mu b M^2 \cos^2 v}{b^2 - M^2\cos^2 v}\left[\frac{1}{b^2 - M^2\cos^2 v} + \frac{1}{b^2 - M^2}\right] + O(\psi_1^2)\right\} \quad . \tag{3.21}$$

The proper distance ϖ can be obtained as a function of v from the metric (3.1), so this can be solved for Z. Performing the integrations exactly is problematical, but an approximate solution is possible.

The first term in (3.21) is the contribution from the unperturbed spherical geometry; the second term, proportional to μ, is the perturbation contribution. In the strong-perturbation regime the latter should dominate, at least near the pole. This occurs if and only if the configuration satisfies the constraint

$$\psi_1 M/(b-M) \gg 1 \quad , \tag{3.22}$$

which can be expressed in terms of the model parameters as

$$b - M \ll (\mu M)^{1/2} \quad . \tag{3.23}$$

This can be taken to be the quantitative criterion for the strong-perturbation regime; it is precisely the opposite of the criterion (3.13) for the weak-perturbation regime. For configurations satisfying (3.23), the zeroth-order (in ψ_1) term in (3.21) can be neglected, except near the equator where the factor $\cos^2 v$ suppresses the first-order term. This still leaves an unwieldy expression for $dZ/d\varpi$. The expression becomes tractable, however, in the limit $\varpi \ll M$ or equivalently, $v \ll 1$, i.e., in the immediate vicinity of the pole. It is thus possible to examine the strongly perturbed horizon geometry in the region almost directly under the nearby moon.

According to the metric (3.1), $v=[\varpi/(2M)][1+O(\psi_1)]$. In the aforementioned limit, this is a small quantity, so the higher-order terms on the right can be neglected, and $\sin v$ and $\cos v$ can be expanded in powers of $\varpi/(2M)$. Also, let s_0 be defined as the proper distance from the north pole of the horizon along the symmetry axis to the coordinate location of the upper moon in the unperturbed Schwarzschild geometry (in the full black-hole-plus-moons geometry this distance is actually infinite, because of the peculiarities of the Curzon geometry near the moons). The metric (2.10) implies that if u_0 is the prolate spheroidal u-coordinate value at the moons' locations ($M\cosh u_0 = b$), then $s_0/(2M) = u_0 + O(u_0^3)$. Constraint (3.22) and the $|\psi_1| \ll 1$ condition on the horizon ensure $u_0 \ll 1$. Thus b can be expanded in powers of the small quantity $s_0/(2M)$ in this regime. With these two expansions, some terms which appear repeatedly in this analysis take the forms:

$$1/(b-M) = (8M/s_0^2)[1+O(s_0^2/M^2)] \quad , \tag{3.24}$$

$$1/(b+M) = [1/(2M)][1+O(s_0^2/M^2)] \quad , \tag{3.25}$$

$$1/(b-M\cos v) = [8M/(s_0^2+\varpi^2)][1+O(s_0^2/M^2)+O(\varpi^2/M^2)+O(\psi_1)] \quad , \quad (3.26)$$

$$1/(b+M\cos v) = [1/(2M)][1+O(s_0^2/M^2)+O(\varpi^2/M^2)+O(\psi_1)] \quad , \quad (3.27)$$

The terms which arise in $\psi_1^{(-)}$ and $\gamma_1^{(-)}$, viz., (3.25) and (3.27), are negligible in comparison to those from $\psi_1^{(+)}$ and $\gamma_1^{(+)}$, viz., (3.24) and (3.26). This fits the physical situation: in this regime, with the moons very close to the horizon in comparison to its size, the horizon geometry near the north pole is influenced far more by the nearby upper moon than by the lower moon on the other side of the hole. This contrasts with the situation in the distant weak-perturbation limit, where it was seen that the effect of one moon was just half the effect of two, i.e., the two moons contributed equally.

If (3.21) is expanded in powers of $\varpi/(2M)$ and $s_0/(2M)$ and only the dominant terms are retained, it takes the form

$$(dZ/d\varpi)^2 = \varpi^2/(4M^2) + (32\mu M/s_0^2)[\varpi^2(2s_0^2+\varpi^2)/(s_0^2+\varpi^2)^2] \quad , \quad (3.28)$$

where the omitted higher-order terms take the form of a factor like those in (3.26) and (3.27). As above, the strong-perturbation-regime criterion states that the first (unperturbed) term is negligible compared to the second (perturbation) term; in the expansion used here, the criterion (3.23) becomes

$$\mu M^3/s_0^4 \gg 1 \quad . \quad (3.29)$$

If the unperturbed term in (3.28) is neglected, then that equation implies

$$dZ/d\varpi = \pm(32\mu M/s_0^2)^{1/2}\varpi(2s_0^2+\varpi^2)^{1/2}/(s_0^2+\varpi^2) \quad . \quad (3.30)$$

This can be integrated, with the result

$$Z(\varpi) = \pm\left(\frac{8\mu M}{s_0^2}\right)^{1/2}\left\{2[(2s_0^2+\varpi^2)^{1/2}-(2s_0^2)^{1/2}]\right.$$

$$\left. + s_0\left[\log\left(\frac{(2s_0^2+\varpi^2)^{1/2}-s_0}{(2s_0^2+\varpi^2)^{1/2}+s_0}\right) - \log\left(\frac{2^{1/2}-1}{2^{1/2}+1}\right)\right]\right\} \quad . \tag{3.31}$$

to leading order. Equation (3.17) implies

$$\tilde{\rho} = \varpi[1+O(\varpi^2/M^2)+O(\psi_1)] \quad . \tag{3.32}$$

so to dominant order ϖ can simply be replaced by $\tilde{\rho}$ in (3.31), to describe the embedding surface entirely in terms of the Euclidean-space coordinates.

Equations (3.31) and (3.32), then, define an embedding surface of the form $\tilde{z}=Z(\tilde{\rho})$ which reproduces the horizon-section geometry in the neighborhood of the pole in the strong-perturbation case. This result reveals that in the limit $s_0 \ll \varpi \ll M$, i.e., in the region far from the pole compared to the moon's distance but not compared to the size of the horizon, the horizon geometry is conical. In this region $dZ/d\varpi$ or $dZ/d\tilde{\rho}$ approaches the constant value $\pm(32\mu M/s_0^2)^{1/2}$, which behavior corresponds to a right circular cone. The shape of this embedding surface is shown in Figure 3.

Because of the approximations used in its derivation, the embedding surface defined by (3.31) and (3.32) does not fix the "orientation" of the perturbation of the horizon geometry; it cannot distinguish between a "bulge" and a "depression." (These terms are to be understood in terms of the intrinsic geometry; the question whether the horizon is displaced up or down in the external space is ill-defined.) But in equations (3.21) and (3.28) the unperturbed and perturbation terms contribute with the same sign, and the relative size of the perturbation term is greatest at the pole, decreasing monotonically to zero at the equator. This means the perturbed horizon-section geometry is prolate. In the strong-perturbation regime as well as in the weak--in fact for any choice of

model parameters--the moons can be said to raise a tidal bulge on the horizon.

Equation (3.31) can be compared with a result in the same form for the weak-perturbation regime. If the model parameters are chosen so that the conditions $(\mu M^3)^{1/4} \ll s_0 \ll M$ hold, then the configuration belongs to the weak regime, but in the neighborhood of the pole the expansions in powers of s_0/M and ϖ/M used above can still be applied. The embedding surface profile $Z(\varpi)$ can be obtained by taking the square root of both sides of Equation (3.30), using the weak regime condition that the unperturbed term is dominant and expanding the root of the right side in powers of the perturbation term, and integrating. Alternatively, it can be obtained by a change of coordinates in the embedding space: $Z = \pm[\mathscr{R}(\bar{\theta})\cos\bar{\theta} - \mathscr{R}(0)]$, $\tilde{\rho} = \mathscr{R}(\bar{\theta})\sin\bar{\theta}$. Both methods yield the result

$$Z(\varpi) = \pm\left\{\varpi^2/(4M) + (16M^2\mu/s_0^2)\left[\frac{\varpi^2}{s_0^2+\varpi^2} + \log\left[\frac{s_0^2+\varpi^2}{s_0^2}\right]\right]\right\} \quad , \qquad (3.33)$$

to first order in the small quantities. This profile differs markedly from the strong-perturbation form (3.31). Here $Z(\varpi)$ is dominated by the unperturbed term, which gives the spherical shape of the Schwarzschild horizon section. The small perturbation contribution is superposed on this. The perturbation terms also differ in the two regimes. Notably, in the limit $s_0 \ll \varpi \ll M$, the perturbation term in this weak case does not correspond to the conical geometry to which the surface described by (3.31) tends; rather, its behavior is governed by the logarithmic term in (3.33). This implies that away from the pole the horizon deformation it describes flattens out like a "pith helmet." This profile is compared with that described by (3.31) in Figure 3. Of course the horizon-section shape itself remains nearly spherical everywhere, in accord with the original definition of the weak-perturbation regime.

It is in the strong-perturbation regime that the solution constructed here for a tidally deformed Schwarzschild black hole can be compared to the calculations by Suen and Price[10] for a tidally deformed Rindler horizon. The Rindler horizon is flat; Rindler space is a good approximation to Schwarzschild spacetime only in a region very near the horizon and very small in extent in comparison to the horizon size M. Equivalently, Rindler space corresponds to a limit $M \to \infty$ of the Schwarzschild geometry, in which the distance measures s_0 and ϖ are held fixed. In such a limit the strong-perturbation-regime criterion takes the form (3.29). The parameter μ is not held fixed in the limiting process, but as is shown in Section IV, it scales as $1/M$. Consequently, the criterion (3.29) is satisfied in the limit, which means the Rindler-space problem corresponds to the strong-perturbation regime of the Schwarzschild tidal-distortion problem as formulated here. Suen and Price construct a solution with a single mass suspended above the Rindler horizon, in contrast to the two moons used here. But as noted above, in the two-moons solution the horizon geometry near a pole ($\varpi \ll M$) is dominated by the influence of the nearby moon, the effects of the second moon near the other pole being negligible, when $s_0 \ll M$. So the two solutions are indeed comparable. Solving the linearized Einstein equations in flat spacetime, Suen and Price calculate the intrinsic geometry of the tidally deformed Rindler horizon, and obtain an embedding diagram of the form $\tilde{z} = Z(\tilde{\rho})$. Their result matches exactly the embedding surface obtained here, defined by equations (3.31) and (3.32), for the appropriate limit of the distorted Schwarzschild horizon.

C. The Scalar Curvature for the Horizon-Section Geometry

The horizon-section geometry associated with the metric (3.1) can also be characterized by its two-dimensional scalar curvature ${}^{(2)}R$, without reference to any embeddings. The calculation of ${}^{(2)}R$ from (3.1) is straightforward; it yields

$$ {}^{(2)}R = [1/(2M^2)]e^{2(\psi_1-\gamma_1)}[\,1+\partial^2\psi_1/\partial\upsilon^2+(\partial\psi_1/\partial\upsilon+\partial\gamma_1/\partial\upsilon)\cot\upsilon $$

$$ -(\partial\psi_1/\partial\upsilon)(\partial\gamma_1/\partial\upsilon)] \ . \qquad (3.34) $$

Expanding this to linear order in ψ_1 and γ_1 and utilizing the expressions for those functions from (2.25) and (2.26) gives

$$ {}^{(2)}R = [1/(2M^2)]\{1+4\mu b/(b^2-M^2\cos^2\upsilon)-8\mu b/(b^2-M^2) $$

$$ +[4\mu M^2 b/(b^2-M^2\cos^2\upsilon)^3][\,4(b^2-M^2)-5(b^2-M^2)\sin^2\upsilon+2M^2\sin^4\upsilon]\} \ , \qquad (3.35) $$

with the higher-order terms omitted. This somewhat unwieldy result is in accord with the results of the preceding sections on the horizon-section geometry. For example, ${}^{(2)}R$ is related[16] to the principal radii of curvature a_1, a_2 of the two-surface by ${}^{(2)}R = 2/(a_1a_2)$. On the symmetry axis, with $a_1=a_2=a$, equation (3.35) implies

$$ a = 2M[\,1-4\mu b/(b^2-M^2)+16\mu M^2 b/(b^2-M^2)^2\,]^{-1/2} \ , \qquad (3.36) $$

to leading order. But this radius can also be obtained from an embedding diagram of the form $\tilde{z}=Z(\tilde{\rho})$ by evaluating $|(1/\tilde{\rho})dZ/d\tilde{\rho}|^{-1}$ on the symmetry axis.[17] Using equations (3.17), (3.19), and (3.21) for this gives precisely the same expression as (3.36).

All the perturbation terms in (3.35) are of order ψ_1 except the term $16\mu M^2 b\,(b^2-M^2)/(b^2-M^2\cos^2\upsilon)^3$, which is of order $\psi_1 M/(b-M)$. This term dominates the scalar curvature if the strong-perturbation-regime criterion (3.22) is

satisfied; the unperturbed term dominates if the configuration belongs to the weak-perturbation regime and condition (3.12) obtains. Thus the distinction between strong- and weak-perturbation regimes is a coordinate-invariant geometric one: in the strong regime the horizon-section curvature is dominated by the perturbation, while in the weak regime the unperturbed curvature is the primary contribution.

Equation (3.35) takes on a simpler form in the limit $s_0 \ll M$, $\varpi \ll M$. If only the leading terms are kept, it becomes

$$^{(2)}R = [\,1/(2M^2)]\,[\,1-(16\mu M/s_0^2)(s_0^2+2\varpi^2)/(s_0^2+\varpi^2) + (256\mu M/s_0^2)(M^2 s_0^4)/(s_0^2+\varpi^2)^3]\quad , \tag{3.37}$$

via the expansion used in the previous section. As above, the horizon-section radius of curvature at the pole can be extracted from this. In the weak-perturbation regime, where the first term in (3.37) dominates, the calculation yields

$$a = 2M\,[\,1-128\mu M^3/s_0^4\,] \tag{3.38}$$

to leading order, which agrees with the value obtained from the embedding function Z given by (3.33). In the strong-perturbation regime, the last term in (3.37) dominates, hence

$$a = [s_0^2/(4\mu M)]^{1/2} s_0/4\quad , \tag{3.39}$$

with all smaller terms neglected. This result likewise agrees with that obtained from the corresponding embedding function, equation (3.31).

The results of Suen and Price[10] for the Rindler horizon can also be formulated in terms of the horizon intrinsic curvature. Their formulae agree with the strong-perturbation-regime expressions above, i.e., equations (3.37) and (3.39),

in the appropriate limit.

IV. DYNAMICAL MASSES IN THE "BLACK HOLE AND MOONS" SOLUTION

The solution constructed here for a tidally distorted black hole is characterized in part by the mass parameters M and μ, for the black hole and moons respectively. The relationships between these parameters and the physical masses in the problem can be extracted from the solution itself. The boundary condition (2.5) on the Weyl potential ψ, and the expression (2.25) for ψ in this solution, imply that the total active gravitational mass of the system of black hole and moons is $M + 2\mu$. This includes the combined effects of the black hole, the moons, their gravitational binding energy, and the contributions of the "ropes." More detailed calculations are needed to determine what masses are to be attributed to these components separately.

A. The Mass of the Black Hole

Since this solution is stationary and axisymmetric, the mass of the black hole itself can be determined by means of the generalized Smarr Formula [18,19]:

$$M_H = 2\Omega^H J_H + [\kappa/(4\pi)]\mathcal{A} \quad . \tag{4.1}$$

Here the black hole mass M_H is defined[18] as $1/(8\pi)$ times the integral over the horizon section of the curl of the stationary Killing vector field $\partial/\partial t$. The first term on the right consists of the horizon angular momentum J_H, defined as a similar integral with the axisymmetric Killing vector $\partial/\partial\varphi$, and the horizon angular velocity Ω^H. As the solution here is static, both of these quantities are zero. The factors in the last term are κ, here the proper acceleration of a static observer at the horizon, renormalized to compensate for the redshift of the observer's proper time with respect to coordinate time[20] (also termed the

surface gravity of the horizon), and $\mathcal{A}$, the proper area of the horizon section.

The horizon surface gravity κ can be evaluated in several ways; a simple formula is[21]

$$\kappa^2 = -\lim_{u\to 0}\frac{(\nabla_\alpha|\vec{l}\,|^2)(\nabla^\alpha|\vec{l}\,|^2)}{4|\vec{l}\,|^2} \quad , \tag{4.2}$$

where the limit given means the limit on the horizon, and the four-vector $\vec{l}$ is the tangent to the horizon generators; in this static case $\vec{l}$ is $\partial/\partial t$. The index α runs over all four spacetime coordinates; it is convenient to use (t, u, v, φ) here. Of course $|\vec{l}\,|^2$ is just the metric coefficient g_{tt}. With the metric given by (2.1), transformed into prolate spheroidal coordinates, and the potentials ψ and γ given by (2.25) and (2.26), the above formula for κ takes the form

$$\begin{aligned}
\kappa^2 &= -\lim_{u\to 0}\{[\,1/(4g_{tt}g_{uu})\,][(\partial g_{tt}/\partial u)^2+(\partial g_{tt}/\partial v)^2]\} \\
&= -\lim_{u\to 0}\{(g_{tt}/g_{uu})\operatorname{csch}^2 u\,[(1+\sinh u\,\partial\psi_1/\partial u)^2+\sinh^2 u(\partial\psi_1/\partial v)^2]\} \qquad (4.3)\\
&= [\,1/(16M^2)]\exp(4\psi_1|_{u=0}-2\gamma_1|_{u=0}) \quad .
\end{aligned}$$

The derivatives of ψ_1 and γ_1 do not contribute to κ^2 because they are finite on the horizon and are multiplied by factors which vanish in the limit $u\to 0$. The result (4.3) is exact. The potential ψ_1 in (2.25) is exact, but γ_1 from (2.26) is only accurate to first order in ψ_1. Substituting these into (4.3) gives the result

$$\kappa = [\,1/(4M)]\exp[\,-4\mu b/(b^2-M^2)]\,[\,1+O(\psi_1^2)] \quad . \tag{4.4}$$

To this order in the perturbation, κ is independent of v, i.e., it is uniform over the horizon; actually this is a general feature of the horizon surface gravity for any stationary black hole.[22]

The horizon-section area $\mathscr{A}$ is easily calculated directly from the metric (3.1):

$$\mathscr{A} = 8\pi M^2 \int_0^{\pi} e^{\gamma_1 - 2\psi_1} \sin v \, dv$$

$$= 16\pi M^2 \exp[\,4\mu b / (b^2 - M^2)\,][\,1 + O(\psi_1^2)\,] \quad . \tag{4.5}$$

Substituting these results into the Smarr Formula (4.1) gives the desired relation:

$$M_H = M\,[\,1 + O(\psi_1^2)\,] \quad . \tag{4.6}$$

To the accuracy of these calculations, the black-hole mass parameter M is the actual black-hole mass.

The issue of the interpretation of the black-hole mass parameter arose in Subsection III.A above, in the comparison of the horizon geometries obtained from this solution and from the Hartle[1] calculation in the distant weak-perturbation limit. As equations (3.14) and (3.15) show, the same shapes are obtained once the different number of moons is taken into account, but the distinct overall factors indicate that the mass parameters "M" in the two formalisms must be different. The above result shows that the mass parameter in the Hartle calculation, which I now label M_{Hartle} to avoid confusion, is not the actual black-hole mass as defined for the Smarr Formula. That is, equation (3.14) describes a black hole of mass M, but equation (3.15) does not. However, these equations imply the relations

$$M_{\text{Hartle}} = [\,\mathscr{A} / (16\pi)\,]^{1/2}[\,1 + O(\psi_1^2)\,] = M \exp[2\mu b / (b^2 - M^2)\,][\,1 + O(\psi_1^2)\,] \tag{4.7}$$

among the Hartle mass parameter, the horizon area, and the black-hole mass.

The physical effect of the perturbation on the black-hole mass is not clear in the relations (4.7); it is necessary to specify more precisely what perturbed and unperturbed configurations are to be compared and how the comparison is to be made. One possible comparison is between unperturbed and perturbed configurations linked by a specified physical process. For example, consider the following process: the initial state is an unperturbed Schwarzschild black hole of mass M_0, with the perturbing moons arbitrarily far away. Let the moons be lowered slowly on ropes from infinity, symmetrically along a common axis, until a given configuration of the type described by the solution constructed here is reached. If the moons are lowered slowly enough, i.e., quasi-statically, the area of the horizon will be conserved in this process. (The rate of change of the area for such a process is determined by the square of the shear rate,[23] and is inversely proportional to the square of the process timescale. The total change in area is thus proportional to the inverse of the timescale, so it vanishes for an arbitrarily slow process.) This area is just $16\pi M_0^2$ in terms of the initial mass. The Smarr Formula and the result (4.4) for κ imply that the mass M in the final configuration obeys

$$M = (M_0^2/M)\exp[-4\mu b/(b^2-M^2)][1+O(\psi_1^2)] \quad . \tag{4.8}$$

This has the solution

$$M = M_0\exp[-2\mu b/(b^2-M_0^2)][1+O(\psi_1^2)] \quad , \tag{4.9}$$

which also implies

$$\kappa = \kappa_0\exp[-2\mu b/(b^2-M_0^2)][1+O(\psi_1^2)] \quad , \tag{4.10}$$

where $\kappa_0=1/(4M_0)$ is the initial unperturbed horizon surface gravity. Thus for the process described here, the gravitational field of the moons causes a

reduction in the horizon surface gravity. In accord with the Smarr Formula, with the horizon-section area conserved in the process, the mass of the black hole is reduced proportionately by the perturbation.

B. The Masses of the Moons and the Contributions of the Ropes

The physical masses of the moons in this solution can be obtained by several methods. The different methods confirm each other's results and reveal a variety of features of the solution.

One way to obtain the active gravitational mass of a moon in this geometry is to examine the metric encountered by observers much closer to the moon than to the black hole.[24] Consider a neighborhood of the upper moon much smaller in (coordinate) extent than the moon/horizon separation $b-M$, but much larger than μ. In this neighborhood the black-hole contributions to the Weyl potentials defining the metric can be approximated by their values at the moon location: $\psi_0=\log[\tanh(u_0/2)]$ and $\gamma_0=0$. In that portion of this neighborhood away from the moon and from the supporting rope, e.g., near the axis between the moon and the hole, the perturbation term γ_1 can also be approximated by zero. The metric in this region then assumes the form

$$ds^2 = -\tanh^2(u_0/2)\,e^{2\psi_1}dt^2 + \tanh^{-2}(u_0/2)\,e^{-2\psi_1}(d\rho^2+dz^2)$$

$$+\rho^2\tanh^{-2}(u_0/2)\,e^{-2\psi_0}d\varphi^2 \quad . \tag{4.11}$$

When re-expressed in local proper time/distance coordinates defined by

$$\hat{t} = \tanh(u_0/2)\,t \quad , \tag{4.12}$$

$$\hat{\rho} = \coth(u_0/2)\,\rho \quad , \tag{4.13}$$

and

$$\hat{z} = \coth(u_0/2)\, z \quad , \tag{4.14}$$

this metric takes on the very simple form

$$\begin{aligned} ds^2 &= -e^{2\psi_1} d\hat{t}^2 + e^{-2\psi_1}(d\hat{\rho}^2 + d\hat{z}^2 + \hat{\rho}^2 d\hat{\varphi}^2) \\ &= -(1+2\psi_1) d\hat{t}^2 + (1-2\psi_1)(d\hat{\rho}^2 + d\hat{z}^2 + \hat{\rho}^2 d\hat{\varphi}^2) \quad , \end{aligned} \tag{4.15}$$

where $\hat{\varphi}=\varphi$ and the metric is expanded to first order in ψ_1 in the last line. But this is just the form of a weak-field metric[25] with Newtonian potential ψ_1. In the hatted coordinates, ψ_1 is given by

$$\psi_1 = -\mu \coth(u_0/2)\,[\hat{\rho}^2 + (\hat{z} - \hat{b})^2]^{-1/2} + \psi_1^{(-)} \quad , \tag{4.16}$$

where $\hat{b} \equiv b \coth(u_0/2)$ and the lower-moon contribution $\psi_1^{(-)}$ is in this approximation a small constant which can be ignored. Equation (4.16) has the form of the Newtonian potential generated by the mass

$$\tilde{\mu} = \mu \coth(u_0/2) = \mu\,[(b+M)/(b-M)]^{1/2} \quad . \tag{4.17}$$

This is the active gravitational mass of the moon, to leading order, as detected by local observers.

The physical mass of the moons also manifests itself in the tension in the ropes. This is determined by the nonzero value of the function γ on the symmetry axis in the region of the ropes. This value can be obtained by integrating the Weyl equations (2.3) and (2.4) along a curve from a point on the symmetry axis between a moon and the hole, where γ is zero, to a point on the axis on the other side of the moon, i.e., on the rope. If ψ is written as $\psi_0 + \psi_1$ and equations (2.3) and (2.4) are expanded out, three groups of terms appear. The ψ_0^2 terms, when integrated, just give the value of γ_0 on the rope, namely zero. The ψ_1^2 terms give the value of γ for the moon's Curzon geometry by itself, also zero,

plus a cross term describing the influence of one moon on the other, which can be neglected. The desired value of γ_1 on the rope comes only from the $\psi_0\psi_1$ cross terms.

A convenient choice of integration path is the coordinate semicircle $\rho=\bar{r}\sin\bar{\theta}$, $z=b-\bar{r}\cos\bar{\theta}$, with the restriction $\bar{r}\ll b-M$. The desired integrand is

$$d\gamma/d\bar{\theta} = (\partial\gamma/\partial\rho)\,d\rho/d\bar{\theta} + (\partial\gamma/\partial z)\,dz/d\bar{\theta}$$

$$= \bar{r}\cos\bar{\theta}\,\{2\rho[(\partial\psi_0/\partial\rho)(\partial\psi_1/\partial\rho) - (\partial\psi_0/\partial z)(\partial\psi_1/\partial z)]\} \qquad (4.18)$$

$$+\bar{r}\sin\bar{\theta}\{2\rho[(\partial\psi_0/\partial\rho)(\partial\psi_1/\partial z) + (\partial\psi_0/\partial z)(\partial\psi_1/\partial\rho)]\} + \ldots$$

where the ellipsis represents all the terms which give zero when integrated. All the necessary quantities are given in Subsections II.B and II.C; some manipulation yields

$$d\gamma/d\bar{\theta} = [2\mu\sin\bar{\theta}/(M\sinh^2 u_0)]\{1+O[\bar{r}/(b-M)]\} + \ldots \qquad (4.19)$$

Since γ is constant on the symmetry axis between the moon and the hole and is also constant above the moon, the integral of (4.19) over $\bar{\theta}$ from 0 to π cannot depend on $\bar{r}$; neglect of the $O[\bar{r}/(b-M)]$ terms entails no approximation. The integral gives

$$\gamma|_{\rho=0,\,|z|>b} = 4\mu/(M\sinh^2 u_0) = 4\mu M/(b^2-M^2) \quad . \qquad (4.20)$$

This is accurate to first order in ψ_1, the only approximation in its derivation being the neglect of the interaction of the two moons with each other.

The stress-energy of the rope corresponding to this value of γ on the symmetry axis can be derived by calculating the Riemann curvature tensor for the spacetime geometry in the immediate vicinity of the rope. This calculation is given in Appendix A; it shows that the rope is characterized by a proper linear

mass density λ and tension T obeying

$$\lambda = T = \gamma/4 \quad , \tag{4.21}$$

to leading order in the perturbation, with γ the value in (4.20). But this tension supports the weight of the moon; it should equal the (passive) gravitational mass $\tilde{\mu}$ of the moon times the proper acceleration of a static body at the moon's position. This acceleration is easily calculated; it is the magnitude of the vector $U^\alpha \nabla_\alpha U^\beta$, where ∇_α is the covariant derivative in this geometry and U^α is the four-velocity of a static object. In the (t, u, v, φ) coordinate system, U^α has components $[(-g_{tt})^{-1/2}, 0, 0, 0]$. If the acceleration is calculated in the unperturbed Schwarzschild spacetime (neglecting the gravitational attraction between the moons), the "force-balance" equation becomes

$$T = \tilde{\mu}/[4M\cosh^4(u_0/2)\tanh(u_0/2)] \quad , \tag{4.22}$$

accurate to first order in the perturbation. This and the above results imply

$$\tilde{\mu} = \mu/\tanh(u_0/2) = \mu[(b+M)/(b-M)]^{1/2} \quad , \tag{4.23}$$

in agreement with the result of the active mass calculation (4.17).

The result (4.21) for the rope tension does not depend on position along the rope; in accord with (2.3), γ is constant over the entire length of the rope. This means that the rope is weightless--no additional tension is needed to support any length of it. This property is a consequence of the "equation of state" $\lambda = T$. The "equation of motion" for a static radial rope in the Schwarzschild geometry, derived in Appendix B, takes the form of a force-balance equation:

$$\{1/[2M\cosh^2(u/2)]\}\, dT/du = (\lambda - T)\{1/[4M\cosh^4(u/2)\tanh(u/2)]\} \quad , \tag{4.24}$$

expressed here in the prolate spheroidal Weyl coordinates. The left-hand side of

this equation is the derivative of the tension with respect to proper distance along the rope; the quantity in braces on the right is the proper acceleration of a static object. Thus $\lambda - T$ must be the proper density of passive gravitational mass; the negative contribution of the tension to that mass is a relativistic effect. If λ and T are equal (the highest tension or lowest density any rope can have, according to the strong energy condition) then the gravitational mass of the rope vanishes. Thus the ropes in this solution for a black hole with moons contribute no gravitational mass to the configuration.

It appears, therefore, that the ropes give rise to no gravitational effects here except for the curvature located in the ropes themselves. Even the conical geometry in the neighborhood of the ropes is flat everywhere but on the ropes. A curious coincidence arises in connection with this conical geometry, however. As shown in Appendix A, the geometry in the neighborhood of any point on the ropes can be described by a cone, with angle α between its axis and generators, given by

$$\begin{aligned} \alpha &= \arcsin\left(e^{-\gamma(P)}\right) \\ &\cong \pi/2 - [8\mu M/(b^2 - M^2)]^{1/2} \\ &\cong \pi/2 - (32\mu M/s_0^2)^{1/2} \quad \text{if} \quad s_0 \ll M \ , \end{aligned} \tag{4.25}$$

where the last two expressions are to first order in the perturbation, and the last involves the expansion used in Subsection III.B. In that section it was found that the horizon-section geometry of a strongly perturbed black hole approached a conical form at distances ϖ from its poles large compared to the moon-pole separation s_0 but small compared with M. The comparable angle α describing that cone is given by

$$\alpha = \pi/2 - \arctan(|dZ/d\tilde{\rho}|)$$

$$\cong \pi/2 - (32\mu M/s_0^2)^{1/2} \quad . \tag{4.26}$$

The same conical geometry is found in both instances. This appears to indicate that away from the pole on the strongly perturbed horizon, the tidal influence of the moon drops off with increasing ϖ and the geometry is dominated by the presence of the rope on the axis. This interpretation, although intuitively appealing, is complicated by the fact that in the $\varpi \ll M$ limit in which this result is seen, the horizon geometry is influence by the "half rope" extending from the nearby moon to infinity. An arbitrarily small neighborhood of a point on the rope, as treated in Appendix A, is influenced by a "full rope" extending in both directions. I have not found any simple physical explanation of these results which resolves this difficulty and accounts for the coincidence of the conical geometries.

The difference between the total gravitational mass of the perturbed-black-hole system measured at infinity, $M + 2\mu$, and the sum of the locally measured gravitational masses of the three bodies, $M + 2\tilde{\mu}$, is the gravitational binding energy of the system (since the ropes contribute no gravitational mass). Since, as shown in Subsection IV.A, above, the mass M attributed to the black hole is the same by both measures, the binding energy can be determined by comparing μ and $\tilde{\mu}$. Alternatively, calculating the binding energy by other methods provides an independent way to obtain $\tilde{\mu}$.

One way to do this calculation is to examine the energy of a mass μ allowed to fall freely from infinity to the desired moon position in the field of the black hole[26]; the kinetic energy released in such a fall is the negative of the binding energy of a static mass at the moon position. For the purposes of this calculation, the moon can be regarded as a test particle in the static, unperturbed

Schwarzschild spacetime. This neglects the moon-moon interaction, as in the previous calculations, and gives results accurate to first order in the perturbation. It also means that the covariant time component of the four-momentum of the particle, p_t, is conserved in the fall[27]; it retains its value at infinity, viz., $p_t = -\mu$. The total energy of the particle measured by a static observer in the Schwarzschild spacetime is $-U^\alpha p_\alpha = -(-g_{tt})^{-1/2} p_t = \mu \coth(u/2)$, where U^α is the observer's four velocity, given above, and u is the prolate spheroidal "radial" coordinate of the observer's position. If the particle is stopped at the desired moon position u_0 and its total energy in the local static frame converted into rest mass, the resulting particle has mass $\tilde{\mu}$ given by

$$\tilde{\mu} = \mu \coth(u_0/2) \quad . \tag{4.27}$$

This mass is the mass of the moon at infinity plus the negative of its binding energy, i.e., this mass plus the binding energy is the mass-at-infinity of the moon. Hence this is the desired proper mass of the moon. This result is in agreement with the previously obtained values for $\tilde{\mu}$, in (4.17) and (4.23), and thus confirms the accounting of total energy described above.

In comparing the results of this study to other calculations of tidal effects on black holes, it is very important to make the correct identification of parameters for the perturbing mass. In the comparison of the horizon-section geometries obtained here and in Hartle's[1] calculation in the distant weak-perturbation limit [equations (3.14) and (3.15)], no distinction was made between μ and $\tilde{\mu}$. In that limit, however, u_0 is large and $\coth(u_0)$ is very near unity. The discrepancy between μ and $\tilde{\mu}$ would give rise to a correction of higher than leading order in b/M, so the distinction does not affect the agreement between the two results. In physical terms this just shows that the binding energy of a moon is a negligible fraction of its mass in the distant weak-

perturbation limit.

The binding energy is significant, however, in the strong-perturbation regime. In the limit $s_0 \ll M$, the expressions (4.17), (4.23), and (4.27) take the form

$$\tilde{\mu} = 4M\mu / s_0 \quad , \tag{4.28}$$

to leading order; clearly $\tilde{\mu} \gg \mu$ characterizes this regime. This expression appears in all the strong-perturbation-regime results in Subsections III.B and III.C. It is this expression which is to be identified with the perturbing mass in the Rindler-space calculations of Suen and Price[10] (hence the statement in the closing paragraph of Subsection III.B that the mass parameter μ scales as $1/M$ in the $M \to \infty$ limit matching the Schwarzschild and Rindler geometries). Complete agreement is obtained, as stated previously, between the strong-perturbation-regime results obtained here and the corresponding Rindler-space results, when this identification of the moon's proper mass $\tilde{\mu}$ with the Rindler-space mass (which is unaltered by any binding energy) is made.

V. RIEMANN TENSOR COMPONENTS IN THE VICINITY OF THE DISTORTED HORIZON

In dynamical situations the evolution of the horizon of an interacting black hole is governed by the Riemann curvature at the horizon (plus any inflowing stress-energy).[28] The components of the Riemann curvature tensor near the horizon of the tidally distorted Schwarzschild black hole described here can be obtained from the metric solution of Subsection II.C. The results give additional information on the nature of the tidal deformation, and provide a means of comparison as a starting point for dynamical calculations.

To facilitate such comparisons, the components are calculated here in the orthonormal frame of a static observer near the horizon. The basis vectors for

such a frame can be written so:

$$\mathbf{e}_{\hat{t}} = (-g_{tt})^{-1/2}\,\partial/\partial t = \coth(u/2)e^{-\psi_1}\,\partial/\partial t \tag{5.1}$$

$$\mathbf{e}_{\hat{u}} = (-g_{uu})^{-1/2}\,\partial/\partial u = [1/(2M)]\,\mathrm{sech}^2(u/2)\,e^{\psi_1-\gamma_1}\,\partial/\partial u \tag{5.2}$$

$$\mathbf{e}_{\hat{v}} = (-g_{vv})^{-1/2}\,\partial/\partial v = [1/(2M)]\,\mathrm{sech}^2(u/2)\,e^{\psi_1-\gamma_1}\,\partial/\partial v \tag{5.3}$$

$$\mathbf{e}_{\hat{\varphi}} = (-g_{\varphi\varphi})^{-1/2}\,\partial/\partial\varphi = [1/(2M)]\,\mathrm{sech}^2(u/2)\,\mathrm{csc}v\,e^{\psi_1}\,\partial/\partial\varphi \quad , \tag{5.4}$$

using the metric of Subsection II.C in the prolate spheroidal Weyl coordinates.

The Riemann-tensor components in this orthonormal frame are related to those in the coordinate frame in a simple manner. For example,

$$R_{\hat{t}\hat{u}\hat{t}\hat{u}} = [1/(4M^2)]\,\mathrm{sech}^4(u/2)\coth^2(u/2)\,e^{-2\gamma_1}R_{tutu} \quad , \tag{5.5}$$

The calculation of the coordinate-frame components such as R_{tutu} is straightforward, although the results are unwieldy, e.g.

$$\begin{aligned} R_{tutu} = -e^{2\psi_1}[\,&\tanh^2(u/2)\,\mathrm{sech}^2(u/2) - \tanh^2(u/2)\,\partial^2\psi_1/\partial u^2 \\ &+ \tanh^2(u/2)\,(\partial\psi_1/\partial v)\,(\partial\psi_1/\partial v - \partial\gamma_1/\partial v) \\ &+ \tanh^2(u/2)\,(\partial\psi_1/\partial u)\,(\partial\gamma_1/\partial u - \partial\psi_1/\partial u) \\ &- \tanh^2(u/2)\,(\partial\psi_1/\partial u)^2 + (1/2)\tanh(u/2)\,\mathrm{sech}^2(u/2)\,\partial\gamma_1/\partial u \\ &-(3/2)\tanh(u/2)\,\mathrm{sech}^2(u/2)\,\partial\psi_1/\partial u + \tanh^3(u/2)\,\partial\psi_1/\partial u\,] \quad . \end{aligned} \tag{5.6}$$

Expanding this to linear order in ψ_1, using the expressions for ψ_1 and γ_1 from (2.25) and (2.26), specializing to the neighborhood of the horizon ($u \ll 1$), and substituting all into (5.5) yields, after considerable manipulation,

$$R_{\hat{t}\hat{u}\hat{t}\hat{u}} = \{-[1/(4M^2)] + (2\mu b/M^2)/(b^2-M^2)$$

$$-(\mu b/M^2)(b^2+3M^2\cos^2 v)(b^2-M^2)/(b^2-M^2\cos^2 v)^3\}[1+O(\psi_1^2)+O(u^2)] \quad , \quad (5.7)$$

as the desired Riemann-tensor component.

The first term in (5.7) represents the Riemann curvature of the unperturbed Schwarzschild geometry; the other two terms give the tidal curvature. It can be seen that the ratio of the third term to the first is of order $\psi_1 M/(b-M)$ (the second term is smaller than the first by a factor of order ψ_1). This implies another invariant interpretation of the weak- and strong-perturbation regimes: in the weak-perturbation regime [condition (3.12)], the Riemann curvature near the horizon is dominated by the unperturbed geometry; in the strong-perturbation regime [condition (3.22)], the tidal curvature dominates.

The principal aim in this calculation of Riemann-tensor components is to provide a standard of comparison, in the static limit, for dynamical calculations of tidal effects on black holes. Of particular interest is the comparison with the Rindler-space results of Suen and Price[10] in the static limit. Thus it is useful to express (5.7) in the "Rindler limit": $M\to\infty$ at fixed ϖ, s_0, and $\tilde{\mu}$. It is also convenient to introduce notation appropriate to the Rindler geometry: As ϖ is proper distance on the horizon away from the pole in the v or $\hat{v}$ direction, let $\mathbf{e}_{\hat{\varpi}} = \mathbf{e}_{\hat{v}}$ denote the orthonormal basis vector in that direction. Further, let $\mathbf{e}_{\hat{n}} = \mathbf{e}_{\hat{u}}$ denote the orthonormal basis vector in the radial (u or $\hat{u}$) direction, i.e., the direction normal to the horizon. In this notation, the component in (5.7) is given in the Rindler limit by

$$R_{\hat{t}\hat{n}\hat{t}\hat{n}} = -16\tilde{\mu}s_0^3/(s_0^2+\varpi^2)^3 \quad , \quad (5.8)$$

to leading order; the neglected terms give a factor $[1+O(\psi_1^2)+O(u^2)+O(s_0^2/M^2)+O(\varpi^2/M^2)]$. The mass $\tilde{\mu}$ is as calculated in

Subsection IV.B.

Other components of the Riemann tensor in this geometry can be calculated in the same manner. In the Rindler limit, the components are

$$R_{\hat{t}\varpi\hat{t}\varpi} = +8\tilde{\mu}s_0^3/(s_0^2+\varpi^2)^3 \quad , \tag{5.9}$$

$$R_{\hat{t}\hat{\varphi}\hat{t}\hat{\varphi}} = +8\tilde{\mu}s_0^3/(s_0^2+\varpi^2)^3 \quad , \tag{5.10}$$

$$R_{\hat{n}\varpi\hat{n}\varpi} = -8\tilde{\mu}s_0^3/(s_0^2+\varpi^2)^3 \quad , \tag{5.11}$$

$$R_{\hat{n}\hat{\varphi}\hat{n}\hat{\varphi}} = -8\tilde{\mu}s_0^3/(s_0^2+\varpi^2)^3 \quad , \tag{5.12}$$

and

$$R_{\varpi\hat{\varphi}\varpi\hat{\varphi}} = +16\tilde{\mu}s_0^3/(s_0^2+\varpi^2)^3 \quad , \tag{5.13}$$

also to leading order; the neglected terms give the same factor as for equation (5.8). A slight complication enters into the calculation of the remaining components. For example, the component $R_{\hat{t}\hat{n}\hat{t}\varpi}$ is given by

$$R_{\hat{t}\hat{n}\hat{t}\varpi} = [1/(4M^2)]\,\mathrm{sech}^4(u/2)\,e^{2(\psi_1-\gamma_1)}\{2\mathrm{csch}u\,[1-\sinh^2(u/2)]\,\partial\psi_1/\partial v$$

$$-\mathrm{csch}u\,\partial\gamma_1/\partial v + \partial^2\psi_1/\partial u\,\partial v\} \quad , \tag{5.14}$$

to first order in ψ_1. This vanishes at $u=0$, though not above the horizon. Calculating it requires obtaining the derivatives of ψ_1 and γ_1 to second order in u. These can be computed by expanding ψ_1 from (2.25) and $\partial\gamma_1/\partial v$ from (2.19) and (2.23) in powers of u, retaining the *two* leading terms in each, and then differentiating and integrating as needed. In this way the remaining Riemann-tensor components can be obtained to first order in u. In the Rindler limit, these components are:

$$R_{\hat{t}\hat{n}\hat{t}\hat{\varpi}} = +48\tilde{\mu}s_0^3\,\varpi s / (s_0^2+\varpi^2)^4 \quad , \tag{5.15}$$

and

$$R_{\hat{n}\hat{\varphi}\hat{\varpi}\hat{\varphi}} = +48\tilde{\mu}s_0^3\,\varpi s / (s_0^2+\varpi^2)^4 \quad , \tag{5.16}$$

where $s \cong 2Mu$ is the proper distance from the field point to the horizon, measured normal to the horizon. These are "leading-order" expressions like those above; the neglected terms give the same factor as before.

Equations (5.8) through (5.13), (5.15), and (5.16), then, give the components of the Riemann curvature tensor measured in the orthonormal frame of a static observer near the pole of the horizon, in the strong-perturbation case. All other components not related to these by index symmetries are zero. As might be expected, they show that the tidal curvature fields are greatest near the pole, and fall off rapidly for $\varpi \gg s_0$, in this configuration with a moon very close to the horizon.

These results show that the Riemann tensor in this geometry possesses an interesting symmetry retained from the unperturbed Schwarzschild spacetime.[29] Let $V^{\hat{\alpha}} = (V^{\hat{t}},\ V^{\hat{n}},\ 0,\ 0)$ be the four-velocity of an observer moving radially, i.e., in the u direction, normal to the horizon, in the vicinity of the horizon pole; the components given are in the static observer's orthonormal frame. Let $R'_{\hat{\alpha}\hat{\beta}\hat{\gamma}\hat{\delta}}$ be a Riemann-tensor component measured in this moving observer's orthonormal frame. Certain of these components obey a special relation, viz.,

$$\begin{aligned} R'_{\hat{t}\varpi\hat{t}\varpi} &= R_{\hat{\alpha}\varpi\hat{\beta}\varpi}\,V^{\hat{\alpha}}\,V^{\hat{\beta}} \\ &= [8\tilde{\mu}s_0^3 / (s_0^2+\varpi^2)^3]\,[(V^{\hat{t}})^2 - (V^{\hat{n}})^2] \\ &= 8\tilde{\mu}s_0^3 / (s_0^2+\varpi^2)^3 \end{aligned} \tag{5.17}$$

hence

$$R'_{\hat{t}\varpi\hat{t}\varpi} = R_{\hat{t}\varpi\hat{t}\varpi} \quad . \tag{5.18}$$

Similarly,

$$R'_{\hat{t}\hat{\varphi}\hat{t}\hat{\varphi}} = R_{\hat{t}\hat{\varphi}\hat{t}\hat{\varphi}} \tag{5.19}$$

and

$$R'_{\hat{t}\varpi\hat{t}\hat{\varphi}} = R_{\hat{t}\varpi\hat{t}\hat{\varphi}} \; (= 0) \quad . \tag{5.20}$$

This symmetry of the Riemann-tensor components implies that the components with two time indices and two indices in directions tangential to the horizon are the same measured in the orthonormal frame of any observer static or moving normal to the horizon.

Suen and Price[10] have calculated the corresponding Riemann-tensor components for the geometry of a Rindler horizon perturbed by a static suspended mass. Their results are in complete agreement with those obtained here.

VI. SUMMARY

Using the Weyl formalism for static, axisymmetric, vacuum geometries, I have here constructed a solution to the Einstein field equations describing a Schwarzschild black hole perturbed by two suspended "moons." The dynamical masses of the bodies in the configuration, the binding energy of the system, and the tension in the supporting ropes are all derived from the solution. The relations among these quantities are completely consistent: the total gravitational mass of the system, measured at infinity, is found to be equal to the dynamical masses of the hole and the moons plus the (negative) binding energy, the ropes contributing no gravitational mass; the tension in the ropes is shown to be the

value required to support the moons in the gravitational field of the hole.

This solution reveals a number of features of the tidal deformation of such a black hole in the static limit. The intrinsic geometry of the distorted horizon is obtained directly from the solution metric; it can be represented with embedding diagrams such as are defined by equations (3.8), (3.14), and (3.33) for the case of weak perturbations, and by equation (3.31) in the strong-perturbation case (see Figures 2 and 3). In all cases the horizon geometry is prolate, i.e., a tidal bulge is produced. For strong perturbations the intrinsic shape of the tidal bulge approaches a conical form away from the horizon's pole; for weak perturbations the bulge "flattens out" intrinsically. Another geometric measure of the tidal effects, the Riemann curvature tensor, can also be calculated from the solution metric, in the vicinity of the horizon. The components of this tensor in the orthonormal frame of a static observer near the horizon are given by expressions such as equation (5.7), or in the strong-perturbation regime, in the neighborhood of the horizon pole, by equations (5.8)--(5.13), (5.15), and (5.16).

The horizon geometry obtained here accords with that obtained by Hartle[1] in the limit in which the moons are far from the horizon compared to its size. In the opposite limit of moons near the horizon, this solution approaches the Rindler approximation of Suen and Price.[10] Thus the results of this study confirm the validity of the Rindler-space approximation to the Schwarzschild geometry for static, strong-perturbation tidal-effect calculations; consequently, they lend support to the use of the Rindler approximation for the more complicated problem of dynamical tides.

ACKNOWLEDGEMENTS

I wish to thank Professor Kip S. Thorne, who provided valuable ideas at many stages of this work, and Professor Richard H. Price, who also provided much assistance and who painstakingly checked these results. I would also like to acknowledge the help of my other colleagues in the "Black Hole Paradigm Society," with whom I collaborated on the program of studies of which this work is a part: Dr. Ronald J. Crowley, Dr. Wojciech H. Zurek, Douglas A. Macdonald, Wai-Mo Suen, Milan Mijic, L. Sam Finn, and Xiao-He Zhang.

This work was supported in part by the National Science Foundation via Grant AST82-14126.

APPENDIX A: SPACETIME CURVATURE AND STRESS-ENERGY OF THE ROPES

The Riemann curvature tensor at the rope singularity can be obtained from an examination of the spacetime geometry near the rope; from this the stress-energy of the rope follows via the Einstein equations.[30] Let P be a point on one of the ropes. In an arbitrarily small neighborhood of P, the spacetime metric is given by equation (2.1), with the potentials ψ and γ evaluated at the point P. Local proper time/distance coordinates can be defined in the neighborhood:

$$\hat{t} = e^{\psi(P)} t \quad , \tag{A1}$$

$$\hat{\rho} = e^{\gamma(P)-\psi(P)} \rho \quad , \tag{A2}$$

$$\hat{z} = e^{\gamma(P)-\psi(P)} z \quad , \tag{A3}$$

and of course $\hat{\varphi}=\varphi$. The metric in these coordinates takes the form

$$ds^2 = -d\hat{t}^2 + d\hat{z}^2 + d\hat{\rho}^2 + \hat{\rho}^2 e^{-2\gamma(P)} d\hat{\varphi}^2 \tag{A4}$$

in the neighborhood of P. This expression shows that the $\hat{\rho}-\hat{\varphi}$ plane in the neighborhood of P has the geometry of a right circular cone, one with angle α between its axis and any generator, defined by

$$\alpha = \arcsin(e^{-\gamma(P)}) \tag{A5}$$

(see Figure 4). Here $\gamma(P)$ is positive and small, as equation (4.20) shows, so α is a real angle near $\pi/2$; this cone is nearly planar. The curvature associated with this geometry is all concentrated at the apex of the cone, i.e., on the rope. The Riemann-tensor components describing this curvature can be obtained by evaluating the rotation of a vector parallel-transported around a closed curve and utilizing the formula[31]

$$\delta A^{\alpha} = -1/2 \int_{S} R^{\alpha}{}_{\beta\gamma\delta} A^{\beta} \, {}^{*}d\Sigma^{\gamma\delta} \quad . \tag{A6}$$

Here A^{α} is the four-vector parallel-transported around a small closed curve C, and the integration is over the planar region S bounded by C, with differential area two-form ${}^{*}d\Sigma^{\gamma\delta}$. This formula is valid in the limit of small areas S and small changes in A^{α}.

The rotation of a vector upon such transport in the geometry represented by (A4) can be seen easily if that metric is written in the form

$$ds^2 = -d\hat{t}^2 + d\hat{z}^2 + d\hat{\rho}^2 + \hat{\rho}^2 \, d\varphi^{*2} \quad , \tag{A7}$$

where $\varphi^{*} \equiv e^{-\gamma(P)} \hat{\varphi}$. This is just a flat spacetime geometry, but with the property that the surface $\varphi^{*}=0$ is identified with the surface $\varphi^{*}=2\pi e^{-\gamma(P)}$. (The transformation performed here is equivalent to slicing a cone radially and unrolling it out flat.) From this form for the geometry in the neighborhood of P it is easy to see that vector components in the $\hat{t}$ and $\hat{z}$ directions are unchanged by parallel transport around any curve; that vectors in the $\hat{\rho}-\hat{\varphi}$ plane are unchanged unless

they are transported around the symmetry axis, i.e., from the surface $\varphi^*=0$ to the surface $\varphi^*=2\pi e^{-\gamma(P)}$; and that such vectors so transported are rotated in the $\hat{\rho}-\hat{\varphi}$ plane. If such a vector makes an angle β with the ray $\varphi^*=0$ in the $\hat{\rho}-\varphi^*$ plane and is parallel-transported around the axis to the ray $\varphi^*=2\pi e^{-\gamma(P)}$, it will make an angle $\beta+2\pi(1-e^{-\gamma(P)})$ with the latter ray. Since the two rays are identified, the vector undergoes a rotation in transport by an angle Δ given by

$$\Delta = 2\pi(1-e^{-\gamma(P)}) \cong 2\pi\gamma(P) \quad , \tag{A8}$$

where, as (4.20) shows, the approximation here is accurate to first order in the perturbation ψ_1 as evaluated on the horizon. This rotation is shown pictorially in Figure 4. As (A6) requires, Δ is small. The changes in the components of the transported vector A^α are given by

$$\delta A^{\hat{\rho}} = -A^{\hat{\varphi}}\Delta \tag{A9}$$

and

$$\delta A^{\hat{\varphi}} = +A^{\hat{\rho}}\Delta \quad , \tag{A10}$$

again to linear order in the perturbation. Here and below, $\hat{\varphi}$ and φ^* components are used interchangeably; the discrepancies involved are of higher order in the perturbation, i.e., in $\gamma(P)$ here.

The form of the Riemann tensor at the rope follows from these parallel-transport properties. The only nonzero components are $R^{\hat{\varphi}}{}_{\hat{\rho}\hat{\varphi}\hat{\rho}}$ and those related to it by index symmetries. Equations (A6) and (A10) imply

$$A^{\hat{\rho}}\Delta = \delta A^{\hat{\varphi}} = -1/2\int_S [R^{\hat{\varphi}}{}_{\hat{\rho}\hat{\rho}\hat{\varphi}} - R^{\hat{\varphi}}{}_{\hat{\rho}\hat{\varphi}\hat{\rho}}]\, A^{\hat{\rho}} d^2\sigma$$

$$= A^{\hat{\rho}}\int_S R^{\hat{\varphi}}{}_{\hat{\rho}\hat{\varphi}\hat{\rho}}\, d^2\sigma \quad , \tag{A11}$$

where $d^2\sigma$ is the area element, the antisymmetric components of the two-form ${}^*d\Sigma^{\gamma\delta}$ being explicitly summed over. The integration region S is a small area in the $\hat{\rho}$-$\hat{\varphi}$ plane around the axis, bounded by the transport curve C. Since this integral gives the same result for any curve about the axis, no matter how small, the Riemann tensor component must have the form

$$R^{\hat{\varphi}}{}_{\hat{\rho}\hat{\varphi}\hat{\rho}} = \Delta\,\delta^2(\hat{\rho}) \quad , \tag{A12}$$

where $\delta^2(\hat{\rho})$ is the ordinary two-dimensional Dirac delta function. The integral has been treated here as an ordinary flat-space integral, once again neglecting the discrepancy between φ^* and $\hat{\varphi}$, which would contribute a factor $\{1+O[\gamma(P)]\}$ to this result.

The components of the Einstein tensor follow immediately from the Riemann-tensor components[32]; the stress-energy tensor for the rope is then given by the Einstein field equations. The components of this tensor are, to leading order,

$$T^{\hat{t}\hat{t}} = -\,T^{\hat{z}\hat{z}} = [\Delta/(8\pi)]\,\delta^2(\hat{\rho}) \quad , \tag{A13}$$

with all others zero. But this is just the stress-energy tensor of a rope on the axis, with linear density $\lambda=\Delta/(8\pi)$ and tension $T=\Delta/(8\pi)$. By (A8), the "equation of state" of the rope can be written

$$\lambda = T = \gamma(P)/4 \quad , \tag{A14}$$

to first order in the perturbation.

APPENDIX B. EQUATION OF STRESS BALANCE FOR A ROPE IN SCHWARZSCHILD SPACETIME

The equation of stress balance for a static rope in a gravitational field is obtained from the requirement that the covariant divergence of the rope's stress-energy tensor vanish.[33] Let the four-velocity of the elements of the rope be U^α, and let W^α be a unit spacelike vector, orthogonal to U^α, defining the direction of the rope. Let the proper mass-energy density of the rope be ε, and let η be the stress in the rope. The rope can only support stresses in the W^α direction; thus, its stress-energy tensor has the form

$$T^{\alpha\beta} = \varepsilon U^\alpha U^\beta + \eta W^\alpha W^\beta \quad . \tag{B1}$$

The desired equations of motion are the two projections $U_\alpha \nabla_\beta T^{\alpha\beta} = 0$ and $W_\alpha \nabla_\beta T^{\alpha\beta} = 0$. In terms of the quantities in equation (B1), these equations are

$$-U^\beta \nabla_\beta \varepsilon - \varepsilon \nabla_\beta U^\beta + \eta U_\alpha W^\beta \nabla_\beta W^\alpha = 0 \tag{B2}$$

and

$$\varepsilon W_\alpha U^\beta \nabla_\beta U^\alpha + W^\beta \nabla_\beta \eta + \eta \nabla_\beta W^\beta = 0 \quad . \tag{B3}$$

The first of these is a time-evolution equation; the second gives the tension distribution in the rope. In the case of a static rope in a static geometry, (B2) becomes trivial; (B3) gives the condition for static equilibrium.

For the case of a static rope in Schwarzschild spacetime, the metric is given by equation (2.13) in the familiar (t, r, θ, φ) coordinates. The rope can be taken to occupy an infinitesimal coordinate solid angle $\delta\Omega$ on the polar axis. In these coordinates, the vectors U^α and W^α have components

$$U^\alpha = [\,(1-2M/r)^{-1/2},\ 0,\ 0,\ 0\,] \tag{B4}$$

and

$$W^{\alpha} = [\,0,\,(1-2M/r)^{1/2},\,0,\,0\,] \quad . \tag{B5}$$

The covariant derivatives in the equations of motion are evaluated by standard methods; with the above components for the vectors, equation (B2) becomes $0 = 0$, as expected, and (B3) takes the form

$$(\varepsilon+\eta)(M/r^2)(1-2M/r)^{-1/2} + (1-2M/r)^{1/2}(d\eta/dr + 2\eta/r) = 0 \quad . \tag{B6}$$

The stress-energy components ε and η can be expressed in terms of the more familiar linear parameters for a rope: let the rope have linear density λ and tension T. The proper cross-sectional area of the rope is $r^2\delta\Omega$. Hence the rope parameters are related by $\varepsilon = \lambda/(r^2\delta\Omega)$ and $\eta = -T/(r^2\delta\Omega)$, the negative sign denoting a tension rather than a pressure. Substituting these relations into (B6) and simplifying gives the desired equation:

$$(1-2M/r)^{1/2}\,dT/dr = (\lambda - T)\,(M/r^2)(1-2M/r)^{-1/2} \quad , \tag{B7}$$

where the solid angle factors $\delta\Omega$ have cancelled out. This is the equation of stress balance for the rope: the left side is the derivative of the tension with respect to proper distance along the rope; the right side is the linear gravitational mass density times the "acceleration of gravity," i.e., it is the linear weight density. This is just the equation to be expected from elementary statics, except for the relativistic contribution of the tension to the gravitational mass.

Equation (B7) takes the form

$$[1/(2M)]\,\mathrm{sech}^2(u/2)\,dT/du = (\lambda - T)\,\{1/[4M\cosh^4(u/2)\tanh(u/2)]\} \tag{B8}$$

in the Weyl prolate spheroidal (t, u, v, φ) coordinates.

REFERENCES

[1]James B. Hartle, Phys. Rev. D 8 , 1010-1024 (1973).

[2]James B. Hartle, Phys. Rev. D 9 , 2749-2759 (1974).

[3]S. W. Hawking and J. B. Hartle, Commun. math. Phys. 27 , 283-290 (1972).

[4]Saul A. Teukolsky, Ph. D. thesis, California Institute of Technology, University Microfilms #74-14,289 (1974).

[5]William G. Unruh and Robert M. Wald, Phys. Rev. D. 25 , 942-958 (1982).

[6]Jacob D. Bekenstein, Phys. Rev. D. 26 , 950-953 (1982).

[7]R. Geroch and J. B. Hartle, J. Math. Phys. (NY) 23 , 680-693 (1982).

[8]Kip S. Thorne and Douglas Macdonald, Mon. Not. R. astr. Soc. 198 , 339-343 (1982).

[9]Douglas Macdonald and Kip S. Thorne, Mon. Not. R. astr. Soc. 198 , 345-382 (1982).

[10]Wai-Mo Suen and Richard H. Price, unpublished.

[11]H. Weyl, Ann. Phys. (Leipzig) 54 , 117-145 (1918).

[12]J. L. Synge, *Relativity: The General Theory* (North Holland, Amsterdam, 1966), p. 315.

[13]H. E. J. Curzon, Proc. London Math. Soc. 23 , 477-480 (1924).

[14]Brandon Carter, J. Math. Phys. (NY) 10 , 70-81 (1969).

[15]J. L. Synge, *Relativity: The General Theory* (North Holland, Amsterdam, 1966), pp. 313-315.

[16]C. W. Misner, K. S. Thorne, and J. A. Wheeler, *Gravitation* (W. H. Freeman, San Francisco, 1973), p. 336.

[17]C. W. Misner, K. S. Thorne, and J. A. Wheeler, *Gravitation* (W. H. Freeman, San Francisco, 1973), p. 335.

[18]Brandon Carter, in *General Relativity: An Einstein Centenary Survey*, edited by S. W. Hawking and W. Israel (Cambridge University Press, Cambridge, 1979), p. 353. Note that Carter's equation (6.297) contains a typographical error; equation (4.1) of the text is correct.

[19]L. Smarr, Phys. Rev. Lett. 30, 71-73, (1973).

[20]Brandon Carter, in *General Relativity: An Einstein Centenary Survey*, edited by S. W. Hawking and W. Israel (Cambridge University Press, Cambridge, 1979), pp. 325-326.

[21]Brandon Carter, in *General Relativity: An Einstein Centenary Survey*, edited by S. W. Hawking and W. Israel (Cambridge University Press, Cambridge, 1979), p. 325. Note that Carter's equation (6.118) contains a typographical error; equation (4.2) of the text is correct.

[22]Brandon Carter, in *General Relativity: An Einstein Centenary Survey*, edited by S. W. Hawking and W. Israel (Cambridge University Press, Cambridge, 1979), pp. 326-327.

[23]Brandon Carter, in *General Relativity: An Einstein Centenary Survey*, edited by S. W. Hawking and W. Israel (Cambridge University Press, Cambridge, 1979), p. 309.

[24]Kip S. Thorne, unpublished.

[25]C. W. Misner, K. S. Thorne, and J. A. Wheeler, *Gravitation* (W. H. Freeman, San Francisco, 1973), p. 445.

[26]Richard H. Price, unpublished.

[27]C. W. Misner, K. S. Thorne, and J. A. Wheeler, *Gravitation* (W. H. Freeman, San Francisco, 1973), pp. 650-658.

[28]Kip S. Thorne and Richard H. Price, unpublished.

[29]Richard H. Price, unpublished.

[30]Kip S. Thorne, unpublished.

[31]C. W. Misner, K. S. Thorne, and J. A. Wheeler, *Gravitation* (W. H. Freeman, San Francisco, 1973), pp. 281-282.

[32]C. W. Misner, K. S. Thorne, and J. A. Wheeler, *Gravitation* (W. H. Freeman, San Francisco, 1973), p. 344.

[33]G. W. Gibbons, Nature Phys. Sci. 240 , 77 (1972). Note that Gibbons' equation (5) is incorrect; his conclusions are in error for the case of the relativistic rope.

Figure Captions

FIG. 1. Weyl background-space source configuration for the Schwarzschild black hole under the tidal influence of suspended moons. The two-moon configuration is shown; for the one-moon solution the lower point source is absent and the lower "rope" extends up to the line source.

FIG. 2. Embedding diagram profiles for the weak-perturbation regime, defined in terms of spherical coordinates in the embedding space. *(a)* The profile defined by equation (3.8) for the weak-perturbation regime. *(b)* The profile defined by equation (3.14) in the distant weak-perturbation limit (with the moons far from the horizon, giving pure quadrupole deformation). The dotted figures are the profiles of spheres with the same area as the horizon embedding surfaces. The size of the perturbation is exaggerated here for purposes of illustration.

FIG. 3. Embedding diagram profiles of the horizon tidal bulges, defined in terms of cylindrical coordinates in the embedding space. *(a)* The profile defined by equation (3.31) for the strong-perturbation regime, showing the approach to conical form away from the pole. *(b)* The profile given by equation (3.33) for the weak-perturbation case, showing the "pith helmet" deformation, which flattens out into the unperturbed spherical shape away from the pole. The size of the perturbation is exaggerated.

FIG. 4. The conical geometry of the $\hat{\rho}-\hat{\varphi}$ plane near the ropes. *(a)* A conical embedding diagram for the geometry depicted in $(\hat{\rho},\hat{\varphi})$ coordinates. *(b)* The geometry depicted in $(\hat{\rho},\varphi^*)$ coordinates; the rays $\varphi^*=0$ and $\varphi^*=2\pi\sin\alpha$ are to be identified. The rotation of a vector $\vec{A}$ in the $\hat{\rho}-\hat{\varphi}$ plane upon transport around the axis along the curve C is shown. The angles α and Δ are exaggerated for clarity.

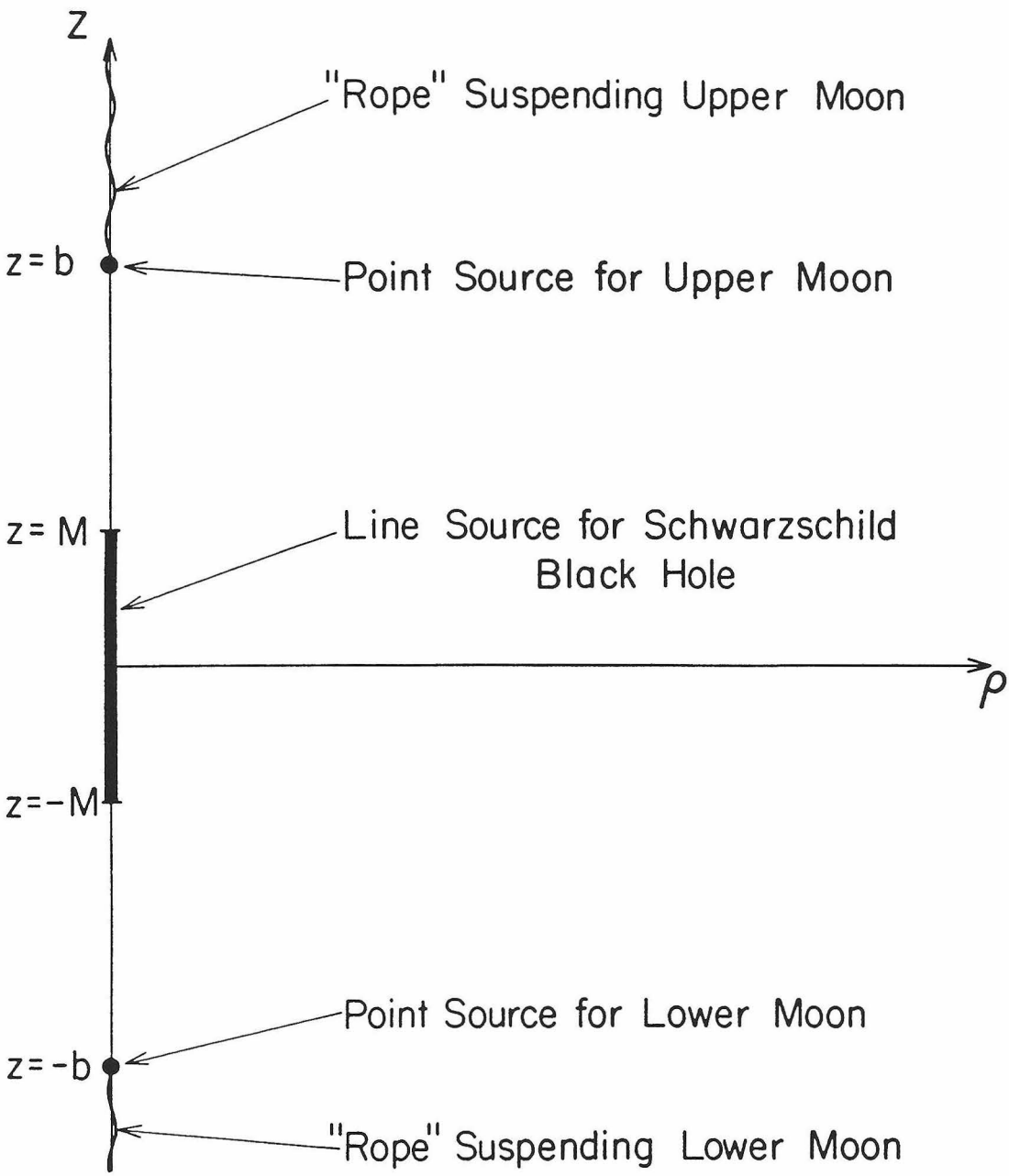
z
"Rope" Suspending Upper Moon
z = b
Point Source for Upper Moon
z = M
Line Source for Schwarzschild
Black Hole
ρ
z = -M
Point Source for Lower Moon
z = -b
"Rope" Suspending Lower Moon

FIG. 1

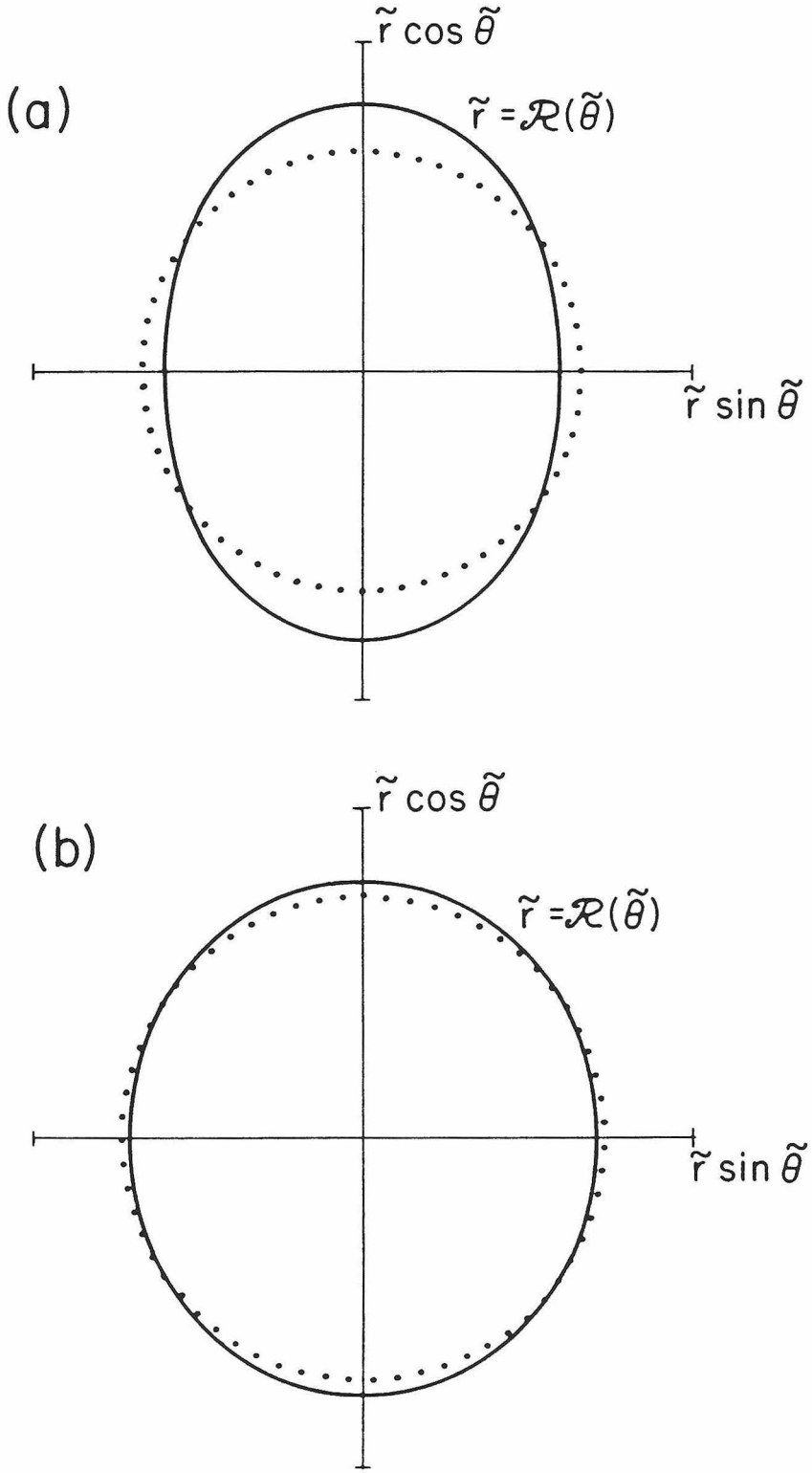
(a)
$\tilde{r}\cos\tilde{\theta}$
$\tilde{r}=\mathcal{R}(\tilde{\theta})$
$\tilde{r}\sin\tilde{\theta}$
(b)
$\tilde{r}\cos\tilde{\theta}$
$\tilde{r}=\mathcal{R}(\tilde{\theta})$
$\tilde{r}\sin\tilde{\theta}$

FIG. 2

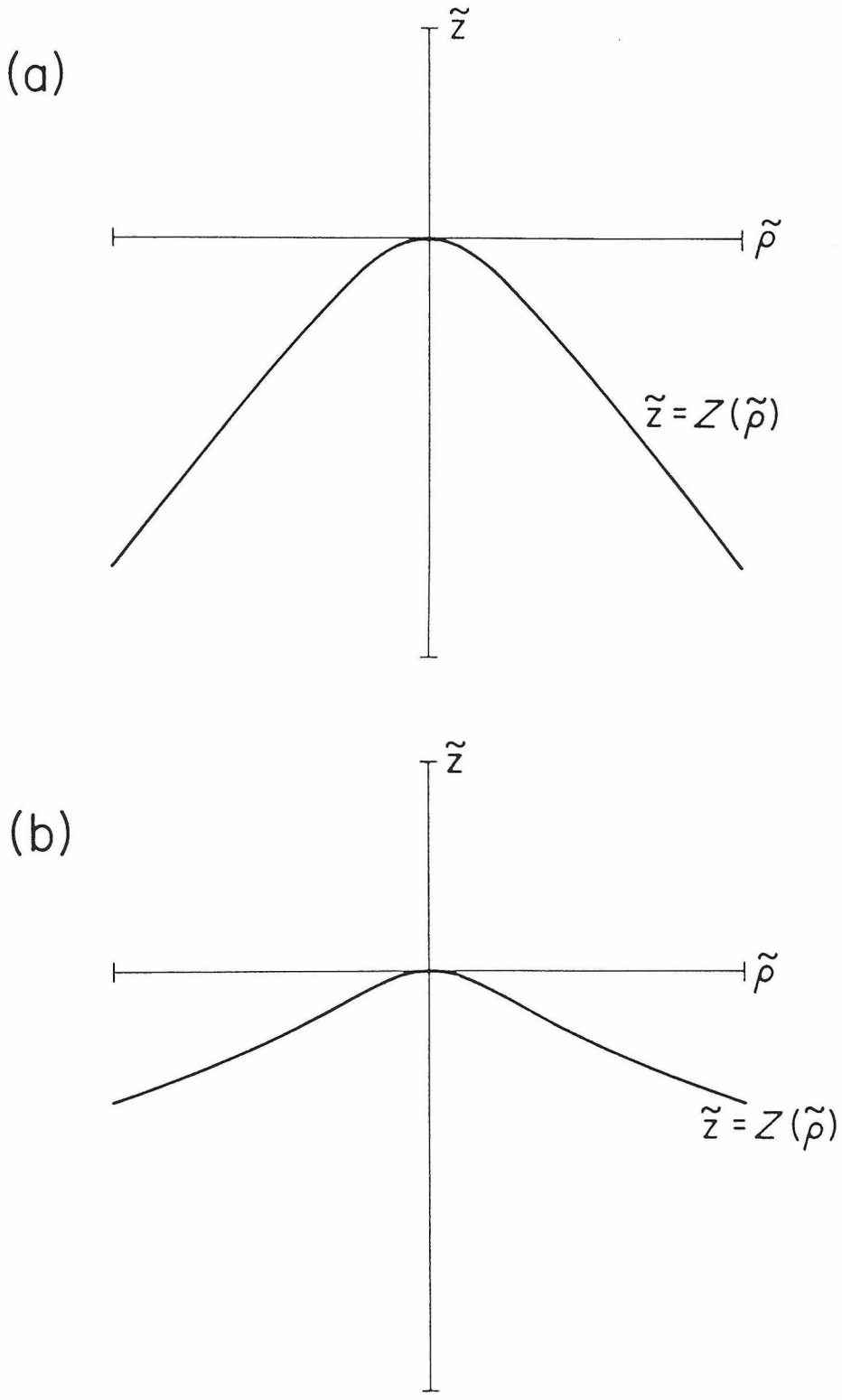
(a)
$\tilde{z}$
$\tilde{\rho}$
$\tilde{z} = Z(\tilde{\rho})$
(b)
$\tilde{z}$
$\tilde{\rho}$
$\tilde{z} = Z(\tilde{\rho})$

FIG. 3

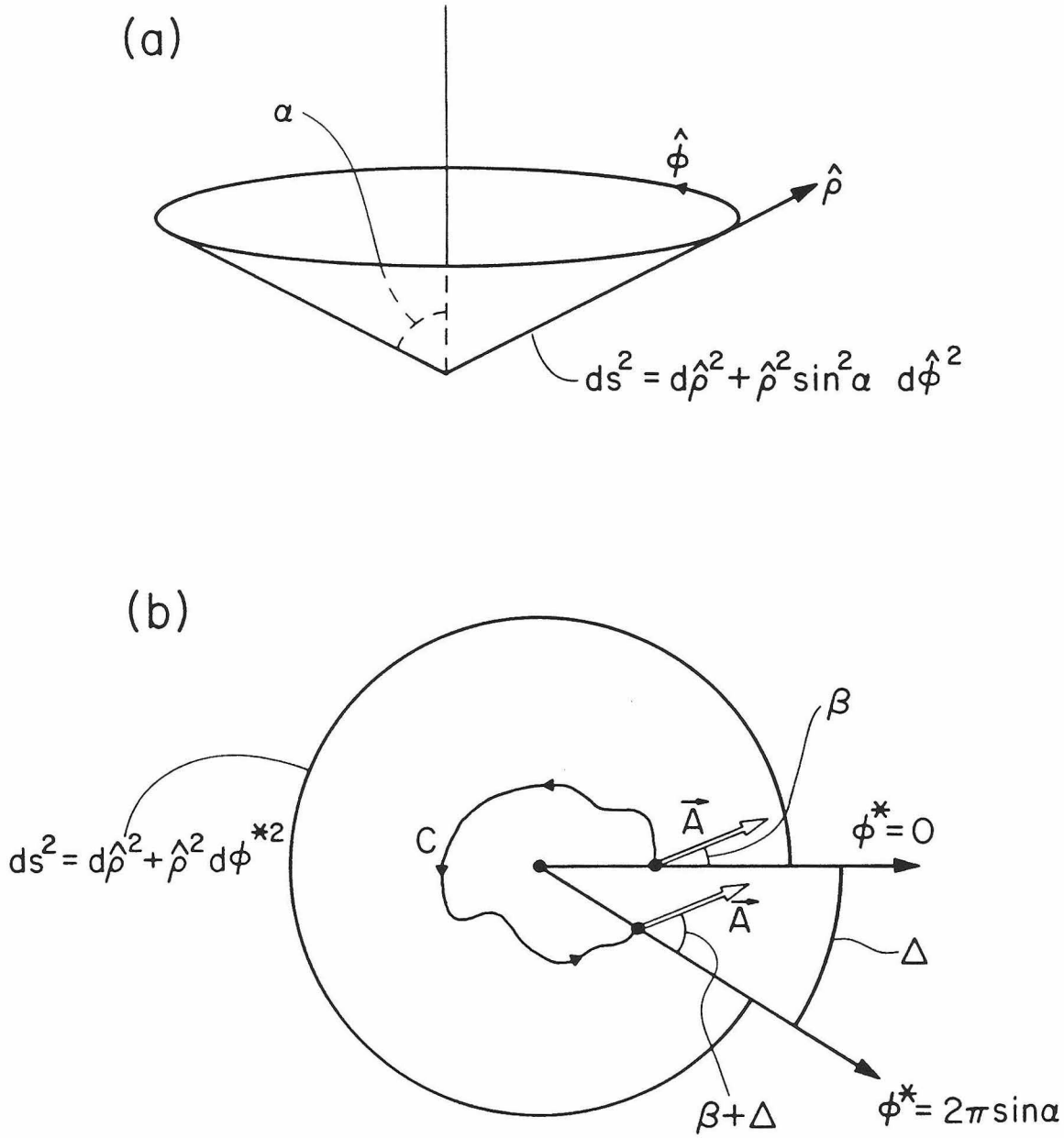
(a)
α
$\hat{\phi}$
$\hat{\rho}$
$ds^2 = d\hat{\rho}^2 + \hat{\rho}^2 \sin^2\alpha \; d\hat{\phi}^2$
(b)
$ds^2 = d\hat{\rho}^2 + \hat{\rho}^2 d\phi^{*2}$
β
C
$\vec{A}$
$\phi^* = 0$
$\vec{A}$
Δ
$\beta+\Delta$
$\phi^* = 2\pi \sin\alpha$

FIG. 4